JPL NO. 9950-279

LOW COST POINT FOCUS SOLAR CONCENTRATOR

Phase I Final Report

March 1979

John H. Laakso
Engineering Manager

Donald K. Zimmerman
Program Manager

Prepared For

Jet Propulsion Laboratory
4800 Oak Grove Drive
Pasadena, California 91103
Project Manager: T.O. Thostesen
Contract No. 955209

By

BOEING ENGINEERING AND CONSTRUCTION
(A Division of the Boeing Company)
Seattle, Washington 98124

1 of 181

ABSTRACT

The preliminary design and economic analysis of a low cost, pneumatically stabilized plastic film point focus solar concentrator are described. Potential applications for the concentrator are in conjunction with Brayton cycle engines or supply of thermal energy. The study objectives were (1) to develop a concentrator having maximum energy collection per unit cost, (2) investigate the related manufacturing, installation and maintenance methods and (3) predict the concentrator costs in mass production. The concentrator has a gore-formed, aluminized polyester parabolic reflector whose shape is stabilized by a slight vacuum. The reflector is mounted on a lightweight conical shell having a rear vacuum membrane. The reflector assembly is supported by a lightweight 2-axis tracking steel framework. The concentrator is completely protected from wind and weather by a pneumatically stabilized clear plastic film enclosure. A sub-scale reflector was fabricated and optically tested by laser ray tracing to determine focal deviations of the surface slope and best focal plane. These test data were then used for comparisons with theoretical concentrator performance modeling and predictions of full-scale design performance. Design concepts and plans for mass-production facilities and equipment, field installation, and maintenance were developed and used for cost analysis. Results of the economic study indicate the concentrator design will have low cost when mass-produced and has cost/performance parameters that fall within current Jet Propulsion Laboratory goals.

ACKNOWLEDGEMENTS

The support the Jet Propulsion Laboratory's contract technical monitor, Tom Thostesen, has provided is greatly appreciated. Thanks are due to the Boeing personnel who contributed to the effort.

Mark Berry-Polymeric Materials Design

Wayne Davidson-Control System

Harry Dursch-Drive Motor Design
Sub-Scale Reflector Fabrication
Cost Analysis

John Laakso-System Design
Control System Design
Structural Analysis

Jesus Mayorga-Testing

Mary Jane Meola-Production Processes

Marv Patterson-Subscale Reflector Fabrication

Joe Reide-Tool Design

Gary Reilly-Testing

Tom Simmons-Plant Architecture

Earl Umbinetti-Drafting

Cheryl Warner-Test Data Analysis
Thermal Analysis

Don Weyer-Concentrator Design

In addition, the following individuals had a significant role in the project.

Larry Johnson-Microelectronics Consultant
Cascade Digital Company
Redmond, Washington

Bill Hochgraef-Tracking System
Government Eletronics Division
Motorola Inc.
Scottsdale, Arizona

Larry Cook-Materials Handling Consultant
Cook-Newhouse and Assoc. Inc.
Bellevue, Washington

Too numerous to acknowledge are all of the vendors that furnished information for the study. Barry Skolnik of National Metalizing (aluminized polyester film), ICI Americas (UV stabilized polyester), Pennwalt (Kynar), Gus Myron of Sheldahl (enclosure fabrication) and Superior Electric Company (stepper motors) were particularly helpful.

TABLE OF CONTENTS

5

1.0 SUMMARY

This report describes the preliminary design and evaluation of a pneumatically stabilized plastic film parabolic concentrator for use in a Brayton cycle system operating with a receiver temperature of 1700°F. The concentrator has a 13 m diameter reflective surface made from metallized film and stabilized with a small differential air pressure. A spherical enclosure made of a clear plastic film completely protects the concentrator and Brayton unit from the environment.

A general goal of this phase, the first of a three-phase project, was to study the pneumatically stabilized plastic film concentrator concept to develop a technical and economic basis for subsequent detailed design approach and implementation. Specific objectives of the project were to:

- Optimize the concentrator design parameters for maximum solar energy collected per concentrator unit cost
- Develop a preliminary design
- Investigate the manufacturing, installation, and maintenance of the concentrator
- Predict the costs for mass production

In Task I of the project, a parameter optimization study was conducted to define an initial optimum design configuration for the concentrator. This design point, with a fixed enclosure and a reflector diameter of 13 m limited by shipping constraints, yielded high net useful energy per unit cost compared to a number of concepts having various reflector support and protection schemes. With JPL's concurrence this design concept was adopted as the baseline concentrator design satisfying the first project objective.

The remaining Phase I project objectives were fulfilled with development of the preliminary concentrator design in a series of tasks: preliminary design, subscale reflector testing, performance analysis, production plant planning, installation studies, maintenance studies and economic analysis.

Preliminary Design

A preliminary design was developed for a concentrator that can be mass-produced at low cost. The concentrator has a gore-formed, aluminized polyester reflector which is supported by a conical shell and a 2-axis tracking steel framework. The reflector is stabilized by a slight vacuum formed in the cavity between the reflector and a rear film membrane also supported by the conical shell.

Because of the light weight of the reflector and protection from wind offered by the enclosure, the reflector's supporting framework is very light weight. Conventional components are utilized in the design of the structural, mechanical and electrical systems. For tracking control, low-cost system and unit controller architectures were defined. Tracking is based on a closed loop control law and uses a photosensor sun tracking unit and stepper motors for accurate tracking.

The protective enclosure has a 14.7 m diameter and is designed as a pressure stabilized clear plastic film structure employing Kynar (poly-vinylidene fluoride) which is inherently stable to ultraviolet radiation. Fabrication of the enclosure would be by an extension of current gore forming techniques. An access door in the enclosure is provided for maintenance of the concentrator. While having a high material cost/unit weight, the enclosure is an essential design feature to achieving low overall concentrator weight and cost with high performance in windy, dusty conditions.

Subscale Reflector Test Program

Feasibility of the pneumatically stabilized reflector was demonstrated by fabrication and testing of a 4.57 m diameter subscale model. Several fabrication issues were resolved which allowed construction of the subscale reflector using (1) simple vacuum-assisted lay-up tooling, (2) taped gore seams which were wrinkle-free, and (3) reflector installation technique that minimized edge mounting errors. The reflector mounting was accomplished by first pneumatically stabilizing the reflector in a holding fixture then attaching the test edge ring which was smaller than the holding fixture. In this manner, the majority of edge mounting related film buckles were outside of the active reflector area and could be trimmed away; a similar mounting technique would be used for rapid field reflector assembly.

In testing the subscale reflector, a laser ray test procedure was used that involved computer-aided data acquisition and post-processing. Final testing collected laser/target intercept data at 72 angular positions (at 5°) and 24 radial points for a total of 1728 data points. These data were analyzed to determine surface slope errors which were used for (1) comparisons with theoretical concentrator performance modeling and (2) predictions for full-scale concentrator performance. Correlations of the surface slope quality with fabrication procedures were found; mishaps in reflector-to-ring mounting were particularly harmful to surface quality.

Taking the "best quadrant" of the reflector and removing systematic radial deviations from a paraboloidal surface, resulted in a computed RMS surface slope error of 3.54 mrad (a significant improvement over previous testing). For all 1728 test points and with systematic errors included, the surface quality was 7.57 mrad RMS. Judging from the results of this single large reflector test, additional fabrication experience and more sophisticated tooling will result in surface quality near the BEC mass production goal.

Performance Analysis

A performance analysis for the full-scale concentrator was performed using the actual surface slopes of the above-mentioned "best quadrant", 3.54 mrad RMS test reflector. Based on the test data, and with 0 mrad tracking error the 13 m concentrator delivers 68 kW of net energy. (61 kW with all test data points considered). For the design goals of 2 mrad for surface quality and tracking errors, the concentrator delivers 71 kW at an optimum F/D of 0.5 and aperture diameter of 0.288 m.

Plant Design

A plant design was conceived for mass production of 100,000 concentrator units per year at a rate of 2.1 units per hour, operating at 2 shifts per day. Operational plans, workstation definition and tooling concepts and plant layout were developed from a study of material flow and plant function isolation zoning.

Automated tooling concepts needed to realize the high production rate were defined for three critical workstations: enclosure gore forming, reflector gore lay-up and joining and reflector support shell panel fabrication. Most of the more conventional parts would be made from vendor-furnished items.

An integrated automatic materials handling system was found to be essential to achieving high production rate at low cost. A key feature of this system is the use of returnable shipping containers, which flow through the plant. Two containers, shipped on a single truck trailer, would be needed for each concentrator. These containers would also provide temporary field storage prior to installation of the concentrators.

The plant design study resulted in a facility having the following characteristics: 732,500 sq. ft. floor area, $41 million building and site cost ($56/ft^2) and $25 million tooling and equipment cost ($34/ft^2).

10

Field Installation and Maintenance

A preliminary field installation plan was developed that will result in rapid assembly and erection of factory pre-assembled concentrator parts. A critical field operation is reflector assembly which is envisioned to be done on portable precision fixtures under shelter. Temporary shelter will be required during reflector and enclosure installation in windy conditions.

An analysis of maintenance requirements over a 30 year lifetime indicates washing of the enclosure will be a major life-cycle cost component followed by enclosure replacement programmed at 15 years. Washing could be done with a mobile washing truck traveling from field to field. Maintenance of the concentrator in the inflated enclosures would be done using portable service equipment having air locks.

Cost Analysis

A cost analysis was performed to determine production, field installations and maintenance costs. The concentrator's estimated selling price based on 1978 dollars is $7835 ($59/m^2) FOB factory. Installed concentrator cost, including related construction site and equipment costs, is $9624 ($73/m^2). With life cycle costs considered, the concentrator cost is $17,510 ($132/m^2).

Economic Analysis

The resulting performance/cost for a life cycle cost including washing is 0.0041 kW_{th}/$. This figure-or-merit would be improved with any reduction of washing and/or enclosure film cost which are the major portions of the total life maintenance cost. In terms of concentrator unit cost/efficiency, the concentrator has an installed cost/efficiency ratio of $125.50/m^2 for a reflector surface quality of 5.52 mrad RMS (representing the full subscale test reflector with systematic errors removed) and $108.17/m^2 for the 2 mrad RMS surface design goal. These ratings compare favorably with JPL's goals for concentrator costs of $100 to 150/m^2 ($111 to 167/m^2 when factored for efficiency) for 1982.

Design Sensitivity Analysis

Design sensitivity studies were done to verify the optimality of the baseline concentrator size. Cost data developed in Task I for various concentrator sizes were updated with the preliminary design cost data. The resulting levelized bus bar energy costs, based on life cycle costs, show the optimum concentrator diameter to be 13 m. Other design trades conducted indicated the concentrator cost to be sensitive to Brayton unit weight, receiver operations temperature, and enclosure cost. In particular, success in current vendor research on inherently stabilized polyester film would result in large concentrator cost savings.

2.0 INTRODUCTION

An approach to achieving significant cost reductions in point focus solar energy concentrators is the use of ultra-lightweight pneumatically stabilized plastic film reflectors. This report describes a preliminary concentrator design having a pneumatically stabilized plastic film reflector and presents an evaluation of the design by subscale reflector testing and economic analysis in a Brayton cycle system application with a receiver operating at 1700°F.

The report summarizes work performed by Boeing Engineering and Construction (BEC) for the Jet Propulsion Laboratory (JPL) under JPL Contract 955209. This project is managed by JPL as part of a broad Department of Energy Program concerned with small solar-thermal power systems for providing thermal and/or electrical power. JPL's overall objectives guiding this project are directed toward developing high temperature point focusing concentrator technology with a major emphasis on low cost in large quantity production.

The BEC concentrator design concept, shown in Figure 2.0-1, is based on a paraboloidal reflective surface consisting of a thin, metallized plastic film which is supported on a conical shell and stabilized with a small differential pressure between the enclosure and a cavity behind the reflector. The film is fabricated in a shape closely approximating the desired paraboloid; final shaping is accomplished with the pressure. The reflector assembly is supported by a structural steel framework which is gimballed for azimuth-elevation sun tracking. The concentrator is placed in a clear plastic film enclosure which is adopted from BEC's heliostat programs. The enclosure is an essential design feature that protects the concentrator from the environment (wind loads, precipitation, dust, hail, etc.).

13

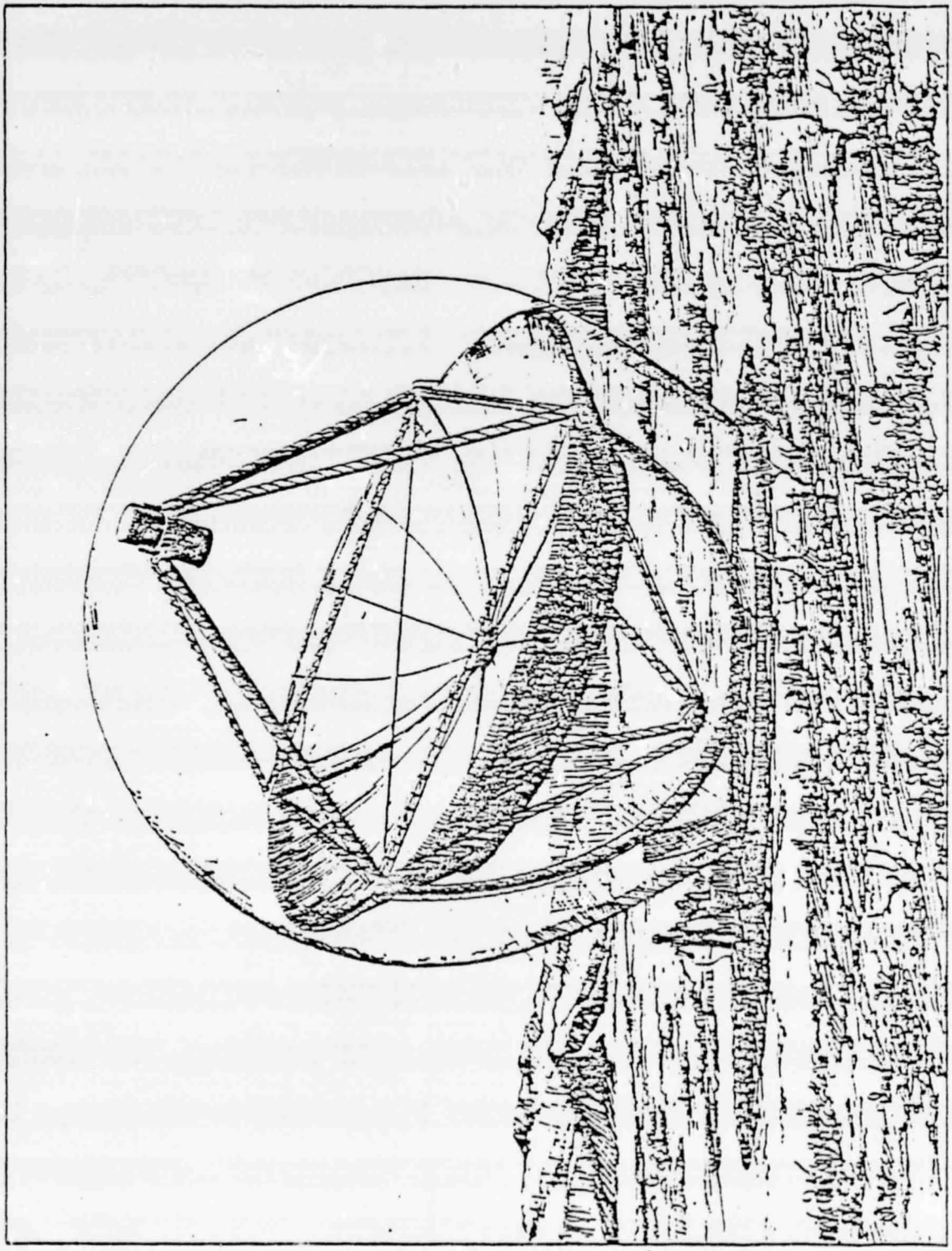

Figure 2.0-1. BEC Low Cost Point Focusing Solar Concentrator

14

Potential advantages of the design concept include:

- o Lightweight structure which minimizes material cost, minimum drive system loads and costs
- o Minimum amount of close tolerance structure
- o Environmental protection for the reflective surface and Brayton unit
- o Elimination of wind-induced distortions of the concentrator
- o Convex outer surface of the enclosure which should remain cleaner than a concave concentrator and maintain higher performance between cleanings.
- o Simple foundation

The design concept draws on much of the design studies, materials evaluations, and processing experience gained in Boeing's work on the ERDA/DOE heliostat development programs. In particular, the basic conceptual design, analysis methods and test procedures for the reflector were developed in a recent BEC program for Sandia Laboratories under Mr. M. W. Edenburn's direction (Ref. 3).

The report is divided in sections that correspond to the Phase I task activities. Section 3.0 gives a summary of work done in Task I Parameter Optimization work, Task II Concentrator Preliminary Design, and Task III Interface Requirements. Section 4.0 presents a subscale reflector test program done in conjunction with the preliminary design development. The results of concentrator performance analysis are given in Section 5.0. Task IV Assessment of Production Implementation studies are described in Section 6.0. As part of the Task II preliminary design evaluation, design sensitivity studies were conducted and are reported in Section 7.0 Conclusions from the Phase I activities are given in Section 8.0.

3.0 CONCENTRATOR DESIGN

The design requirements, interface requirements, design concept studies, preliminary design and design analysis are described in Sections 3.1 through 3.6.

3.1 Design Requirements

The concentrator design was governed by design requirements furnished by JPL. These requirements are given in (1) JPL Document DM 512142, Exhibit II, Design Req'ts. Specification-point Focusing Concentrator (preliminary), 10 February 1979 and (2) JPL Letter, G.E. Saunders to E. J. Valley (BEC), dated 12 January 1979. In general terms, the design requirements are the basis of the following criteria for concentrator design:

- Mass-producible at low cost
- Maximum kW_{th}/S
- Configuration suitable for a wide range of Brayton receiver/engine units
- 30 year life
- Survive environmental extremes
- Full 2-axis tracking capability
- Fail-safe operation
- High reliability
- Easily serviced

3.2 Design Parameter Optimum Study (Task I)

This section presents a brief review of the design configuration studies conducted in Task I. The configuration variables that are important to the development of a low cost pneumatically stabilized film concentrator were identified as:

- Reflective surface stabilization method
  - Vacuum
  - Positive pressure
- Reflector cavity closeout type
  - Separate
  - Integral with enclosure
- Receiver/engine interface
  - Enclosed
  - Partially enclosed
  - Exposed
- Enclosure configuration
  - Separate or fixed
  - Integral or rotating

Each of these variables, singly or in combination, were studied in Task I to arrive at the design concepts shown in Figures 3.2-1 to -4.

Concept 1 shown in Figure 3.2-1 has a lenticular enclosure permitting the concentrator to be feathered in high winds to reduce survival wind load requirements. Investigations showed the shape would be subjected to high lift and gimbal moments while operating during normal winds. This configuration has a double transmittance loss through the enclosure. The latter problem is eliminated in Concept 2, Figure 3.2-2, but some lift and gimbal moment remains for operation in normal winds. The near spherical enclosure of Concept 3, Figure 3.2-3, eliminates the lift and high loads for the survival wind condition. Finally, Concept 4 shown in Figure 3.2-4 completely eliminates the wind loads from the concentrator, at the expense of more difficult access and the need for the intake/exhaust ducting.

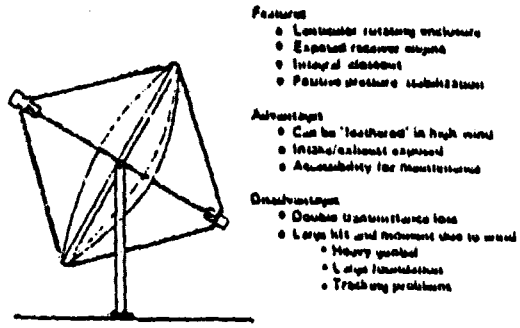

Figure 3.2-1. Concept No. 1

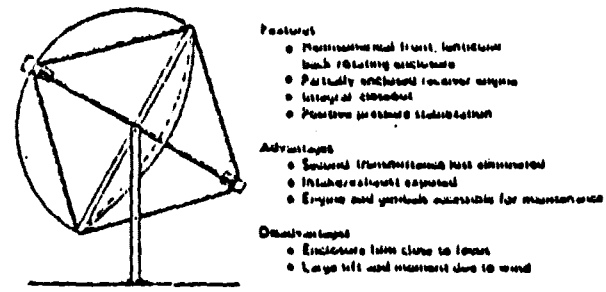

Figure 3.2-2. Concept No. 2

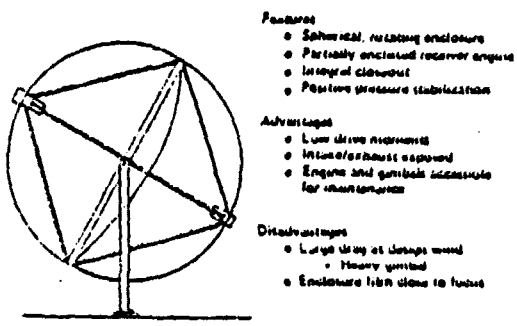

Figure 3.2-3. Concept No. 3

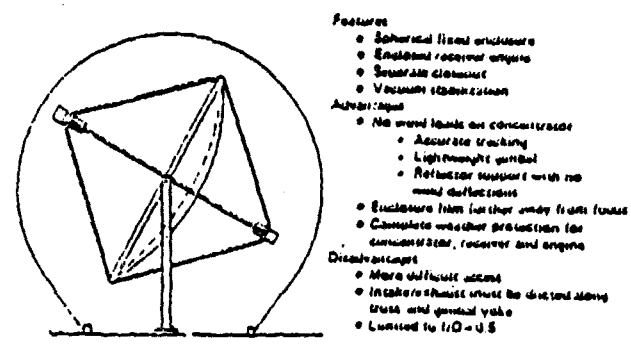

Figure 3.2-4. Concept No. 4

A comparison given in Table 3.2-1, of the configuration candidates with respect to cost-effectiveness, reliability, producibility and state-of-the-art (readiness) indicated two concepts were leading candidates. They are differentiated by their enclosure types: a rotating spherical enclosure and a fixed spherical enclosure (referred to as "rotating" or "fixed").

The parametric design studies in Task I proceeded with balanced comparative studies of the fixed and rotating enclosure concepts; these studies involved conceptual design, fabrication, installation, and maintenance studies and performance/cost analysis. A summary of the performance/cost trades for the candidate concentrator concepts appears in Figure 3.2-5.

Table 3.2-1. Concept Comparison

	No. 1	No. 2	No. 3	No. 4
Support trusses, Concept receiver, Reflector, Protective enclosure	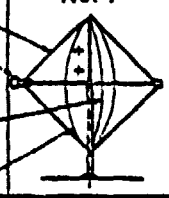	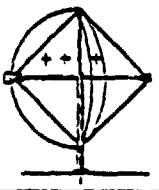	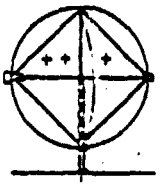	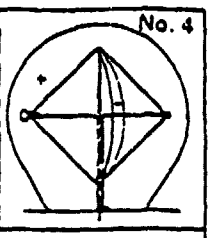
Cost effectiveness				
Thermal performance	Lowest (2 τ's)	Good	Good	Best- τ Higher
Cost	Highest (Drive loads)	Near highest	Near lowest	Lowest
Overall	Lowest	Near lowest	Near best	Best
Reliability	Lower (Gimbal and drive loads)	Lower	Next best (Gimbal loads)	Best (Complete protection)
Producibility	Good	Good	Good	Slightly lower, (Full sphere)
State-of-the-art	Current	Current-- (Enclosure thermoform)	Current--	Current-

No. 3 and No. 4 selected for evaluation

As shown in Figure 3.2-5, the performance/cost figure-of-merit for both enclosure concepts falls off at the larger concentrator diameters. This is due primarily to increased costs for (1) yoke structure, (2) increased field assembly costs, and (3) enclosure replacement. The rotating concept has an overall lower value and more rapid fall-off for the figure-of-merit because of wind load effects on yoke weight. Note that effects of wind-induced yoke deflections are not included in the performance parameters; if considered, the rotating enclosure would have even lower relative figures-of-merit..

Based on the figure-of-merit data developed in Task I, the optimum concentration concept has a fixed enclosure and will have a large size. The concentrator diameter recommended for the following Task II preliminary design was then selected to be 13 m. At this diameter, the concentrator appeared to offer near maximum kW_{th}/S and reaches the limits for reflector and enclosure shipping configurations that allow shipment without special permits.

20

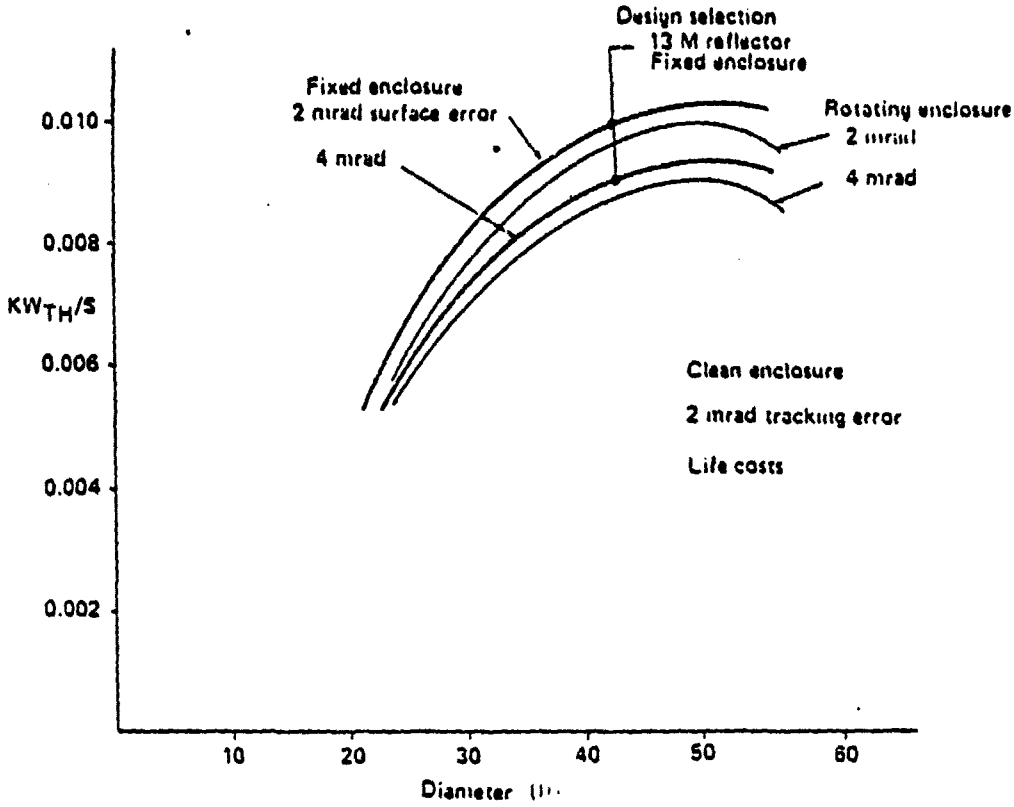

Figure 3.2-5. Concentrator Performance/Cost Summary

3.3 Selected Design Concept

The design concept selected for the baseline preliminary design as a result of the Task I studies is illustrated in Figure 2.0-1. This design is characterized by:

o Fixed enclosure diameter	14.7m
o Reflector diameter	13 m
o F/D	0.5
o Receiver aperture diameter	0.228 m
o Reflector surface slope quality goal	2 mrad RMS
o Tracking system accuracy goal	2 mrad RMS

3.4 INTERFACE REQUIREMENTS

Design of the interfaces between the LCPFC and the receiver/power conversion unit is based on the following requirements:

- Receiver/PCU space envelope is 32 in. diameter x 43 in. long
- Receiver/PCU combined weight is 825 lbs.
- Receiver/PCU support ring is a C6 x 10.5 channel
- Temperature of the PCU exhaust gas is 416°F
- PCU supply/exhaust lines are sized for a mass flow of 0.533 lb/sec with a total pressure drop of 1.6 in. w.c. (.045 psi.)
- PCU supply/exhaust lines are 6 in. pipes with band type clamps
- Receiver/PCU power and instrumentation cables are attached to concentrator structural components

3.5 CONCENTRATOR PRELIMINARY DESIGN

Major components of the LCPFC system are shown in Figure 3.5-1 and consist of the following assemblies:

- Reflector assembly-section 3.5.1
- Structural/mechanical assemblies-section 3.5.2
- Enclosure-section 3.5.3
- Pneumatic systems-section 3.5.4
- Control system-section 3.5.5

22

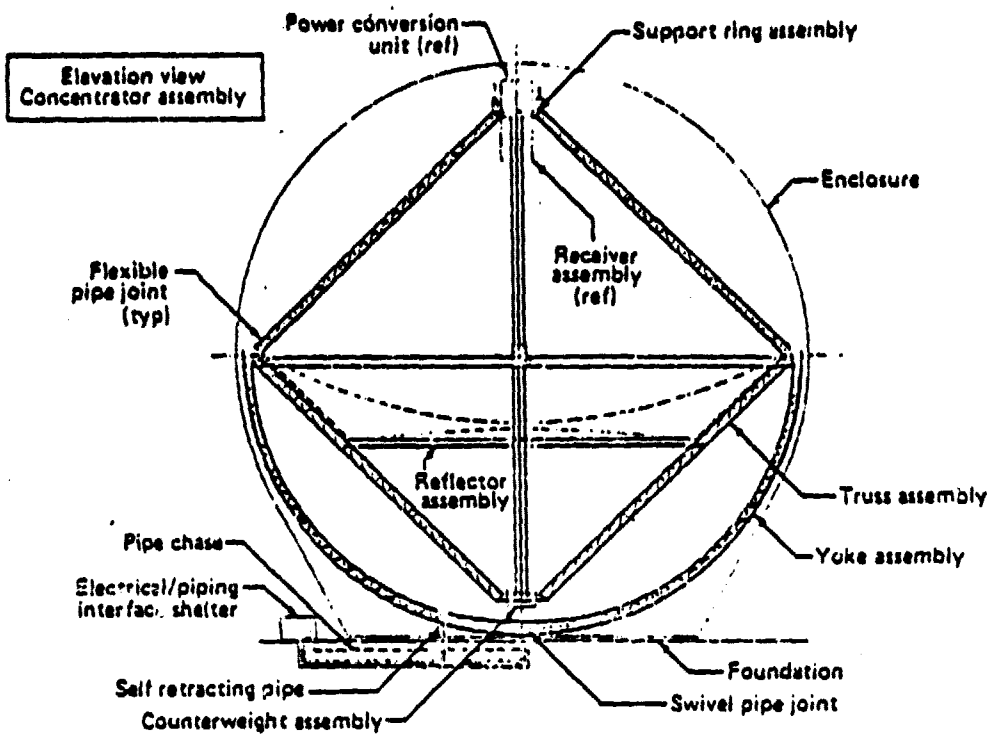

Figure 3.5-1. Structural/Mechanical Design

3.5.1 Reflector Assembly

The reflector assembly consists of a pneumatically stabilized plastic film reflector, a conical reflector support shell and a rear plastic film vacuum membrane. Reflector stabilization is achieved with a vacuum of nominally 0.0037 psi and in this condition the reflector assembly can be safely handled during field installation. As shown in Figure 3.5.1-1. four attachment points are provided to mount the assembly on the concentrator truss. The following describes the reflector assembly components in more detail.

3.5.1-1 Reflector

The reflector is assembled from 18 20° gore sections and is designed to be wrinkle-free at a nominal stabilization pressure of 700 psi. At this pressure level, the maximum film stress is 700 psi. and occurs in the circumferential direction at the perimeter. Based on testing done in a Sandia Laboratories Contract (Ref. 3), a 20° gore configuration is a good compromise between minimizing surface errors related to flat gore facets and lay-up

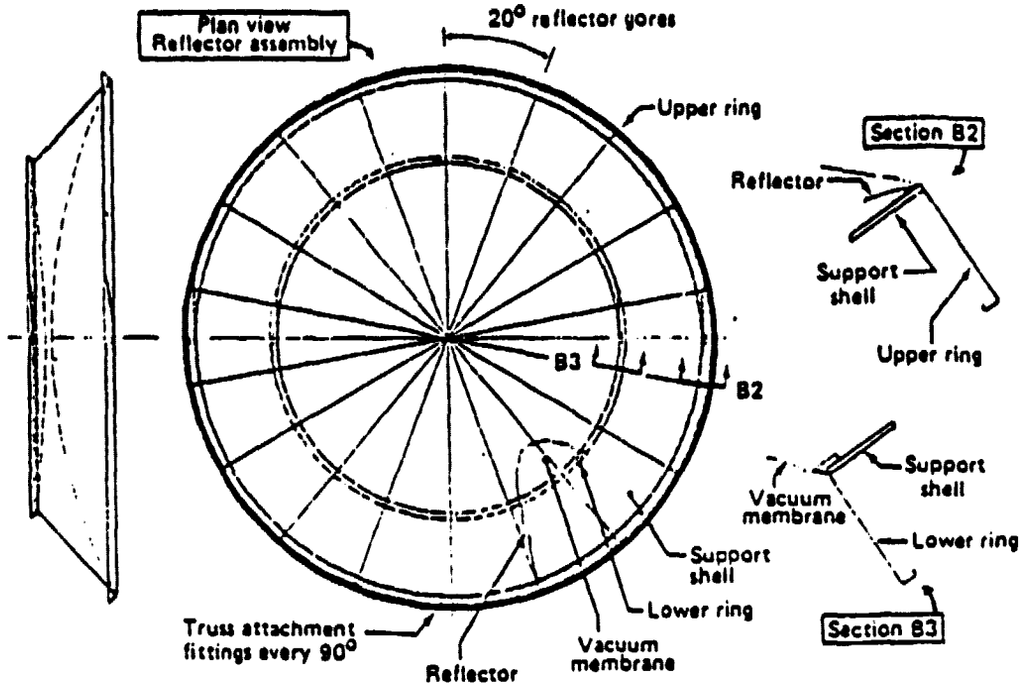

Figure 3.5.1-1. Reflector Configuration

costs. The reflector is designed with a F/D of 0.5 to give good performance, as discussed in Section 5.0, with a compact enclosure. Also, at this F/D, the reflector can be easily rolled on a mandrel for shipping. At the reflector's perimeter, a thermoplastic adhesive would be used to attach the reflector to the support shell in the field using special tooling, discussed in Section 6.2.

The reflector seam configuration is a butt-type joint having adhesive splicing tape on both sides. A tape thickness of 2 mil and width of 0.5 inch are believed to be adequate from strength considerations. One polyester tape product, having a pressure-sensitive acrylic adhesive, Permacel-255, was used in the sub-scale reflector and was found to have impressive adherence. As part of a follow-on detail design program, adhesive studies will be done to insure taped seams will have the requisite 30-year life. Thermoplastic adhesives, such as offered by Sheldahl, will also be considered for reflector seams. One potential problem associated with heat sealing is heat shrinking of the reflector film which may produce surface errors.

The reflective film material is specified to be a UV stabilized aluminized polyester film with an antioxidation coating (first surface reflector). The weatherability of the reflector is expected to be good by virtue of the metalized side protecting the polymer substrate from the ultraviolet solar radiation and the clean, dry environment inside the protective enclosure. Further, the mechanical loading on the film is approximately an order of magnitude below the film's yield point; a substantial margin even if degradation with time did occur.

However, because of the desirability of long life (30 years) and its associated economy in labor and materials, development work has been underway to assure long term stability of properties. Samples of aluminized Mylar were enclosed in Tedlar envelopes and exposed on a rack at Albuquerque, New Mexico for 16 months. The frontside of the samples were south facing and the backside shaded from the sun. At the end of the 16 months the following degradation was observed:

Property	% Loss
Reflectivity	1.4
Yield Strength	0
Ultimate Strength	8
Ultimate Elongation	16

The data suggests the material would be servicable for at least several years, however, it is not known how the degradation mechanisms vary with time and exposure (linear, increasing or decreasing rate, etc.). This has led to a Boeing Plastic Film Industry cooperative program aimed at increasing reflector film life.

Table 3.5.1-1 lists the materials and respective suppliers for candidates received for test. To the right, in the appropriate columns, are shown the specular reflectances taken on the Boeing bi-directional reflectometer at 0.15° cone angle with a 633 nanometer wavelength source. As can be seen, a variety of film processors are represented. The reflectance 's, of course, generally higher as the cone angle is increased from 0.15° upward. It should be noted that the values in the table have been adjusted upward by about 3 percent to convert to integrated solar specular reflectance (air mass 2).

Table 3.5.1-1. Candidate Reflector Film

	Specular reflectance @ .15° cone angle	
	No overcoat	Overcoated
Aluminized (National Metalizing)		.89
Mylar D – Aluminized (National Metalizing)	.91	
Mylar D – Aluminized (Dunmore)	.89	
Melinex 442 – Aluminized (Dunmore)	.86	.79
Melinex "O" – (U/V stabilized) – Aluminized (Martin Processing)	.81	
Melinex "O" – Aluminized (Morton Chemical)	.88	.69
Polyester – (U/V stabilized) – Metalized (OCLI)		
Silverized	.91	.90
Aluminized		.68

The protective coated material supplied by National Metalizing was improved in two iterations from a reflectivity of .71 to .89 (at 633 nm wavelength). This compares with reflectivity of .91 for an unprotected aluminized surface at the same wavelength.

Dunmore provided Mylar D in earlier research and it was seen to have a 633 nm reflectance of 0.89 for the present effort, they provided candidates of overcoated and uncoated aluminized Melinex 442. As seen in the table, the reduction in specular reflectance due to the overcoating was 0.07, an unacceptable loss. Melinex "O" provided by Martin Processing exhibited a large amount of scattering process and its effect on the surface quality of the substrate. Late in the program, Morton Chemical provided aluminized polyester with and without overcoating for evaluation. Test results were a 633 nm reflectance of 0.88 without overcoating, and 0.69 with overcoating. Further iterations may improve the low value obtained for overcoated material. Aluminized polyester with overcoating and silvered polyester with and without overcoatings were provided by Optical Coating Laboratory. The overcoated aluminized material had low reflectivity at all cone angles and was not a viable candidate as received. The overcoated silvered material had comparable reflectance to the best aluminized specimens evaluated thus far.

Accelerated simulated sunlight exposure tests were performed on selected specimens. The purpose of this testing was to evaluate resistance of protective coatings to UV. The testing was quite severe because of the spectral mismatch between the simulator and real sunlight in wavelengths of high sensitivity for polyesters. No attempt was made to relate exposure time under the simulator with equivalent real time under sunlight. The samples submitted for test did not generally have acceptable reflectivities, but were exposed primarily to evaluate the coatings.

Generally, the reflectances remained constant, while the mechanical properties dropped with exposure. The tests revealed no optical degradation of the metalized surface, but did substantiate the need for substrate protection from the ultraviolet.

Based upon the initial and accelerated UV data, samples of National Metalizing and OCLI overcoated materials were selected for real time and accelerated exposure testing in the desert. Although the Dunmore material reflectivity was lower than desired, its survival to the accelerated UV test exposure was good. All samples have been enclosed in weatherable polyester "bags" to simulate the protection they would receive in a protective enclosure. The bag material used was Martin Processing weatherable polyester (Melinex "O").

At the time of this report, data was not yet available from the desert testing. Based upon initial test results, accelerated UV tests and material availability, the reflective film product offered by National Metalizing would be favored for near-term hardware applications.

The 3M Company has recently announced an aluminized polyester film having an acrylic overcoating (product number YS-91). This product has shown promise in real time and accelerated testing and will soon be evaluated by BEC. It is available in both roll widths of 52 in. and tape widths. The later product, called Front Side Seaming Tape, is made with a high shear contact adhesive and is a candidate material for the reflector gore seams.

3.5.1.2 Rear Plastic Film Vacuum Membrane

The rear vacuum membrane would be fabricated from polyester film; UV protection would be provided by either UV stabilization similar to the reflector or by surface cladding with UV screening material. The membrane shape needs to be approximately spherical to minimize film stress and will require fewer gores than the reflector lay-up.

3.5.1.3 Reflector Support Shell

The reflector support shell consists of a conical shell with roll-formed aluminum upper and lower edge rings. An aluminum faced, kraft paper honeycomb sandwich construction is used for the shell panels. Because of light loading, the sandwich faces are 0.007 in. aluminum and the core is 0.5 in. thick and is a minimum weight commercial grade product (2.3 pcf phenolic treated kraft paper, 0.375 in. cell size). The honeycomb sandwich would be bonded with low-cost one-part adhesives (such as Morton's MOR-AD 336 urethane) as are used in the recreational vehicle industry. Structural analysis of the reflector support shell was performed to determine stresses and deflections and is discussed in Section 3.6.1.

28

3.5.2 STRUCTURAL/MECHANICAL COMPONENTS

Structural/mechanical components of the concentrator are shown in Figure 3.5-1 and are described in the following sections:

- Truss beam assembly, including drive system for elevation positioning (section 3.5.2.1)
- Yoke beam assembly, including drive system for azimuth positioning (section 3.5.2.2)
- Receiver/PCU and counter weight support rings (section 3.5.2.3)
- Foundation (section 3.5.2.4)
- Electrical/piping interface skid (section 3.5.2.5)

3.5.2.1 TRUSS BEAM ASSEMBLY

The truss beam assembly shown in Figure 3.5.2.1-1 provides structural support and elevation positioning for the receiver/PCU, counter weight and reflector assembly.

Truss beams are open web equilateral triangle structures with chords of 3/4 in. o. d. tubing and continuous cross bracing. Cross bracing is 1/2 in. o.d. tubing electrically welded to the chord members. The truss beams are fabricated in sections for ease of handling and employ, a double bolted joint for joining sections on site. Figure 3.5.2.1-2 shows a cross section of truss beam and a truss joint.

End plates with welded on end stubs and double bolted joints are used to join the truss beams that make up the truss beam assembly. Figure 3.5.2.1-3 shows the interface of the truss beam assembly with the yoke box beam. 1 1/2 in. o.d. hollow shafts are welded into the truss beam assemoly and plates and are supported by Morse SF series ball bearings. The bearings are sized to support the radial and thrust loads imposed by the truss beam assembly and are fully self-aligning. Elevation drive for the truss beam assembly is provided at one shaft by a Superior Electric Mo 93 stepping motor and Morse 266 speed reducer mounted on the yoke box beam as shown in Figure 3.5.2.1-3. A precision rotary potentiometer

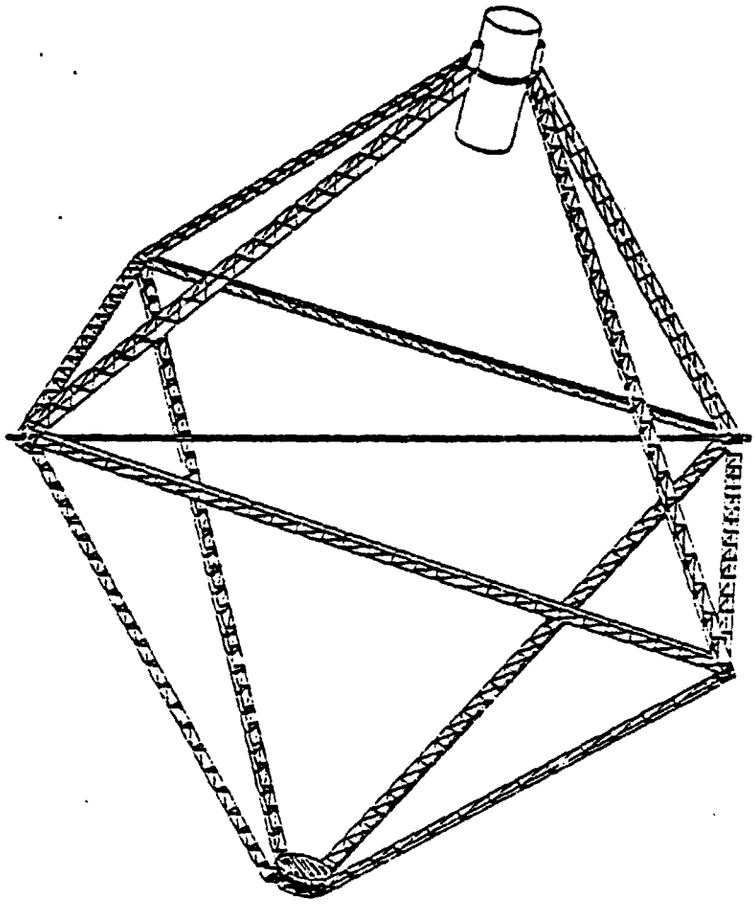

Figure 3.5.2 1-1. Truss Beam Assembly

is connected to the other shaft to provide positioning feedback to the elevation control system. A 3/16 in. aircraft cable between the two shafts prevents lateral spreading of the truss beam assembly at the bearing points.

PCU supply/exhaust air pipes and instrumentation/power cables are attached to and supported by the truss beam structure.

3.5.2.2 YOKE BEAM ASSEMBLY

The yoke beam assembly provides structural support and azimuth positioning for the truss beam assembly.

30

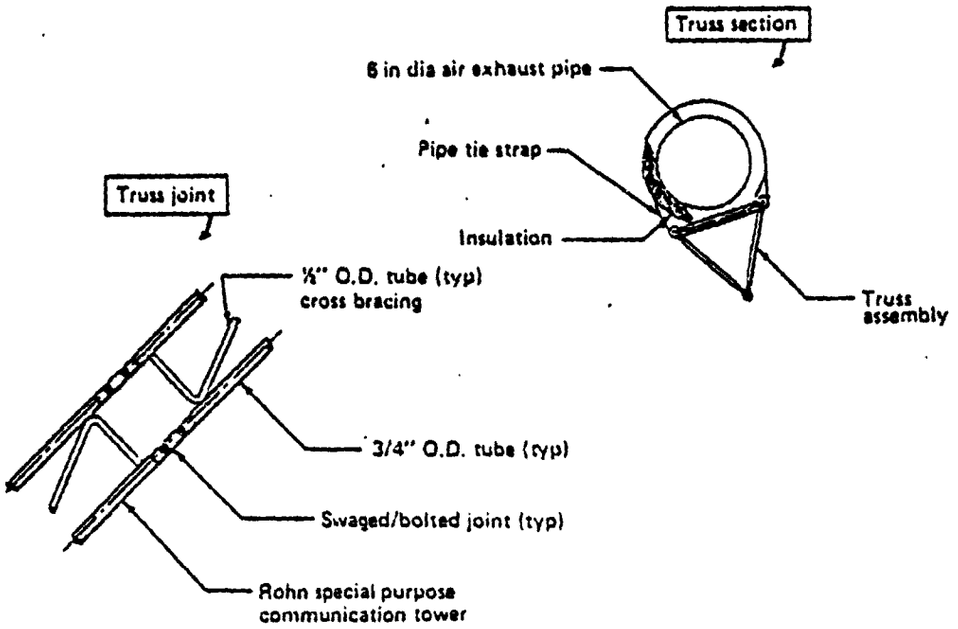

Figure 3.5.2.1-2. Truss Details

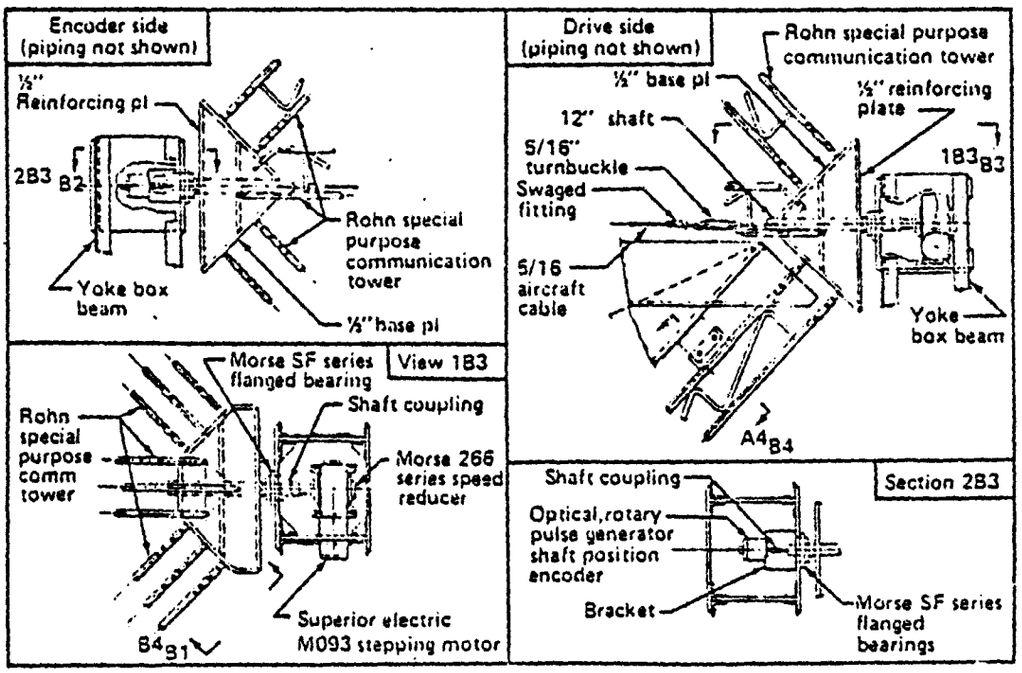

Figure 3.5.2.1-3. Truss Bearing & Elevation Drive

Yoke beams are open web box beam structures with chords of 1 1/4 in. equal leg angles joined together by continuous 1/2 in solid rod Z cross bracing on top and bottom and 1/2 in. solid rod V cross bracing on the sides. The cross bracing is electrically welded to the chord angles. The yoke beam assembly is 10 in. x 14 in. at the bottom bearing point tapering to 10 in. x 10 in. at the interface with the truss beam assembly. Yoke beams are fabricated in sections and joined together on site with a bolted splice plate as shown in Figure 3.5.2.2-1.

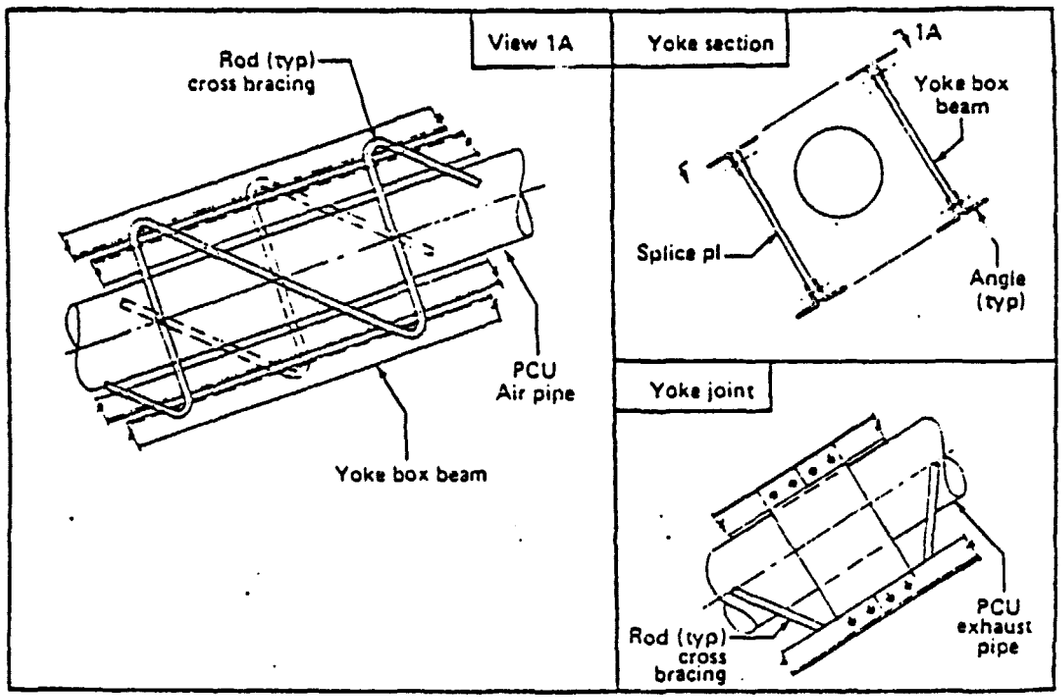

ORIGINAL PAGE IS
OF POOR QUALITY

Figure 3.5.2.2-1. Yoke Details

The yoke beam assembly is supported on a Keene K series turntable bearing sized for the thrust and moment loads imposed by the yoke. The yoke beam assembly is secured to the inner race of the bearing which is free to rotate. The outer bearing race is fixed to the concrete foundation by anchor bolts. Azimuth positioning is accomplished through a stepping motor/gear reducer mounted in the yoke structure as shown in Figure 3.5.2.2-2. The gear reducer spur gear engages exterior gear teeth in

32

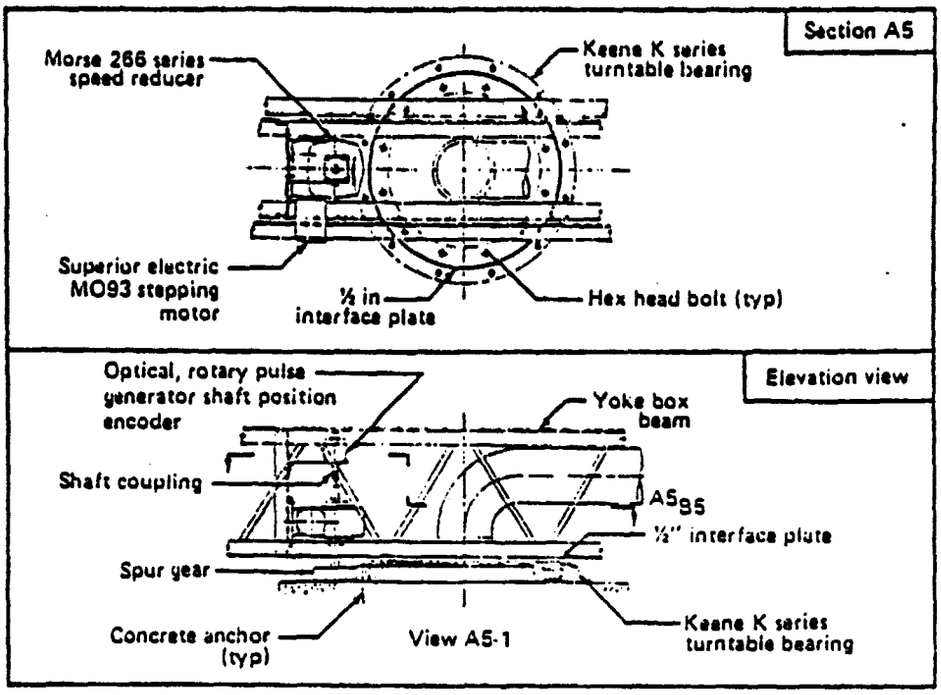

Figure 3.5.2.2-2. Yoke Bearing & Azimuth Drive

the outer bearing race providing the driving force for positioning. A precision rotary potentionmeter is connected to the gear reducer shaft to provide positioning feedback to the azimuth control system.

PCU supply/exhaust air pipes and instrumentation/power cables are attached to and supported by the yoke beam structure.

3.5.2.3 RECEIVER/PCU SUPPORT RING

The receiver/PCU support ring provides the interface between the receiver/PCU and the truss. The support ring is a C6 x 10.5 channel formed to an inside diameter of 32 inches with the flange pointing out. The support ring is joined to the truss beam assembly by a bolted joint as shown in Figure 3.5.2.3-1.

A similar support ring containing a concrete weight is attached to the opposite side of the truss beam to counter balance the receiver/PCU.

33

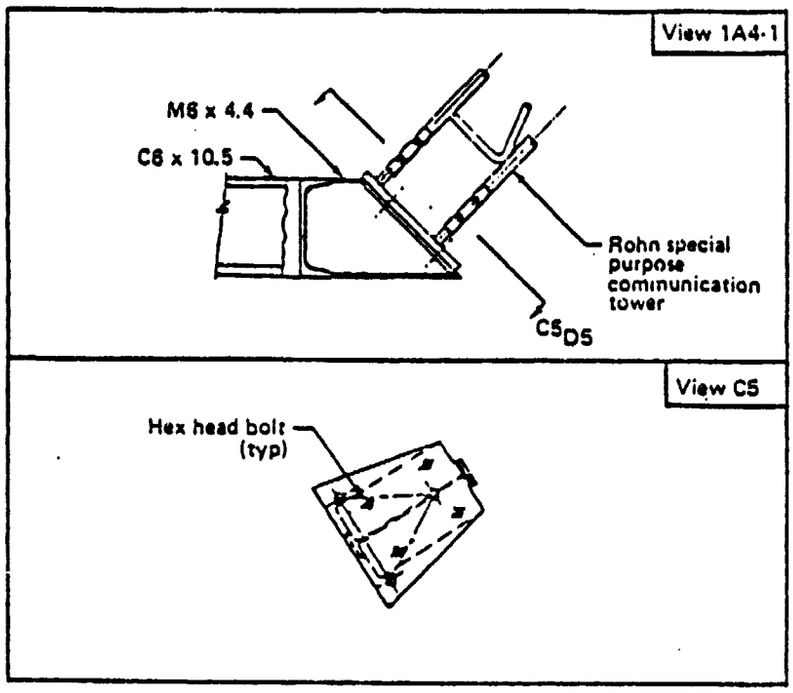

Figure 3.5.2.3-1. Receiver/PCU Support Ring

3.5.2.4 FOUNDATION

The foundation supports the yoke beam assembly, provides a structural attachment for the enclosure and anchors the enclosure against moment and uplift wind loads. The foundation is a reinforced concrete slab-on-grade 6 in thick and 29 ft. in diameter. A 1/4 x 6 in. steel ring integrated with the slab reinforcing steel is used as an outer form during concrete placement. The ring is then used as a clamping plate for the enclosure film and clamp as shown in Figure 3.5.2.4-1.

A door frame is welded to the clamping plate on the north side of the enclosure and a sheet steel door provides access to the inside of the enclosure. To prevent loss of enclosure air during ingress, provisions for attaching an air lock are incorporated into the door frame design.

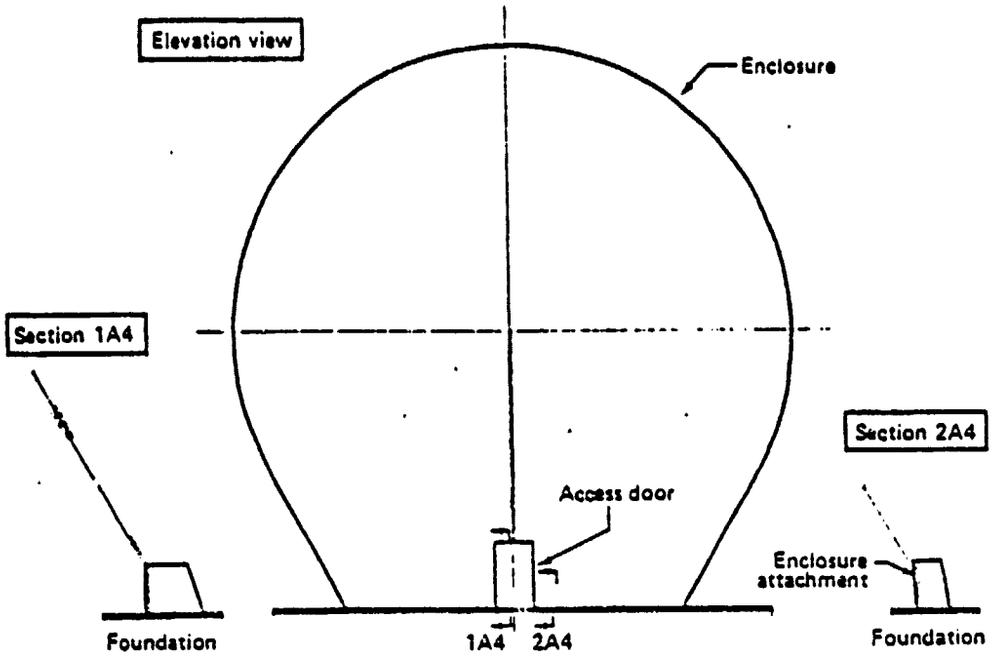

Figure 3.5.2.4-1. Foundation & Enclosure Attachment

3.5.2.5 Electrical/Piping Interface Skid

The electrical/piping interface skid shown in Figure 3.5.2.5-1 contains the enclosure air pressure system, electrical interface panels and PCU pipe terminations. The skid is located outside the enclosure for ease of access and maintenance.

A filtering system for enclosure air contains a pleated pre-filter rated at 55% efficiency and a Mine Safety Appliance final-filter rated at 99.97% efficiency. With normal atmospheric dust conditions, the filters will trap approximately 1 lb. of dirt per year. A set of louvers is located at the air intake to prevent moisture from impinging upon the filters. A power interface panel and an instrumentation interface panel are provided for termination of electrical wiring and for location of the concentrator drive controls. Provisions for remote adjustment and monitoring of control system functions are located in these panels.

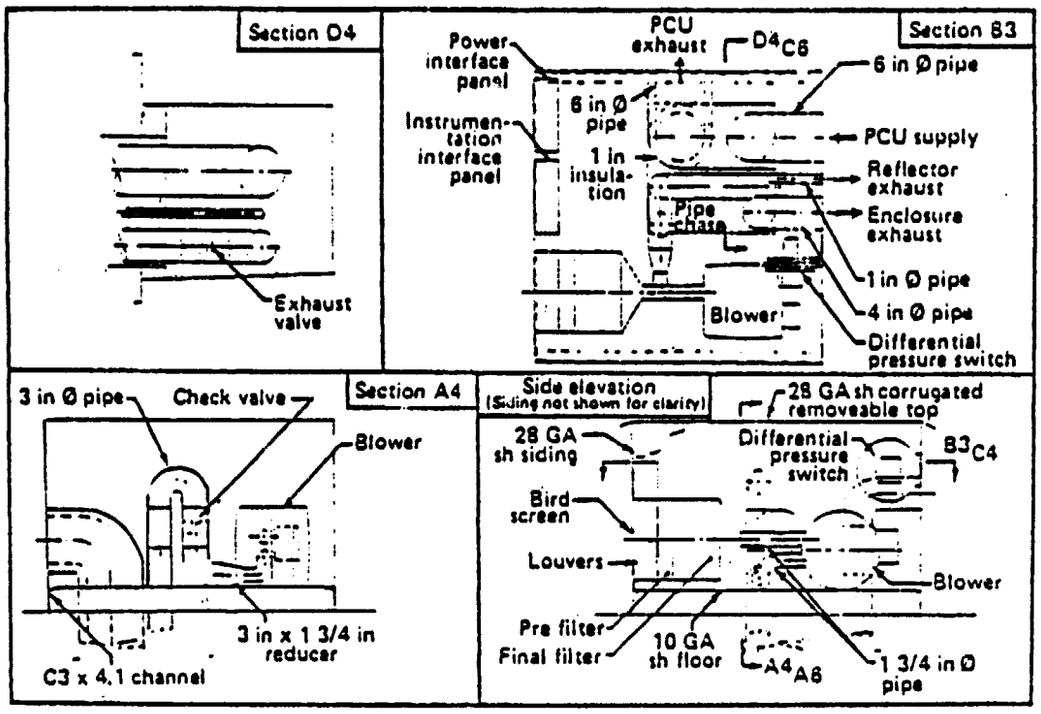

Figure 3.5.2.5-1. Electrical/Piping Interface Skid

Parasitic power comsumption of controls, drive motors and air pressurization systems are shown in Table 3.5.2.5-1. Maximum power consumption for these systems is less than 1% of the concentrator generative capacity.

Table 3.5.2.5-1 Parasitic Power

Air Blower	2.2 KWH/day
Unit Controller	Negligible
Stepper Motors (2)	0.5 KWH/day
Solenoid Valves (2)	Negligible
Total	2.7 KWH/day

36

3.5.3 Enclosure

The enclosure is designed as a spherical, pneumatically stabilized, single wall plastic film structure. The spherical shape is selected to minimize enclosure surface area and membrane loads (i.e. film thickness and cost) without restricting movement of the concentrator, as shown in Figure 3.5.3-1. Near the base of the enclosure, the shape may deviate from a true spherical shape to provide a smooth transition to the foundation perimeter.
Design of the enclosure is governed by static and dynamic pressure loads, material selection, and fabrication method (thermoformed vs. gore-formed). The following discussion treats material selection and enclosure design features; structural analysis and fabrication are discussed in Sections 3.6.1 and 6.1.4 respectively.

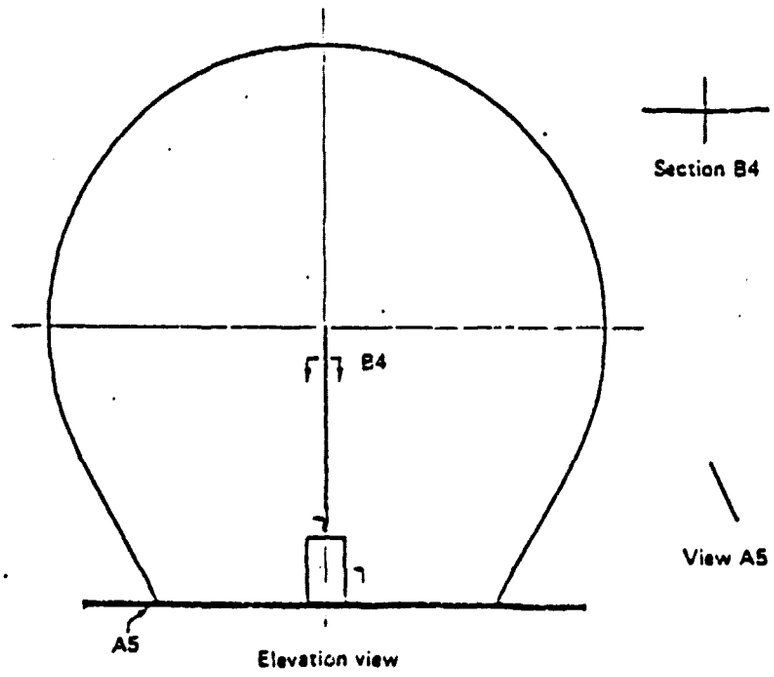

Figure 3.5.3-1. Enclosure Configuration

37

A side seam is provided on the north side of the enclosure; this is required to allow (1) removal of the enclosure from a rigid fabrication mandrel and (2) installation in the field over a completed concentrator. The seam is a hook-and-loop type for ease of field assembly; the seam would be permanently fastened in the field by heat sealing.

An access door would be installed in the field to permit subsequent maintenance operations using air locks. The door is a pre-fabricated unit made from galvanized steel. The door is secured to a light-weight steel door jamb which is attached to the enclosure. A rope-type bead at the enclosure's edge is retained by a continuous clamp at the foundation edge to anchor the enclosure.

In previous work at Boeing, a plastic film industry search was conducted for purposes of determining an optimum enclosure material in terms of specular transmittance, mechanical strength and weatherability. Fourteen companies were visited, several others were contacted by telephone. Ten companies participated by providing sample materials and data where available.

As sample materials were received, they were screen tested to determine applicability to our solar collector needs. Micro tensile coupons were cut and tested for ultimate strength, yield strength and ultimate elongation. (per ASTM D1708). Specular transmittance was measured on a Beckman DK-2A spectrophotometer with integrating sphere within an acceptance cone angle of 0.5°, as a function of wavelength from 250 to 2500 nanometers. Samples showing promise were exposed to accelerated ultra-violet (UV) radiation testing for purposes of ranking materials according to their UV stability.

Due to the lack of real time weatherability data and the inability to correlate accelerated UV test data with real UV life, selected samples were installed on racks at the Desert Sunshine Exposure Test Facility near Phoenix, Arizona to receive outdoor exposure. Samples were mounted on south facing racks, tilted at 45° and on sun tracking racks, equipped with multiple mirrors that provide 8 suns exposure (EMMA). Coupons are removed periodically and returned to the laboratory for optical and mechanical testing. At the time of this writing, 3 month and 6 month exposure data were available.

Table 3.5.3-1 shows the loss in optical and mechanical properties for the 5 candidates after 6 months on the 45° rack, which most closely simulates real time exposure, and after 6 months exposure on the EMMA. EMMA data will eventually be used to predict material life, after the acceleration factor has been determined.

Table 3.5.3-1. Optical/Mechanical Degradation – 6 Months Environmental Exposure

Material identification	6 month degradation, %							
	Real time (1 sun) ▷				Accelerated (8 suns) ▷			
	Ultimate strength	Yield strength	Elongation	Spec. trans.	Ultimate strength	Yield strength	Elongation	Spec. trans.
Kynar – Pennwalt	4	0	0	2	6	0	0	2
Tedlar – DuPont	8	4	17	3	13	2	14	6
Melinex-O – Martin Processing	28	17	56	0	72	78	90	39
Polycarbonate – Cryovac	24	10	39	6	25	7	94	52
Polyester – National Metalizing	38	9	86	0	60	100	97	35
Petra A – Allied Chemical	40	85	98	11	100	100	100	24

▷ Fixed, south facing, 45° rack

▷ Equatorial mount with mirrors for acceleration (EMMA)

Table 3.5.3-2 shows the fluorocarbons, Kynar and Tedlar, to be superior in weather resistance. Examination of the real time data reveals that while other materials may hold up well optically, the degradation in mechanical properties is more severe than the fluorocarbons. In addition, the fluorocarbons showed little or no property loss in the accelerated exposure (EMMA).

Table 3.5.3-2 Enclosure Film Candidate Evaluation

	Availability	Weatherability	Approx. expected life	Status	Joinability	Future cost $/ft²	Transmittance	Concerns
Polyesters	• ICI • Celanese • Allied Chemical • Martin • National Metalizing	Needs U/V stabilizer	5 years	Stabilizer improvement program	Thermosetting adhesive bond	$2.00	0.88	• Tear resistance • Flammability • Handleability • Stabilizer development
Polyvinylidine Fluoride	Pennwalt (Kynar)	Inherently stable in U/V	15 years	Production film stretching process development	Heat sealable	$4.00	0.91	• Production quantity availability
Laminated films	Cryovac							• Exploratory development for solar applications

If one were to simply assume an acceleration factor of 8 (8 suns for 1 year=1 sun for 8 years) the data shown in the accelerated data column would correspond to an equivalent 4 years of 1 sun exposure. Experience has shown this assumption to be invalid, however, as different materials show varying sensitivity to acceleration of exposure. The conclusions to be drawn about the last four materials in the table are that either the materials have a relatively short UV life or the acceleration factors are much larger than for fluorocarbons. It is possible that the real time degradation will level off after the large initial values observed in the first 6 months. For this reason the real time testing of all materials will continue. Accelerated testing will be continued on the fluorocarbons only, since all others have shown damage that renders them impossible to test.

Kynar, which is a polyvinylidene fluoride, shows the most promise of all materials in terms of weatherability and transmittance at this time. While its cost per pound is higher than polyesters, it is likely that its longer life will compensate. Work on polyester stabilization is still being pursued however, and testing of potential candidates will be performed as they become available.

3.5.4 PNEUMATIC SYSTEM

The pneumatic system supplies/exhausts air to maintain inflation air pressures within the enclosure and reflector cavities. Air pressure is controlled as shown in Figure 3.5.4-1 and as follows:

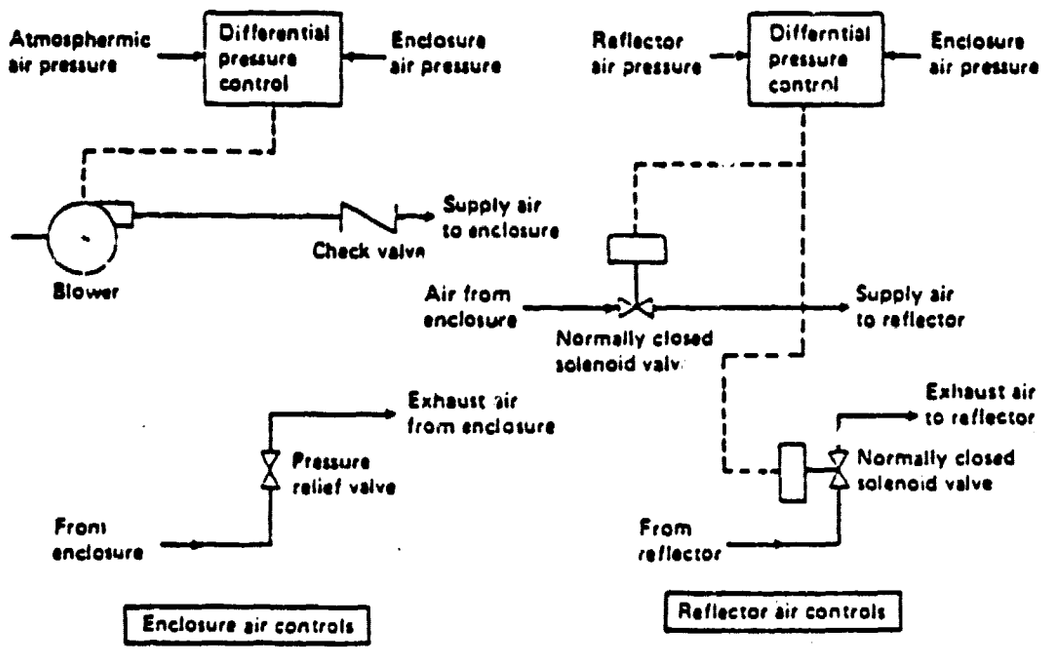

Figure 3.5.4-1. Air Pressurization Control Schematics

Enclosure Air

A Rotron spiral regenerative blower rated at 80 CFM, 10 in. of water, and 530 watts is controlled by a Dwyer differential pressure switch sensing atmospheric and enclosure air pressure. When the enclosure air pressure is below set point the pressure switch starts the blower and air is delivered to the enclosure through a pressure activated check valve. When enclosure pressure reaches set point, the blower stops. When enclosure air pressure is above set point, air is exhausted to the atmosphere by a pressure activated relief valve.

41

Reflector Air

On a call for increased pressure between the reflector cavity and the enclosure, a Dwyer differential pressure switch, sensing reflector air pressure and enclosure air pressure, opens a normally closed solenoid valve to allow air from the enclosure to pressurize the reflector cavity. On a call for decreased pressure between the reflector cavity and the enclosure, the differential pressure switch opens a normally closed solenoid valve and allows reflector air to be exhausted to the atmosphere.

3.5.5 Control System

The control system concept selected for the collector is based on microprocessor technology. A microprocessor based system lends itself well to providing a "sun tracking" capability and the expansion for controlling other components of an energy collection system. Other advantages are:

1) low power consumption
2) compact packaging
3) low production cost
4) easy modification of operational parameters
5) simple interfacing with a data aquisition system

In a typical installation, the control system's primary functions are to:

1) position the collectors toward the sun,
2) reposition the collectors and sound a warning in case of failure,
3) control the system during start-up.

Primary components of the entire sun tracking control system are identified in Figure 3.5.5-1, they are the system controller, unit controller, photosensor, servo-pots, drive motors, and interconnecting serial data busses. General control system architecture is shown in Figure 3.5.5-2 along with the respective functions of the system and unit controllers.

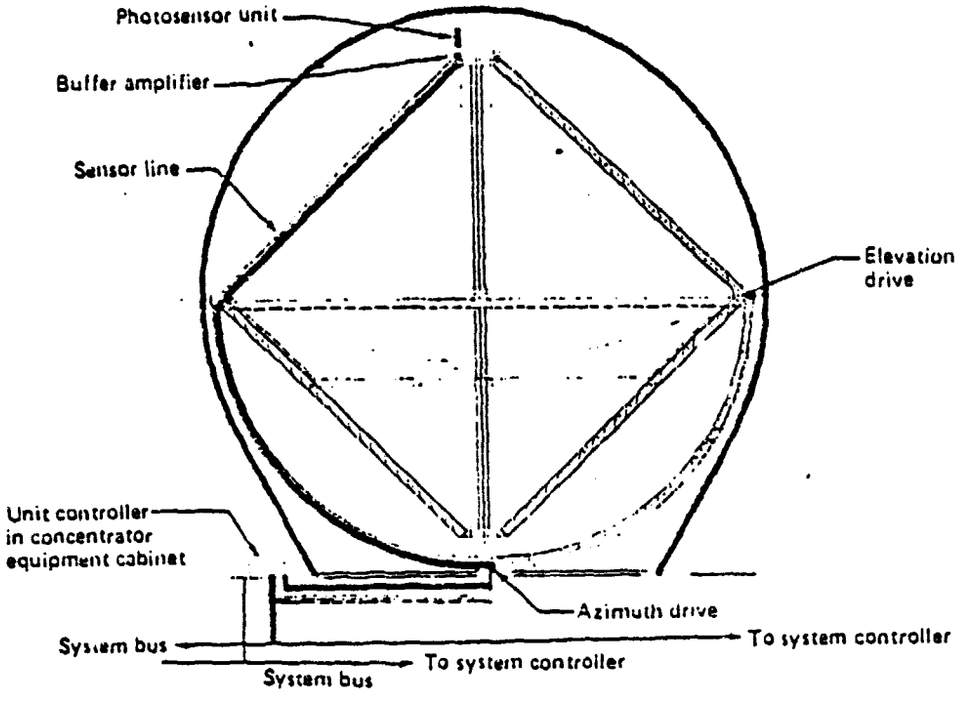

Figure 3.5.5-1. Tracking System Components

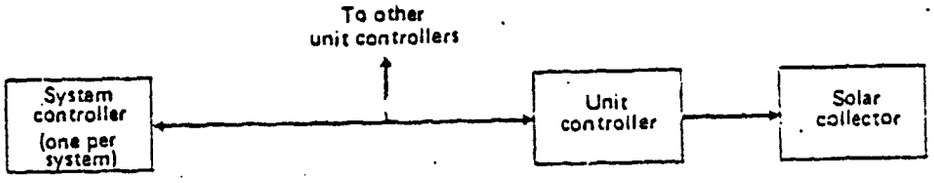

- Provide overall system monitoring, initial alignment, and fault isolation
- Uses triple-redundant processors and control logic
- Communicates over mutiple serial busses to unit controllers
- Provides interface to central power system controller
- Provides independent collector control
- Uses both photosensors and solar calculations to perform tracking
- Has two processors with some redundancy
- Has self checking capability
- Provides off-line control for alignment and maintenance

Figure 3.5.5-2. Tracking System Architecture

43

System Controller

The system controller architecture is illustrated in Figure 3.5.5-3. The architecture utilizes triple redundancy; that is, there are three independent microcomputer systems working in parallel. The outputs of the microcomputers are combined in a majority logic network before being transmitted to the unit controllers.

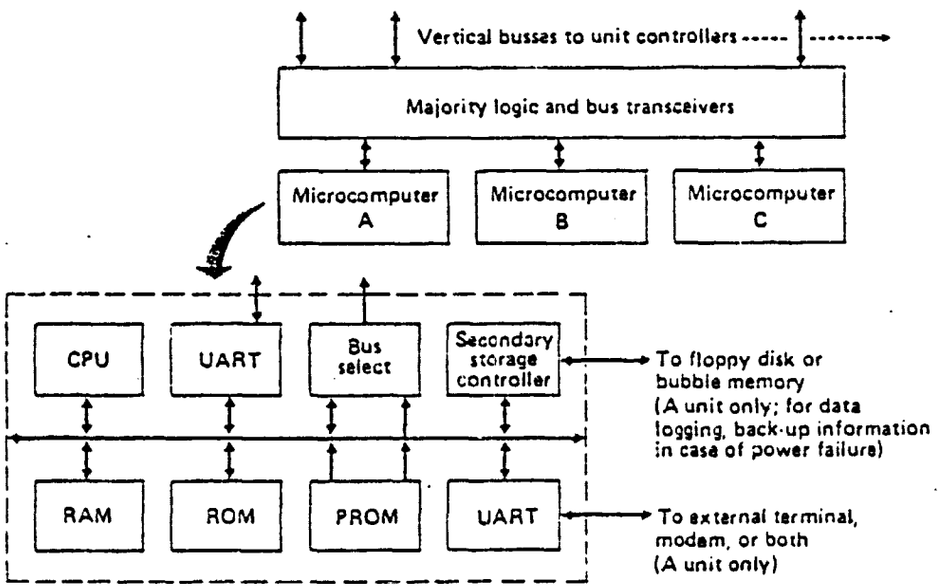

Figure 3.5.5-3. System Controller

Each microcomputer consists of a microprocessor, RAM, a serial interface (UART), ROM and PROM. The ROM holds the system control program, and the PROM holds coefficient data which can change from system to system and from year to year, such as solar ephemeris data. On one of the three microcomputers there is provision for a secondary storage device controller. The controller provides an interface to memory devices such as magnetic bubble memories or floppy disks. These devices can be used to store system parameters, fault location tables, and other system information.

There is also a serial interface on the same microcomputer board which permits connection to an on-site terminal, or to a modem, or both. The modem allows remote monitoring of the system controller from a central station via standard telephone lines.

The added cost of having the triple redundancy in the system is small when compared with the overall system cost and the cost of the possible downtime in a system without redundancy. The cost of one of the redundant microcomputers is expected to be approximately $500, with the total system controller cost (including a disk, terminal and other electronics) being $5,000. A less sophisticated system controller (without data storage) is estimated to have a distributed unit cost of $50 for a field of 50 concentrators.

Unit Controller

The unit controller (Figure 3.5.5-4) provides detailed control of each individual collector. Specifically, the unit controller functions are:

a) Track the sun using photosensors
b) Calculate the sun position using solar equations
c) Position the collector via azimuth and elevation stepping motors (2-axis controls)
d) Monitor possible fault conditions at the collector, such as overheating
e) Communicate with the system controller

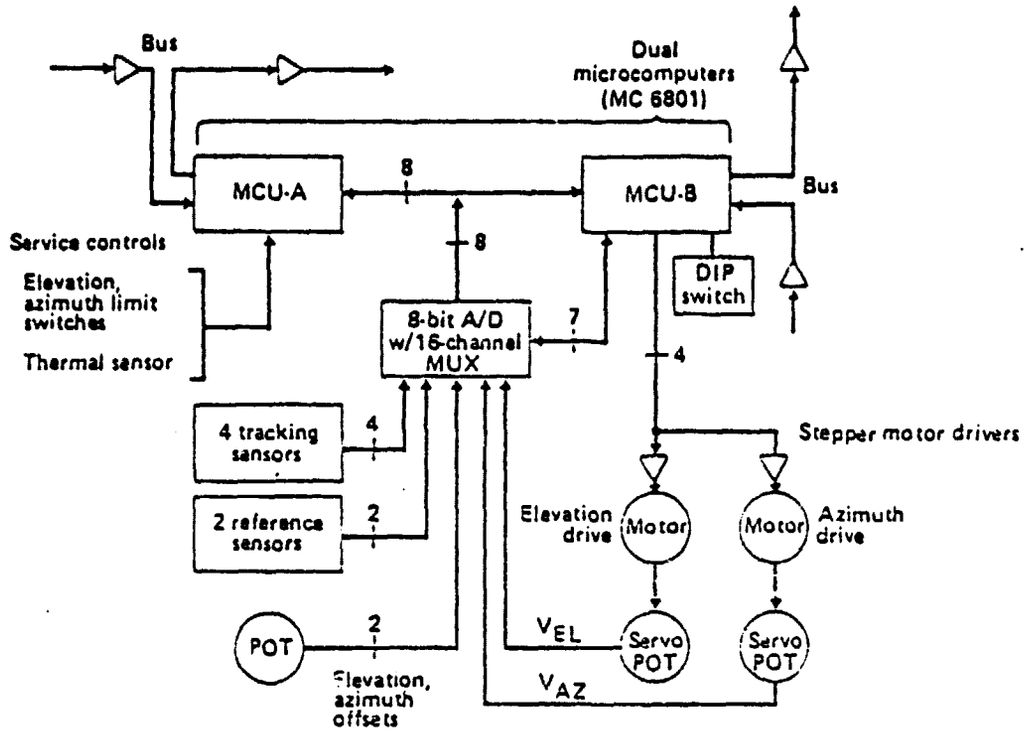

Figure 3.5.5-4. 2-Axis Unit Controller

Physically the unit controller consists of two single-chip microcomputers and associated peripheral circuitry. Each microcomputer is a Motorola 6801 and includes 2K bytes of ROM, 128 bytes of RAM, a timer, a serial interface, and an 8-bit processor. The 6801 processor executes the same instructions (with several additional ones) as the Motorola 6800. Hence, it could use much of the same software already developed on existing 6800-based Motorola sun-tracking system.

The rational for using two microcomputers rather than one was that the 2K of ROM available on one microcomputer is thought to be insufficient for the total control task. As a comparison, the current Motorola sun tracker uses 3.5K of memory for these tasks, plus a mathematical function chip. Hence, it is felt that two 6801 microcomputers providing 4K total of ROM and an enhanced instruction set will be sufficient for the job. Additionally the use of two microcomputers allows two completely redundant serial interfaces (to x and y busses) and improved capability for built-in checking and fault-tolerance.

46

One of the microcomputers, MCU-A, is tasked with providing a calculated position of the sun based on the time of day and information undates from the system controller. It also accepts switch inputs from the collector, including azimuth and elevation limit switches and a thermal overheat switch. In addition there are six switches which select the device address for the unit controller, and two push button switches for manually operating the azimuth and elevation motors.

The other microcomputer, MCU-B, is tasked with positioning the stepper motors and inputting data from an 8-bit analog-to-digital (A/D) converter. The A/D converter has 16-channels, with 10 being used, and accepts analog signals for azimuth and elevation potentiometers, and from photosensors. The offset potentiometers allow for compensation for the imperfect positioning of the photosensor unit. Two pairs of photosensors are used to track the sun with angular errors less than 2 mrad as discussed later.

System and Unit Controller Fabrication

As indicated in Figure 3.5.5-5, the controllers would be rugged single board computers assemblies. Both the unit and system controller can be fabricated using standard double-sided printed circuit (PC) boards. For the unit controller, all the electronics except for a power transformer can be mounted on a single PC board. Holding approximately 20 integrated circuits and miscellaneous discrete components, the board should require approximately 50 square inches of area. For a production quantity of 10,000 or more units over a several-year period, mass production techniques, such as Ragen semi-automatic assembly, can be used in the fabrication process. This will help keep the cost/unit extremely low for the unit controllers. As part of the automated controller fabrication process, circuit burn-in and computer-aided check-out would be performed prior to chassis packaging.

47

- Unit and system controllers are rugged single board computers
- Automated manufacturing processes
  - PC boards are double sided and gang-drilled by N/C
  - Rayen equipment used for parts installation
- Unit controller costs

Parts	$140
No of PCB pins	400
Total fab cost	$228 @ 10,000 units

- Distributed system controller cost – $50/concentrator

Figure 3.5.5-5. Controller Fabrication/Costs

The system controller can be fabricated as three identical PC boards and a mother PC board holding the majority logic and bus transceivers. Each of the three identical microcomputer boards can be fabricated using identical assembly steps. The microcomputer board with the additional electronics (secondary storage controller and spare serial interface) can be fabricated using additional steps. These steps assemble the extra electronics into board positions that are de-populated on the other two boards. With this technique, the number of identical units is essentially increased and the cost is lowered.

Costs for the unit controller were estimated by pricing a preliminary parts list having a total of 75 discrete components. The discrete component cost including chassis is $140; an estimate for total assembled board cost for a 10,000 production run is $228. As mentioned previously, an estimated distributed system controller cost for a typical field is $50/concentrator.

48

System Bus Organization

The system bus organization is depicted in Figure 3.5.5-6. The individual unit controllers would be connected to this network to receive sun tracking position coefficients, as needed for the solar position equations programmed in the unit controller. Also, the system bus would distribute sun tracking position information needed for checking the unit controller computations. Specific unit controllers could be addressed by the system controller to remotely monitor individual unit controller functioning or isolate faults. An orthogonal bus organization provides redundancy in case of breaks in the system bus; in this scheme, each unit controller relays bus information in a daisy-train manner.

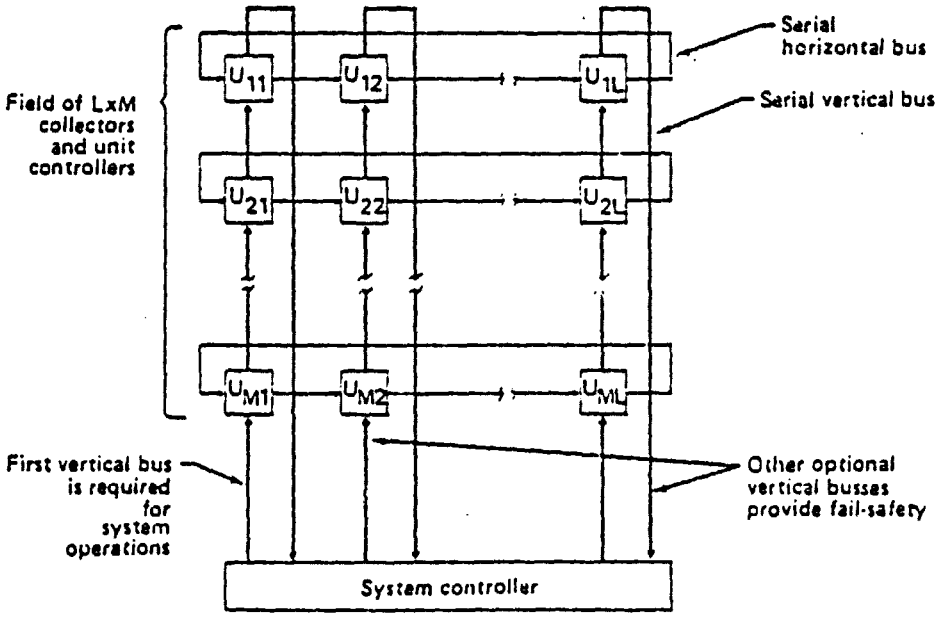

Figure 3.5.5-6. Two-Dimensional Bus Scheme

49

Photosensor Tracking Unit

The photosensor tracking unit consists of a shadow box, two pairs of tracking linear photosensors and two reference photosensor cells. This unit is illustrated in Figure 3.5.5-7 and is patterned after a photosensor tracker developed by Motorola for Sandia Laboratories. The pairs of linear photosensors are used for elevation and azimuth tracking in a closed-loop interface with the unit controller. Two reference photosensors are used in an automatic daily calibration procedure involving programmed elevation and azimuth sweeps. The outputs from the reference photosensors are used to compute numerical software corrections for the tracking photosensor that compensate for sensor aging and temperature effects. With their photosensor unit and self-calibrating software procedure, Motorola has achieved pointing accuracy of ± 7 mrad with a shadow box depth of 7 in.; a shadow box depth of 15 in. is shown in Figure 3.5.5-7 which will offer increased accuracy.

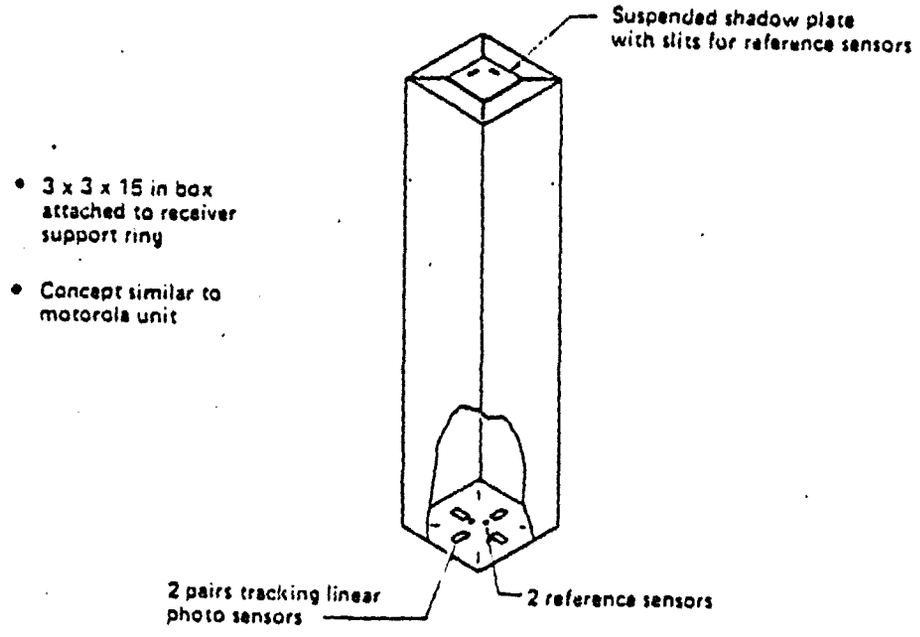

Figure 3.5.5-7. Photosensor Unit

50

Drive Component Features

Table 3.5.5-1 shows the drive component features. It is assumed that slewing need only be done by elevation drives which must accelerate the receiver to a slew rate of 1/2°/sec (JPL requirement) in a distance of 4.5 inches. For this slew condition, a torque of 1013 in. lbs. is required based on rotational mass inertia derived from a finite element ANSYS computer model (see Section 3.6.1).

Table 3.5.5-1. Drive Component Features

	Elevation	Azimuth
Slew rate	½°/sec	
Tracking rate	15°/hr (max)	15°/hr (max)
Inertia	6.332×10^5 in-lb-sec^2	7×10^5 in/lb sec^2
Output torque required	1,013 in-lb	20 in-lb
Stepper motor type	18.75 in-lb 1.8°/step	5 in-lb. 72°/step
Speed reducer type	70:1	20:1

Stepper motors were selected for the drive system because of the following reasons (for example, see Ref. 6):

- o Direct interface with unit controller
- o Provides braking
- o No brushes
- o Competitive cost

The speed reducers have two functions; one of which is to provide enough output torque and the second one is to reduce the angle per step for accurate tracking. Worm gear speed reduces are specified because of their good life, smooth operation, low maintenance requirements and low cost.

51

Non-Normal Tracking Conditions

Possible non-normal tracking conditions are listed in Table 3.5.5-2. The responses to these conditions can be activated by commands sent out by the system controller.

Table 3.5.5-2. Non-Normal Tracking Conditions

Event	Automatic remedial actions to prevent enclosure overheating
Loss of drive power	Pneumatically de-focus reflector with standby power
	De-track with stand-by power (or manual method)
Control system pointing error	De-focus
	De-track
Return-to-service	Re-track
	Re-focus
Brayton unit overheating	De-track per thermal sensor signal to unit controller

52

3.6 Design Analysis

Preliminary design analyses were performed to verify structural adequacy and to determine air flow rates needed to maintain enclosure pressurization. These analyses found the concentrator design to have ample strength margins and low gravity-induced deflections. Several computer models were developed which will be useful for design optimization in the subsequent detail design phase.

3.6.1 Structural Analysis

The structural analyses investigated the major structural components which are categorized as:

Enclosure
Truss
Yoke
Reflector film
Reflector Support Shell
Foundation

3.6.1.1 Enclosure

The enclosure design thickness is governed by combined inflation and wind induced pressure loads. As indicated in Figure 3.6.1.1-1, snow and hail loads are not governing design conditions according to experimental data from previous heliostat enclosure development programs. Inflation pressure is set at a level that prevents enclosure buckling due to wind-induced positive local pressures. This pressure level and the wind-induced local negative pressures superimpose to produce local film loads which determine the enclosure design thickness.

- Internal pressure
  - Combines with most other load conditions
  - Minimum to limit inward deflections or collapse
- Wind
  - Critical design condition
  - Loads based on wind tunnel tests
- Snow
  - Load less than 3/4 P_i to limit deflection
  - Not critical for southwest USA
- Hail
  - Evaluation based on tests with 1 inch iceballs
  - Candidate films withstand southwest USA hail

Figure 3.6.1.1-1. Enclosure Strucutral Analysis Loading Conditions

Analysis of the wind-induced pressures is based on wind tunnel test data. In a previous heliostat enclosure development project, over 140 wind tunnel tests were performed to establish a design nomograph which appears in Figure 3.6.1.1-2. These tests involved various boundary protection conditions, enclosure base shapes, and field arrangements. Using this data, the enclosure design, with a diameter of 48 ft. and assuming a base skirt, has an internal pressure requirement of 0.15 psi and a maximum film membrane load of 105 lb/in. due to combined internal and wind-induced negative local pressure. At this enclosure diameter, the single enclosure and most critical interior field enclosure position cases give equivalent film loads. The maximum film load occurs near the top of the enclosure as shown in Figure 3.6.1.1-3. Integration of the pressure loads gives slightly lower loads at the enclosure base.

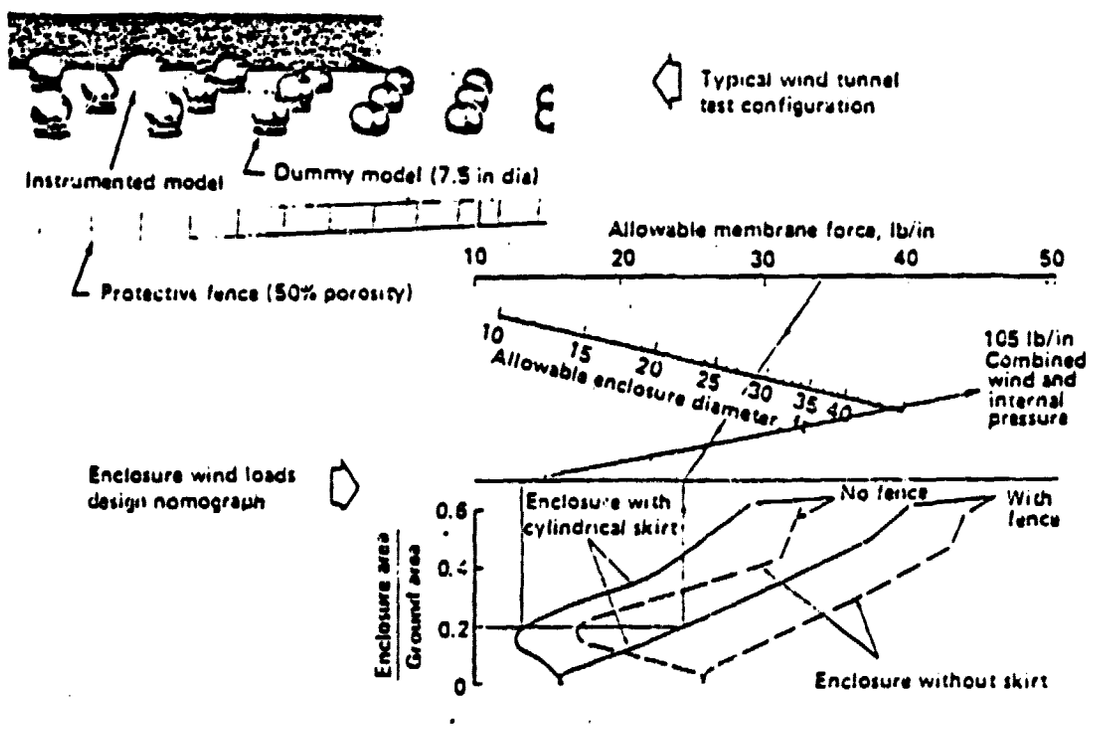

Figure 3.6.1.1-2 Enclosure Wind Loads

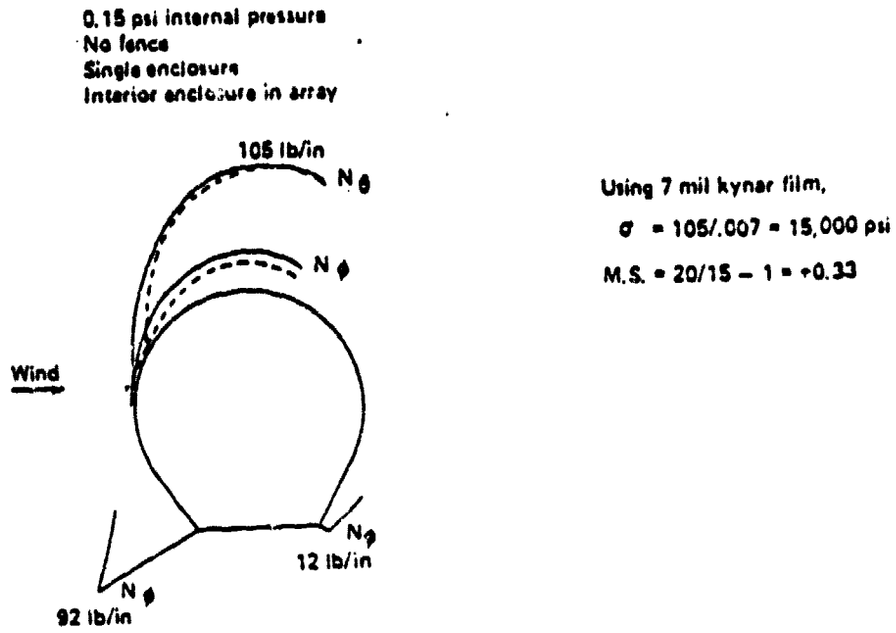

Figure 3.6.1.1-3. Enclosure Film Stresses Combined Wind and Internal Pressure

BEC test data for Kynar film are shown in Figure 3.6.1.1-4. For an allowable ultimate design stress of 20,000 psi, the resulting margin of safety for a Kynar enclosure with a 7 mil thickness is:

$$\sigma = \frac{105}{0.007} = 15{,}000 \text{ psi}$$

$$MS = \frac{20{,}000}{15{,}000} - 1 = +0.33$$

A characteristic of biaxially-oriented Kynar is that it has a low "yield" point and considerable work hardening (non-linear stress-strain curve). The nominal film stress due to internal pressure alone is well within linear behavior. At high wind loadings, the enclosures will develop a limited amount of local permanent strain which is not believed to be detrimental to enclosure performance.

56

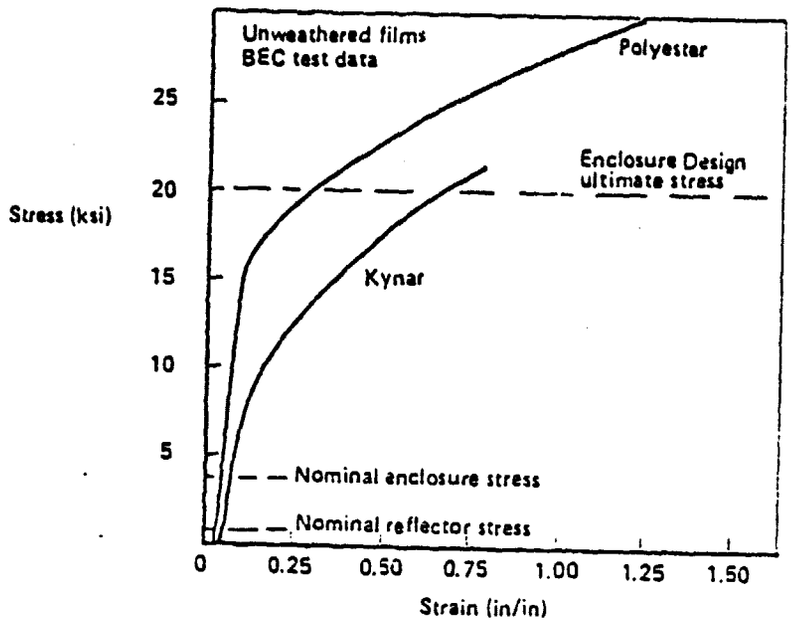

Figure 3.6.1.1-4. Typical Stress-Strain Properties

3.6.1.2 Foundation

The foundation design requirements are to anchor the enclosure and provide a stable footing for the yoke azimuth bearing with a low construction cost. The governing design requirement is enclosure anchoring under the 100 mph design wind load conditions. Because of the light weight of the concentrator, the loads on the foundation in the yoke bearing area are low.

67

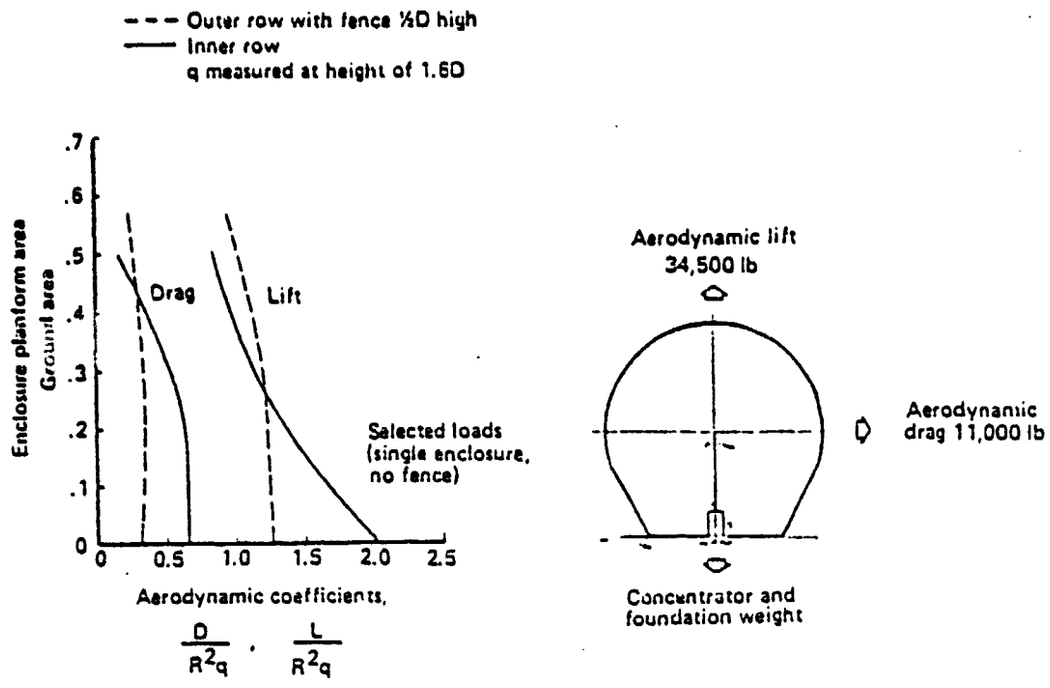

Figure 3.6.1.2-1. Foundation Loads

Enclosure loads transferred to the foundation were determined by integration of the local internal and wind-induced pressures which are based on wind tunnel test data. The resultant lift and drag forces for the enclosure design are shown in Figure 3.6.1.2-1. Based on these forces, three foundation concepts were sized, as illustrated in Figure 3.6.1.2-2, to give ample margin against soil bearing failure and overturning. The slab foundation is the preferred design and requires the least amount of reinforced concrete of the gravity foundation concepts; this advantage is a result of internal pressure acting on the slab to reduce foundation uplift loads. Estimates of the respective in-place foundation costs are given in Table 3.6.1.2-1. The slab foundation cost of $868 is used in the cost analysis discussed in Section 6.4.

58

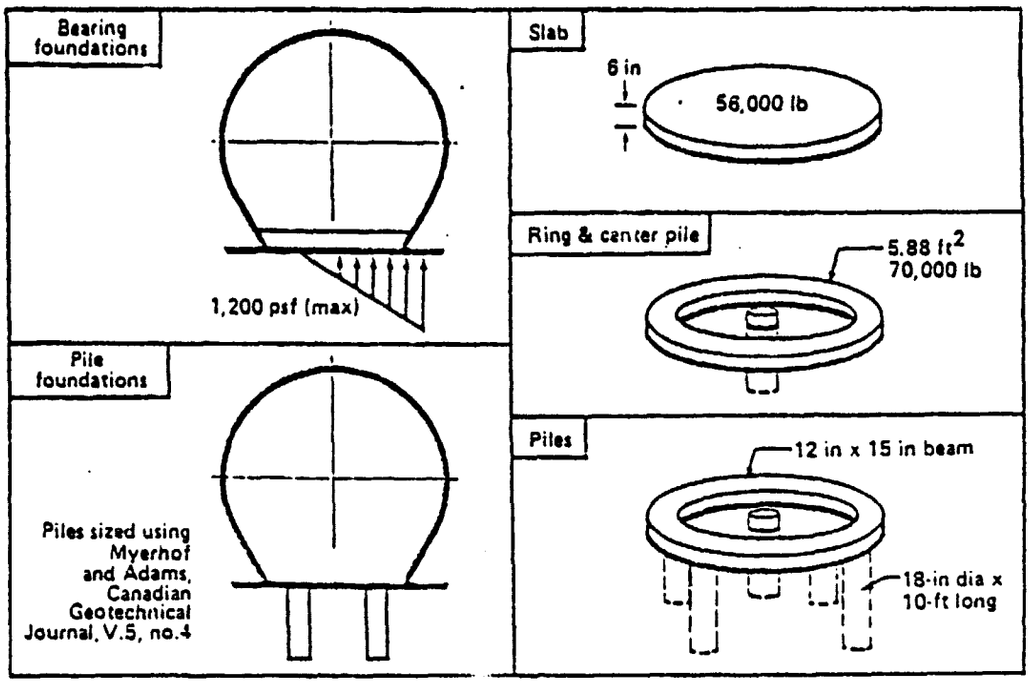

Figure 3.6.1.2-2. Candidate Foundation Sizing

Table 3.6.1.2-1. Foundation Estimated Costs

Foundation type	Cost basis	Estimated cost
Slab	$71/CY less edge forms	$ 868
(Edge form left in place for enclosure attachment)		
Ring	Ring at $170/CY Concentrator support pile @ $11/ft x 10 ft + $95 setup	3,577
Pile	5 piles at $11/ft + $95 setup Ring at $140/CY	1,235

- Ring and pile foundations require enclosure attach provisions and ground seal
- Slab foundation design selected

3.6.1.3 Truss Loads and Reflections

The truss structure functions to support the reflector assembly, Brayton engine/receiver, Brayton system lines, control system components and counterweight. Because of the importance to low cost of minimizing structural weight (a pound saved is 75¢ earned!) while maintaining accurate receiver/reflector alignment, truss loads and deflections were analyzed to verify that the preliminary lightweight truss design was satisfactory.

The finite element model shown in Figure 3.6.1.3-1 was analyzed with the ANSYS code to compute loads and deflections. This model represents a generalized truss and yoke design which furnished the data needed for structural design iterations. Features of the model include rigid joints, 3-D general beam elements, 8 inch eccentricity between the elevation bearing truss point and the yoke neutral axis, and symmetry about the x-z plane. Properties of the elements are given in Table 3.6.1.3-1. The element weights shown correspond to a "half" model. For simplicity, the lattice strut members were modeled with effective axial areas which correspond to the weights shown; the miscellaneous weights include allowances for lattice web parts.

60

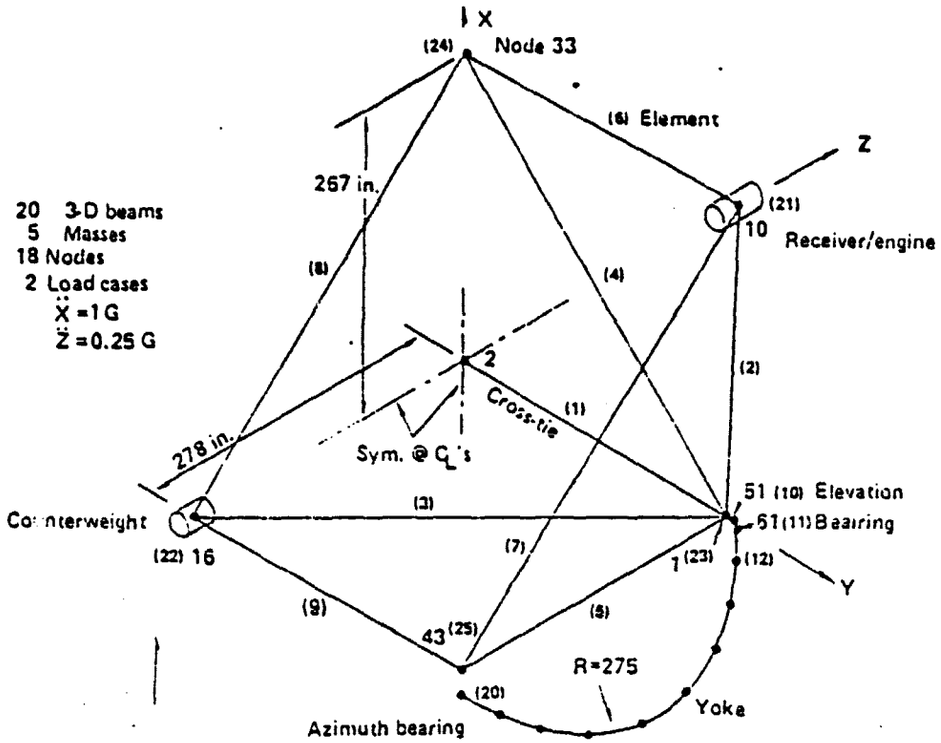

Figure 3.6.1.3-1. ANSYS Half-Concentrator Model

61

Table 3.6.1.3-1. Finite Element Model Properties

Element ID	Part	Weight each LBs.	Area (A) IN^2	Moment of Inertia (I) IN^4	Torsional Property (J) IN^4
1	Rod	40	0.5	-	-
2 to 5	Beam	98	0.5	2.73	1.5
6 to 9	Beam	29	0.25	1.37	0.5
10 to 11	Rigid Links	0	-	-	-
12 to 17	Upper Yoke Beam	44	1.5	58.4	70
17 to 20	Yoke Center Beam	22	1.5	119.4	137.2
21	Brayton Unit	500	-	-	-
22	Counterweight	500	-	-	-
23	Reflector Assembly + misc. wt.	400	-	-	-
24 to 25	Reflector Assembly + misc. wt.	200	-	-	-

Selected load and deflection results from the finite element analysis are given in Figure 3.6.1.3-2. The effective tracking error of 0.37 mrad shown is due to a computed lateral deflection of 0.07 inches for the worst case concentrator orientations for gravity loading. This deflection-related error does not include effects of joint flexibilities and member sag which will be modeled in the subsequent detail design phase.

The maximum truss member load for combined 1 g vertical and 0.25 horizontal (siesmic) accelerations is 1585 lb. in element 4 (see Figure 3.6.1.3-1). This member was checked for Euler buckling and local chord crippling and was found to have a margin-of-safety governed by Euler buckling. For a triangular design lattice strut section having an effective area of 0.339 $in.^2$ and side width of 6.92 in., the margin-of-safety for Euler buckling is:

$$I = 2.73\ in^4$$
$$L = 381\ in$$
$$P_{CR} = \pi^2 EI/L^2 = 5568\ LB$$
$$M.S. = 5577/1585 - 1 = 2.52 >> 0.$$

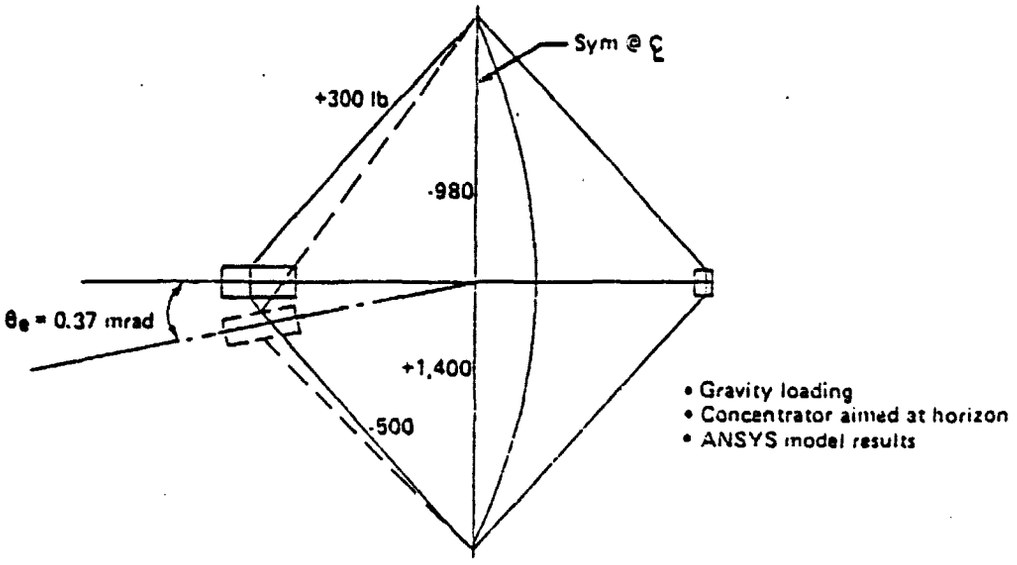

Figure 3.6.1.3-2. Truss Loads and Deflections

3.6.1.4 Yoke Loads and Reflections

Yoke moment loads computed with the finite element model are shown in Figure 3.6.1.4-1. The yoke moments were found to be effectively reduced by the presence of the crosstie (element 1 in Figure 3.6.1.3-1). For a yoke box section varying in depth from 10 in. at the ends to 14 in. at the center and with a constant effective axial area of 2.70 in^2, the critical section is on the yoke arm at the maximum positive moment location. The resulting margin-of-safety with respect to a chord yield strength of 36,000 psi is ample:

$$I = 58.36 \text{ in}^4$$

$$M = +142472 \text{ in lb}$$

$$\sigma = \frac{MC}{I} = \frac{142472\ (5)}{58.36} = 24412 \text{ lb/in}^2$$

$$M.S. = \frac{36000}{24412} - 1 = +0.47$$

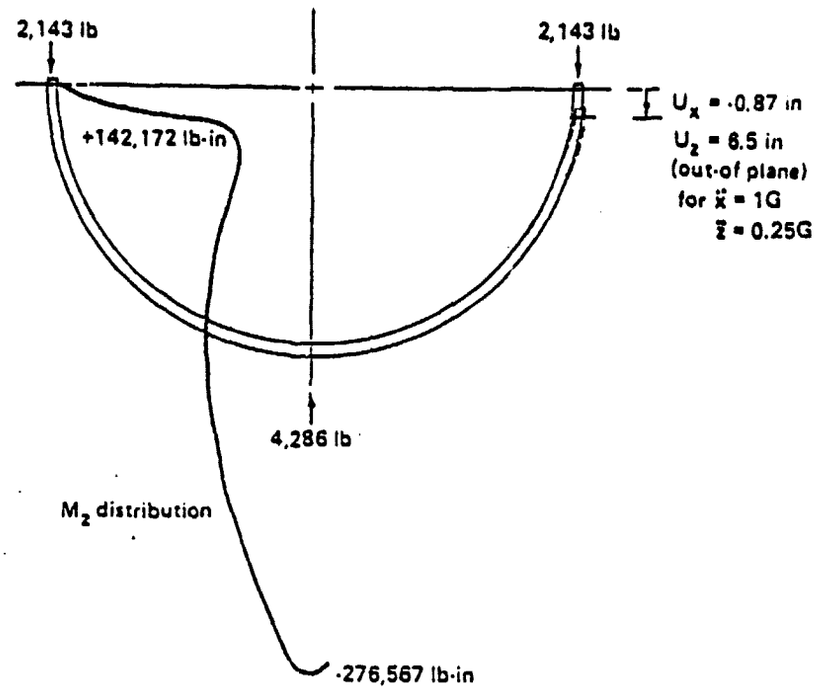

Figure 3.6.1.4-1. Yoke Loads and Deflections

Local buckling of the yoke chords and web bracing are not critical failure modes for the vertical or horizontal load conditions. Under the lateral seismic load condition of 0.25 g, the Brayton unit will deflect 4.4 inches towards the enclosure; this deflection is allowable and is primarily due to torsional flexibility of the yoke. Vertical yoke deflection for gravity loading is 1.77 in. which is acceptable. (Both yoke loads and deflections would be significantly reduced if outrigger supports were added to the design).

64

3.6.1.5 Reflector Shell Analysis

A preliminary structural analysis of the reflector support shell was performed considering film loads, pressure loads and gravity for an upward reflector orientation. This analysis was done using the STAGS-C Computer code and a 5 row by 11 column shell quadrant model illustrated in Figure 3.6.1.5-1. Radial and vertical deflection results from this model are plotted in Figure 3.6.1.5-2; these deflections are very small and are not expected to significantly degrade reflector surface quality. In a subsequent detailed design phase, the ultra-light reflector shell model will be refined to include other tracking orientations and deflecting truss mounting points.

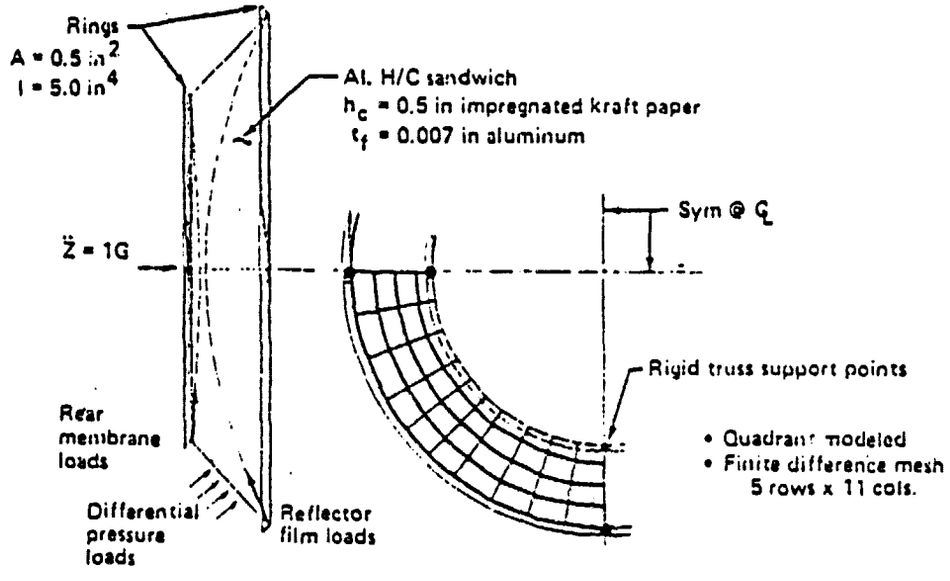

Figure 3.6.1.5-1. Stags-C Model for Gravity-Included Deflections

The maximum shell loads obtained from the STAGS-C model are in the lower edge ring mid-way between the truss support points. The resulting sandwich face stress is 996 psi which is satisfactory. The ring load at this location is 498 lb., which results in a margin-of-safety of +0.27 with respect to local ring flange crippling.

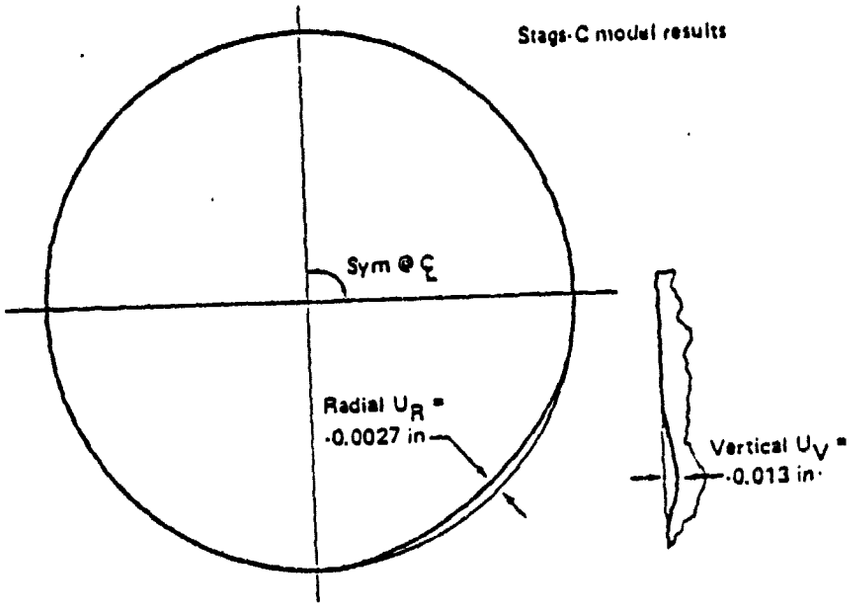

Figure 3.6.1.5-2. Reflector Support Shell Deflections

3.6.1.6 Reflector Film Stress

The reflector film is stabilized with a nominal differential pressure of 0.0037 psi. At this pressure, the maximum film stresses occur at the perimeter:

σ_θ = 609 psi (radial direction)

σ_ϕ = 700 psi (circumferential direction)

66

The above maximum stress is well within the linear elastic behavior range of biaxially-oriented polyester film (see the polyester stress-strain curve in Figure 3.6.1.1-4). Also, this stress is below the assumed creep limit stress of 2000 psi, which gives an ample creep limited margin-of-safety of + 1.86. An evaluation of creep tendencies can also be made based on the logarithmic creep strain law:

$$\varepsilon = \varepsilon_o t^{\beta}$$

where ε = total accumulated creep strain
ε_o = strain at 100 hours
t = time in hours
β = creep exponent

Without having long term creep test data, a conservative value for β is assumed to be 0.06 which gives a total creep strain at 30 years (262080 hours) as follows:

$$\varepsilon = \varepsilon_o t^{\beta} = \varepsilon_o(262080)^{0.06} = 2.1\,\varepsilon_o$$

The initial average strain of the reflector is low (approximately 0.0005 in/in for an average stress level of 300 psi). This strain will be approximately doubled in 30 years and so resultant reflector quality degradation is expected to be insignificant.

3.6.1.7 Margin-of-Safety Summary

The preceeding margin-of-safety analyses are summarized in Table 3.6.1.7-1. Ample margins exist in all of the components.

3.6.1.8 Weight Distribution

The concentrator's weight distribution is itemized in Table 3.6.1.8-1. Because of the results of the structural analysis, some conservatism exists in the concentrator design which may allow future weight (and cost) reductions. (In the detailed design phase, alternate truss and yoke configurations should be investigated that could reduce structural weight and reduce or eliminate the counterweight.)

67

Table 3.6.1.7-1. Margin of Safety Summary

Component	Design condition	Analysis results	Margin-of-safety
Truss strut A_s = .34 in^2 I = 2.73 in^4	Seismic 1 G vertical 0.25 G lateral Concentrator looking at the horizon	Axial load = 1,585 lb (comp) Euler buckling load = 9,568 lb Chord crippling load = 25,500 lb	> +1.0
Yoke A_s = 2.70 in^2 I = 58.38 in^4	Same as above	Max moment = 276,567 in-lb Max chord stress = 24,412 lb/in^2 Allow chord stress = 36,000 lb/in^2	+0.47
Enclosure film Kynar film t = 0.007 in	100 mph wind + 0.18 lb/in^2 inflation pressure	Max film stress = 15,000 lb/in^2 (at top) Allow film stress = 20,000 lb/in^2	+0.33
Reflector film Polyester film t = 0.002 in	Nominal stabilization pressure = 0.0037 lb/in^2	Max film stress = 700 lb/in^2 (at support) Allow stress = 2,000 lb/in^2 (creep limited)	+1.86
Reflector support shell Lower edge ring A = 0.8 in^2	Gravity + external Pressure + film loads	Axial ring load = 488 lb Rig crippling stress = 6,325 lb/in^2	+0.77
Foundation Weight = 56,000 lb Diameter = 29 ft	100 mph wind Dead weight overturning	Lift = 34,500 lb Drag = 11,000 lb	+0.6

Table 3.6 1.8-1. Concentrator Weight Distribution

Brayton engine/receiver	825 lb
Counterweight	825
Reflector assembly	808
Truss	658
Yoke	908
Misc parts	336
Total moving weight	4,360
Enclosure film	436
Misc enclosure/foundation parts	625
	5,421 lb

68

3.6.2 Tracking Error Estimate

Estimates of tracking errors are listed in Table 3.6.2-1. A major source of error is expected to be due to inaccurate alignment of the photosensor unit during installation. Photosensor related errors, however, can be reduced by software corrections that would be performed during installation and routine maintainence. The overall root sum square tracking error is estimated to be 1.43 mrad which compares favorably with a design goal of 2 mrad.

Table 3.6.2-1. Angular Tracking Error Estimates

Errors source	1σ error mrad		
	Component error	Root sum squares	
		Groups	Total
Static errors			
Control system			
Ephemeris data	0.11		
Computations	0.06		
Clock resolution	0.02		
Photosensor calibration	1.30	1.306	
Drive system			
Gimbal axis alignment	0.30	0.30 → 1.40	
Structural deflections		0.40	
Dynamic errors			1.43 mrad
Structural deflections	0.25	.27	
Drive system stepping error	0.10		

3.6.3 Control System Reliability

Reliability of the concentrator system is governed to large extent by the unit and system controllers. Other concentrator components are either unlikely to fail or are less sophisticated and easily maintained.

The MTBF (mean time between failure) estimate for the unit controller is determined by summing the discrete part failure rates as shown in Table 3.6.3-1. The failure rates used in the table were derived from rates used in previous heliostat programs. The actual MTBF is determined by taking the reciprocal of the sum of failure rates. For the unit controller the resulting MTBF is 54,200 hours based on a 90% confidence level. This relatively high MTBF is due to the use of just a few reliable LSI circuits to implement the controller.

The failure rate for the system controller is also based on rates used in previous heliostat programs, and the MTBF is determined to be approximate 8000 hours for a single microcomputer. This relatively lower MTBF (as compared to that of the unit controller) is due to the greater complexity of the individual microcomputer systems. However, the triple redundancy improves the MTBF considerably (about an order of magnitude), and the system controller MTBF is conservatively estimated to be about 50,000 hours or 6 years; that is, about the same as that of the unit controller.

Table 3.6.3-1. Mean Time Between Failure Analysis Data

Component	No. Used	Failures per Million operating hours at a 90% confidence level/ component	Total Parts
microcomputer	2	.2	.4
7400 series logic	8	.6	.48
capacitors	4	.4	1.6
transistors	10	.9	9
resistors	10	.02	.2
transformer	1	.07	.07
regulators	2	3	6
A/D converter	1	.2	.2
bus transceiver	1	.5	.5
Total failure rate			18.45
MTBF			54,200 hours

3.6.4 Enclosure Air Flow Rates

The Boeing Thermal Analyzer computer program (Ref. 1) was used to determine transient temperature profiles for the collector components. The primary components modeled are shown in Figure 3.6.4-1.

Daily ambient temperature profiles were provided by JPL. The profiles were adjusted to the extreme summer and winter temperatures for the Edwards Air Force Base area. The average daily insolation value is 845 w/m^2 with a maximum value of 1000 w/m^2. The insolation profiles are for the winter and summer solstice.

Ground temperature is assumed to be ambient temperature with the sky temperature 6.1°C lower. The aperture temperature profile was obtained from previous transient analyses.

Convection coefficients for the internal components are computed based on data for vertical and horizontal plates; a no wind condition was assumed.

Radiation view factors were calculated by the Boeing AS2814 Thermal Radiative Interchange Factor Program. The program employs a Monte Carlo method; it uses a specular/diffuse reflectance model and can also handle transmitting surfaces with refraction at interfaces.

The temperature profiles for the reflector (with no anti-oxidation coating), enclosure, and enclosure air are shown in Figure 3.6.4-2 for the winter extreme and Figure 3.6.4-3 for summer extreme. Temperatures for the production reflectors will be lower due to use of an anti-oxidation coating which increases emissivity.

The maximum enclosure air temperature change is 0.25°C/minute. This leads to a maximum enclosure air flow of 60 cfm. Negligible air flow in and out of the reflector cavity is required to maintain proper stabilization pressure.

12

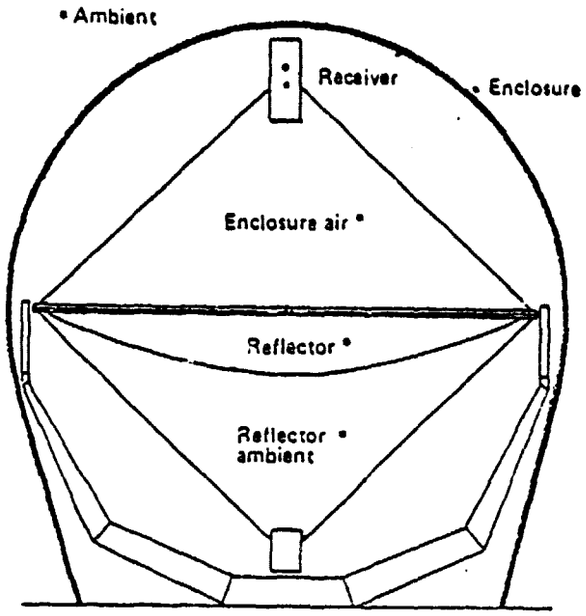

- Transient thermal analysis
- Temperature profiles for extreme summer and winter
- Maximum temperature change T = .25°C/min
- Maximum enclosure flow rate 60 cfm
- Reflector ambient flow rate negligible

Figure 3.6.4-1. Enclosure Air Flow Rates

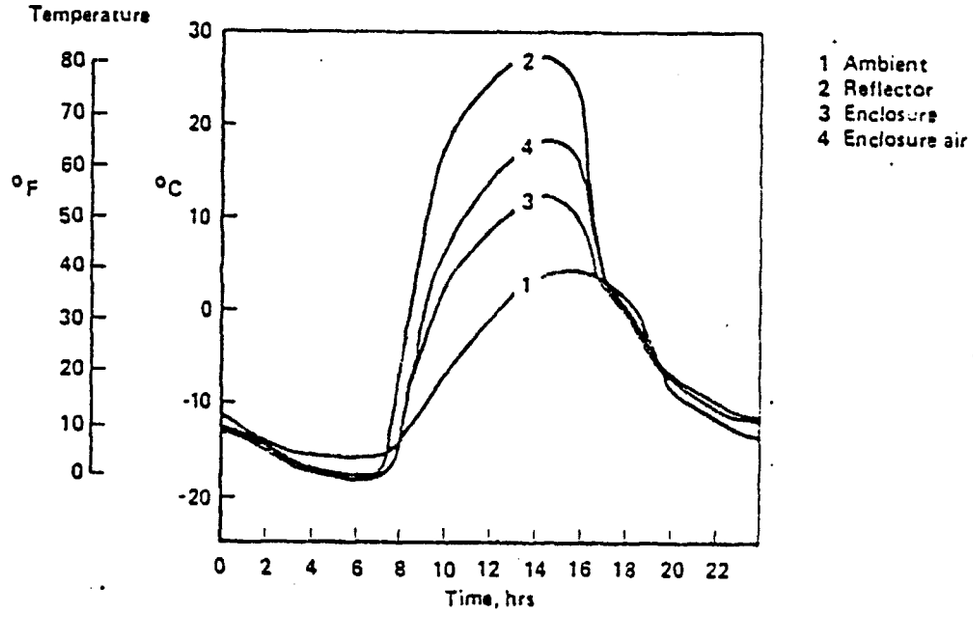

Figure 3.6.4-2. Extreme Winter Temperature Profiles

73

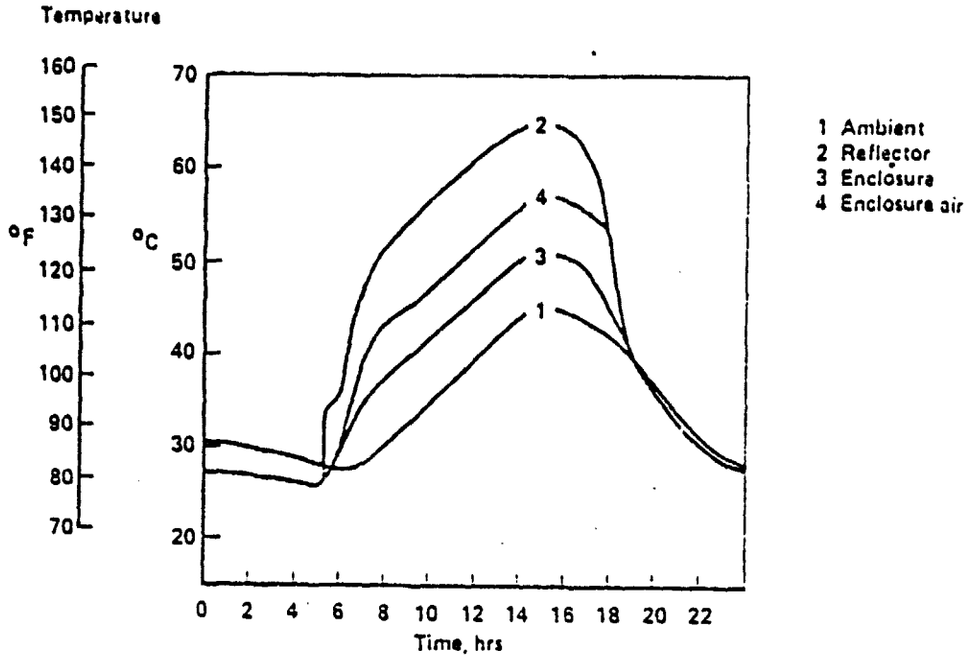

Figure 3.6.4-3. Extreme Summer Temperature Profiles

74

4.0 SUB-SCALE REFLECTOR TEST PROGRAM

A 4.57 m diameter sub-scale reflector was built and tested by laser ray tracing for the purpose of demonstrating a prototype reflector fabrication technique and surface slope errors. The test evaluation of resulting data was subsequently used in performance studies of the full-scale reflector design. The following sections describe the test program activities with respect to:

- o Sub-scale reflector fabrication
- o Reflector testing
- o Test data acquisition
- o Test data analysis

4.1 Sub-scale Reflector Fabrication

Steps followed in the test hardware fabrication are identified in Figure 4.1-1. These steps and related tooling were refined with trial fabrication of four 2 m diameter reflectors. A single 4.57 diameter (active reflector area) was then fabricated and tested by laser ray tracing. Most of the fabrication techniques proved to be successful; difficulties were encountered in reflector mounting which will be discussed in the remaining section.

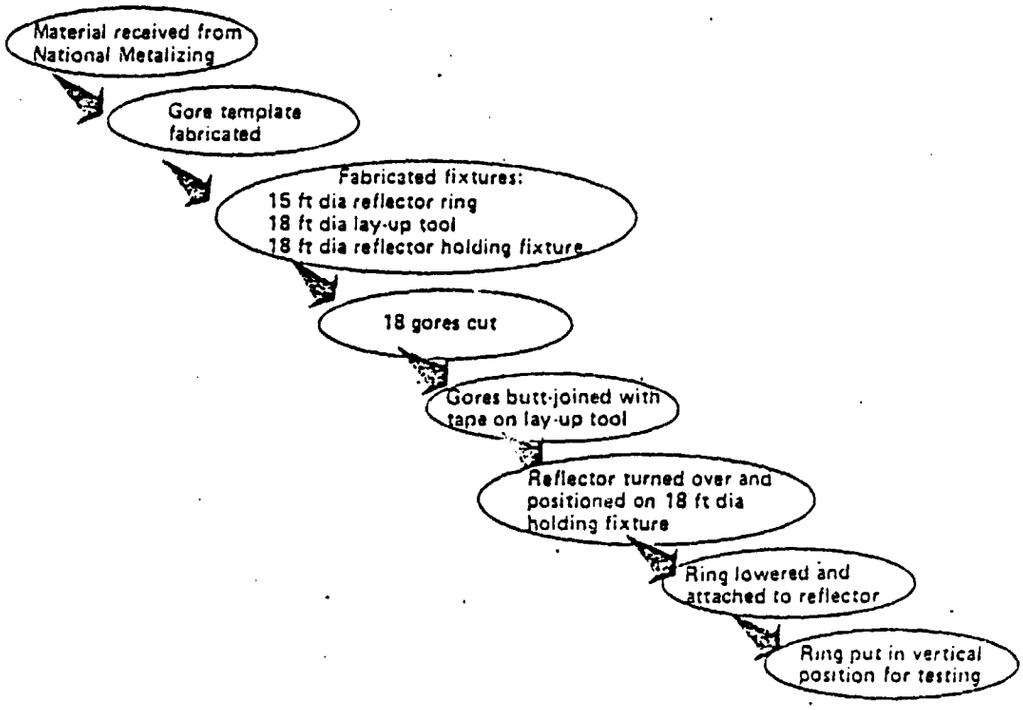

Figure 4.1-1. Prototype Reflector Fabrication Steps

75

The polyester film used for the reflector was Melinex-O aluminized by National Metalizing. Melinex-O is a biaxially-oriented film produced by ICI Americas. This material was selected because of its excellent optical and mechanical properties and availability.

A roll of 2 mil, 56" wide aluminized polyester was received from National Metalizing and was subjected to and passed an acceptance test of 89% minimum reflectance at a cone angle of 0.15°.

Gore Template

The aluminum templates for the 2 m and 4.57 m reflector gores were fabricated at the Boeing Commercial Airplane Division's template shop. The template was made in halves to assure symmetry and was machined to within a 10 mil tolerance.

The same gore shape analysis method that was derived for Sandia Laboratories (Ref. 3) was used for this project. This analysis was coded and executed interactively on Boeing Computer Service's CDC 6600 computer. Figure 4.1-2 shows the offsets for the 4.57 m reflector gore template versus gore center-line distance from the pole.

The template has 1/16 in. holes drilled every foot along the edges. These holes were used to pin-mark the gores which provided indexing marks for positioning on the lay-up tool. Holes were also drilled into the template to index the attachment of the reflector to the holding fixture and the reflector ring.

Using the template as shown in Figure 4.1-3, 18 gores were cut out with a scalpel. Special care was taken to avoid wrinkles in the polyester during cutting. The 21 index marks were then punched in and the finished gore rolled up and placed on the table at the left. To minimize wastage, a second gore was cut along side of the first one. Weights were placed on the template to avoid movement of it during cutting.

	LENGTH	FULL WIDTH	HALF WIDTH
1	0,00	0,00	0,00
2	2,28	,81	,40
3	4,57	1,61	,81
4	6,85	2,42	1,21
5	9,14	3,22	1,61
6	11,42	4,03	2,01
7	13,71	4,83	2,42
8	16,00	5,64	2,82
9	18,30	6,44	3,22
10	20,59	7,25	3,62
11	22,90	8,05	4,03
12	25,20	8,86	4,43
13	27,51	9,66	4,83
14	29,82	10,47	5,23
15	32,14	11,27	5,64
16	34,46	12,08	6,04
17	36,79	12,88	6,44
18	39,13	13,69	6,84
19	41,47	14,50	7,25
20	43,82	15,30	7,65
21	46,18	16,11	8,05
22	48,54	16,91	8,46
23	50,92	17,72	8,86
24	53,30	18,52	9,26
25	55,69	19,33	9,67
26	58,08	20,14	10,07
27	60,49	20,94	10,47
28	62,91	21,75	10,87
29	65,34	22,56	11,28
30	67,77	23,36	11,68
31	70,22	24,17	12,08
32	72,68	24,98	12,49
33	75,15	25,78	12,89
34	77,63	26,59	13,29
35	80,13	27,40	13,70
36	82,63	28,20	14,10
37	85,15	29,01	14,50
38	87,68	29,82	14,91
39	90,23	30,62	15,31
40	92,79	31,43	15,72
41	95,36	32,24	16,12
42	97,94	33,05	16,52
43	100,54	33,85	16,93
44	103,16	34,66	17,33
45	105,79	35,47	17,73

Figure 4.1-2. Gore Template Coordinates

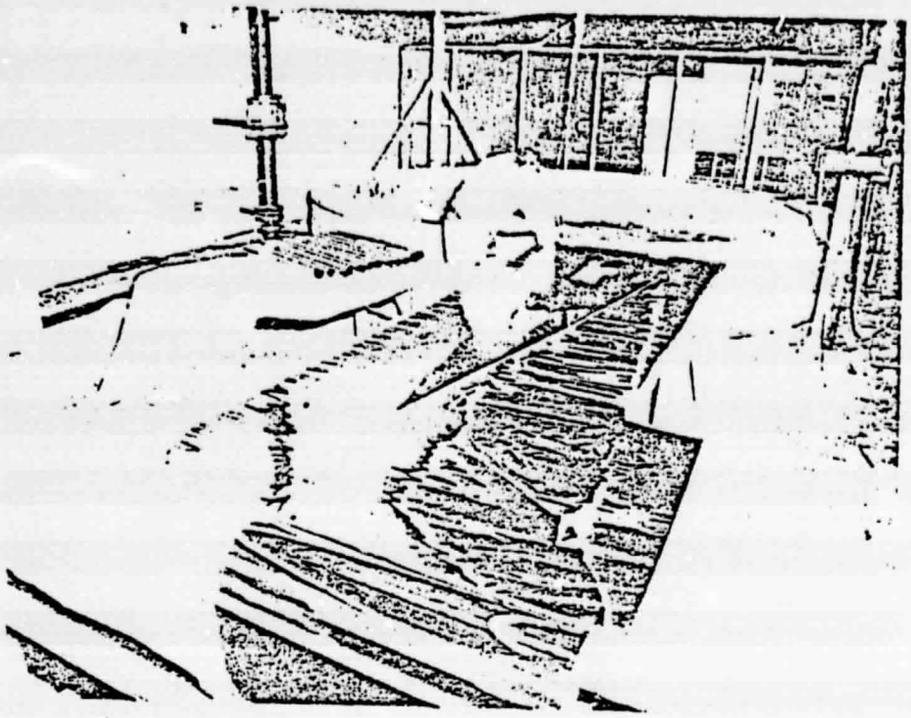

Figure 4.1-3. Gore Cutting

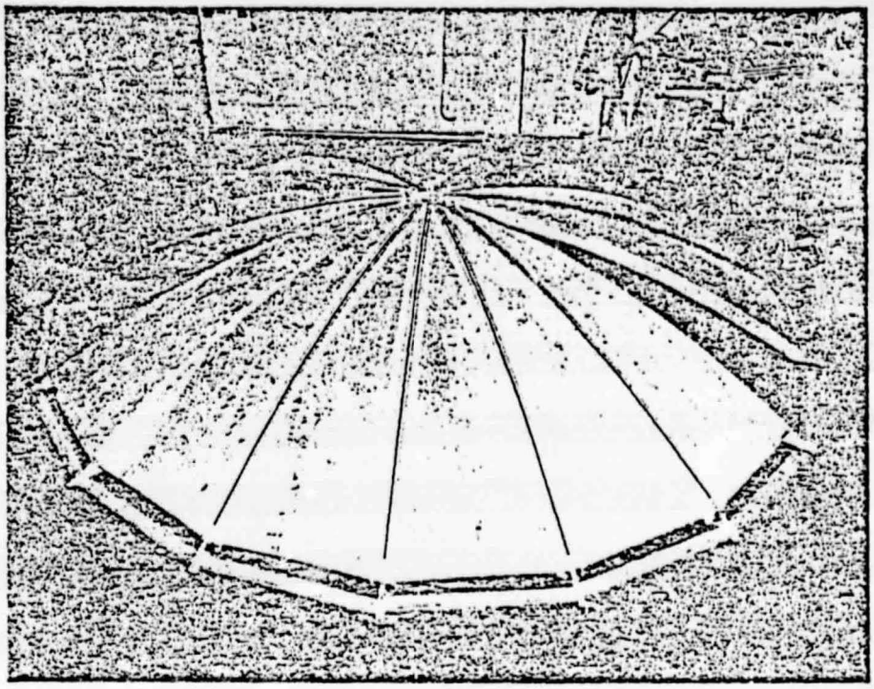

Figure 4.1-4. Lay-up Tool

Lay-up Tool

Because of the large reflector size, a decision was made early in the project to abandon heavy conventional plaster tooling and use instead lightweight portable wooden lay-up tooling. The resulting tooling approach is shown in Figure 4.1-4 and Figure 4.1-5. In this tooling concept, the tooling nearby serves as a holding fixture during taping of the gore seams. Accuracy of the reflector surface is established by the pre-cut core shape and careful butt-joining to the gores prior to taping. Thus, highly accurate lay-up tool contours are not necessary.

The lay-up tool was constructed from plywood by a local cabinet shop. The missing panel in Figure 4.1-4 allowed assembly of the first 17 gores and was replaced for attachment of the final gore. Each rib has a vacuum channel which is covered with a porous tape (lawn chair webbing). A conventional shop vacuum cleaner was attached to the tubing visible in Figure 4.1-5.

79

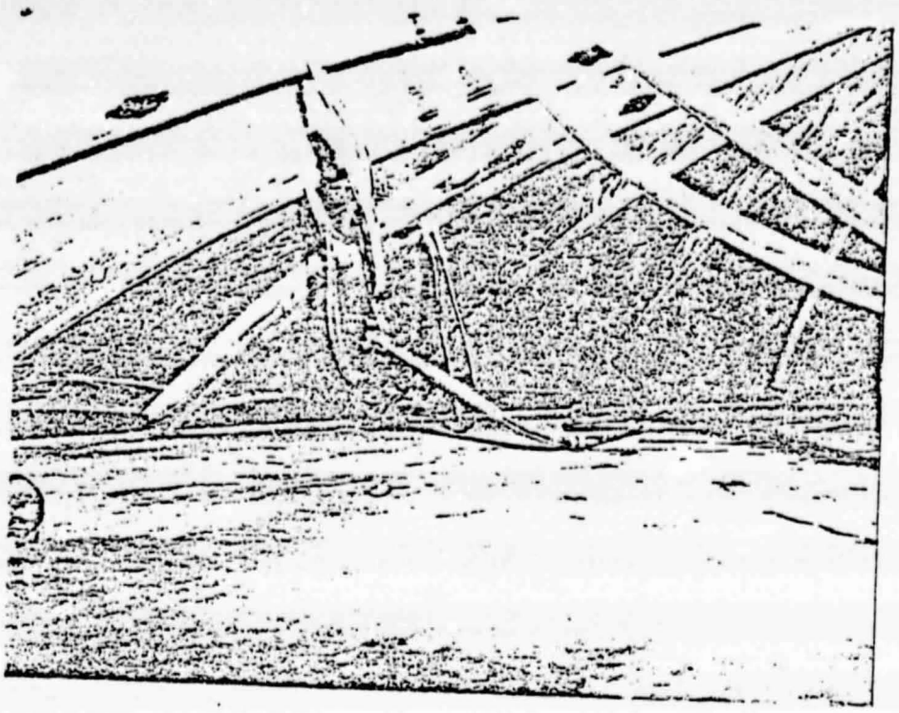

Figure 4.1-5. Vacuum Hold-down

This vacuum hold-down technique was very effective in maintaining gore position during taping (previous static attraction caused gore movement and wrinkled seams).

Reflector Gore Assembly

The gores were placed metalized side down on the lay-up tool. Using the index marks to position the gores along side of each other, they were butt-joined together using 2 mil 1/2 in. polyester tape (Permacel 255). The vacuum hold-down device prevented the gores from moving once they were positioned correctly. Figure 4.1-6 shows the taping together of two gores. Notice that even though there are wrinkles in the polyester, there are none at the joints. Figure 4.1-7 shows the method used for firmly bonding the tape to the reflector film.

70

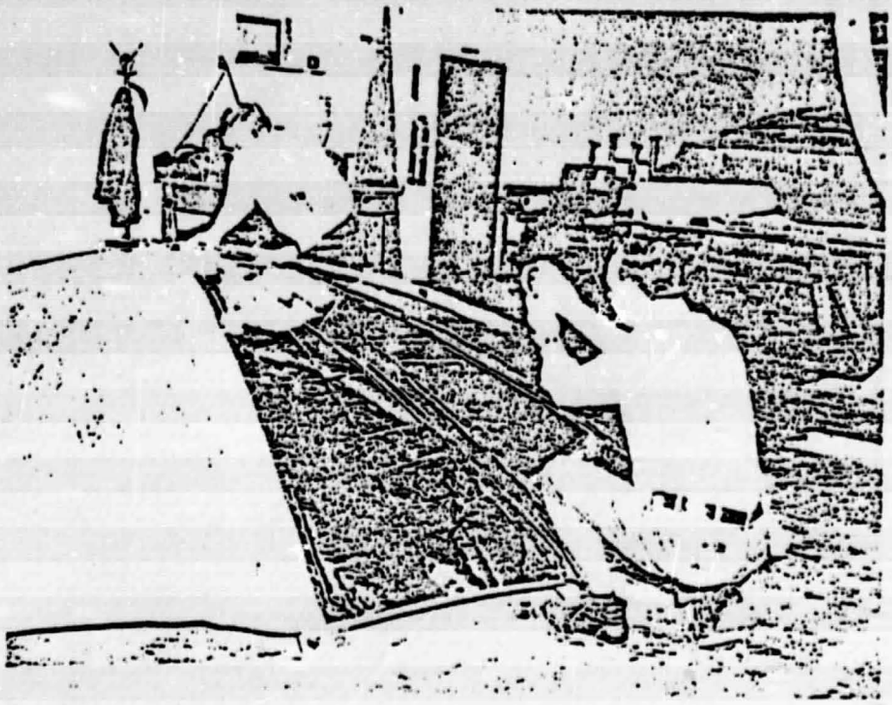

Figure 4.1-6. Taping of Gores

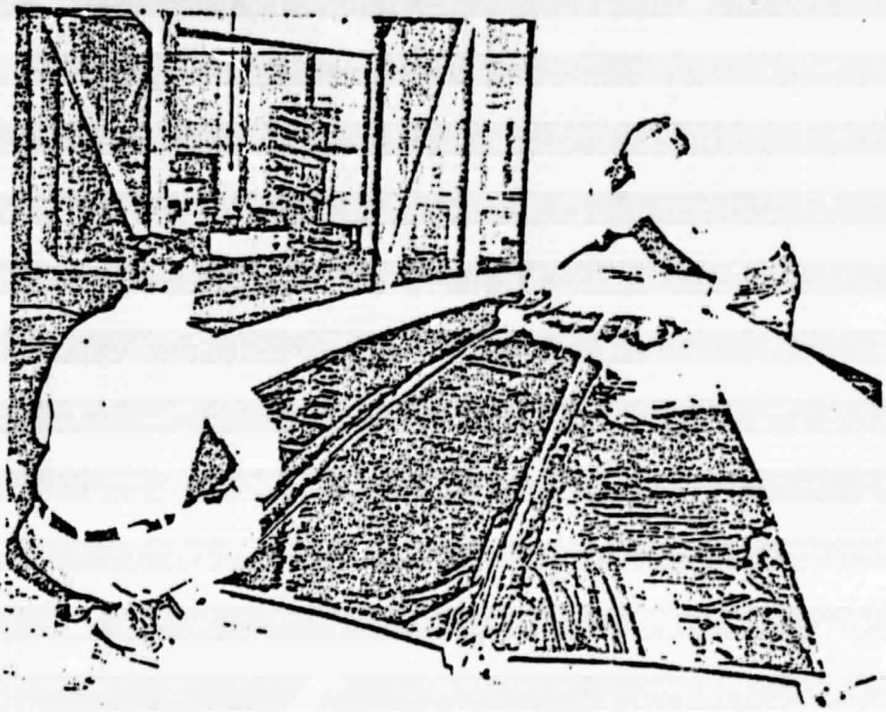

Figure 4.1-7. Final Step in Joining of Gores

81

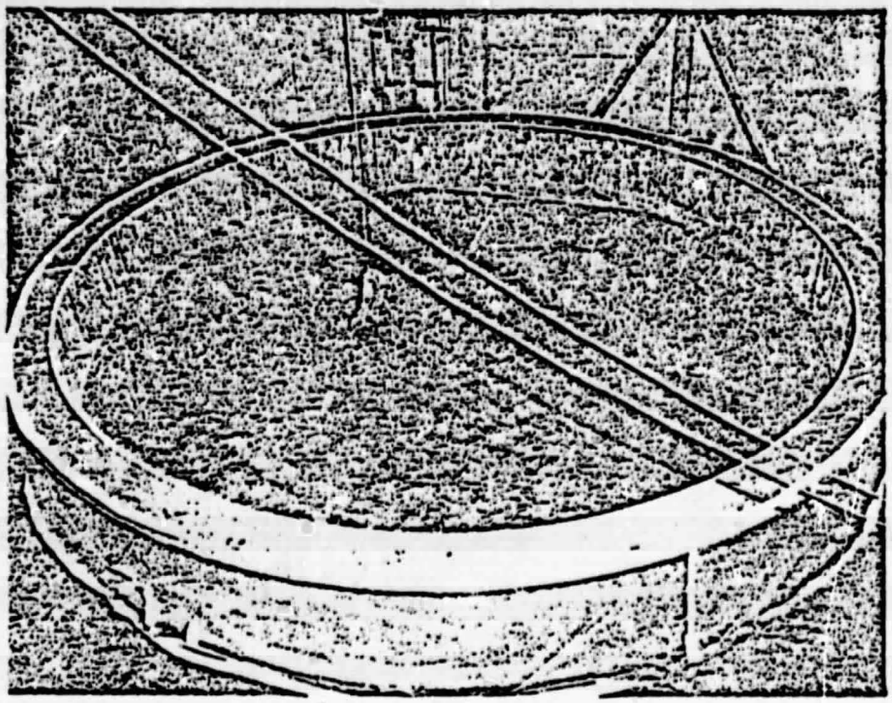

Figure 4.1-8. Reflector Holding Fixture

Reflector Holding Fixture

Figure 4.1-8 shows the reflector holding fixture built from plywood. This tool permitted attachment of a reflector test support ring to the reflector while it was stabilized by vacuum. The reflector-to-ring joining operation is illustrated in Figure 4.1-9. The four hoisting hooks in the middle of the picture were hooked into corresponding eye bolts on the ring. Running the main rope through an overhead pulley permitted lowering and raising the ring.

Reflector Support Ring

The ring is a box-section having 0.5 in. router-cut plywood webs and 0.25 in. plywood inner and outer flanges. Internal stiffening diaphragms were placed every two feet. The "rear" side of the ring had a small plywood circumferential rib that was router-trimmed to form an accurate reflector mounting surface. A clear 5 mil polyester film was attached to the "front" side of the ring. After the reflector was attached it could then be stabilized with air pressure supplied by a blower.

82

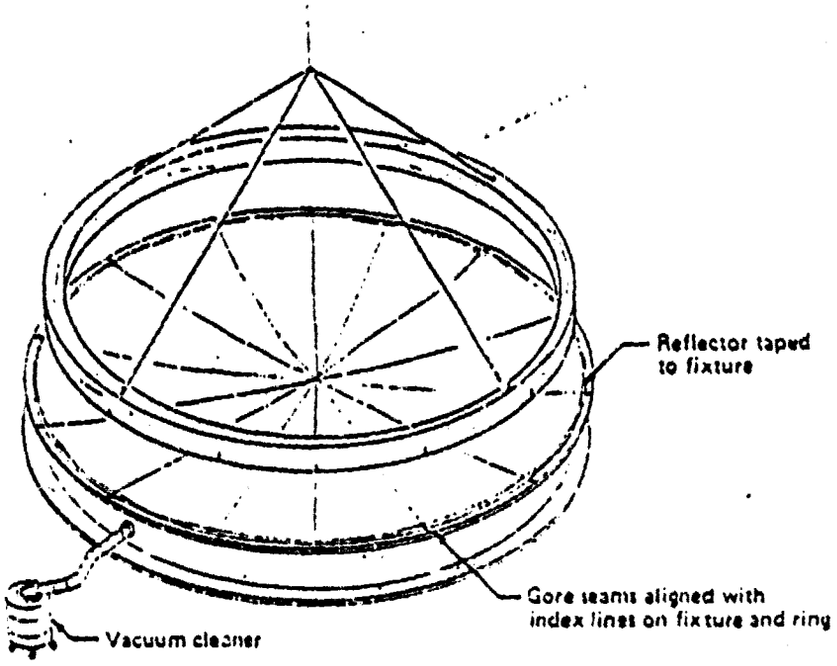

Figure 4.1-9. Reflector Mounting Fixture

Reflector-to-Ring Joining

Once all the reflector gores were joined together, the reflector was inverted and carried to the reflector holding fixture. Great care was taken in fastening the reflector to the holding fixture. The gore seams were aligned with the index marks on the fixture to provide equal tension in the tangential direction. At the same time, index marks put in the gores from the gore template were aligned with the inner edge of the fixture to provide equal tension in the radial direction. Once the reflector was positioned correctly it was taped to the fixture to provide an air-tight seal.

Using the vacuum pump to provide a differential pressure of 0.5 in. of water, the reflector was fully stabilized with all wrinkles removed. The reflector ring which fits inside the holding fixture, was then lowered and fastened to the reflector. Velcro with self-adhesive backing was used for fastening the ring to the reflector. After mounting the reflector, the excess edge

was then trimmed off. A bead of sealant was placed around the Velcro edge to make it air tight, and the edge of the reflector was taped to the ring rib.

An important feature of this tooling concept is that by having an excess width of film around the reflector, mounting errors at the reflector holding fixture would in theory be distant from the ring. In practice, a uniform edge mounting tension was not activated as will be highlighted in the following test data analysis section. Future reflector mounting is planned to be accomplished using pneumatically actuated grips that will produce a uniform edge tension.

Completed Sub-scale Reflector

Views of the completed sub-scale reflector, general fabrication, and test area appear in Figures 4.1-10 to -13. Items appearing in Figure 4.1-10 include: lay-up tool, reflector holding fixture, laser lathe bed (lower left), laser test target stand (in front of the reflector), and the auto-collimation mirror (small square supported by the adjustable cross-frame at the center of the reflector). Figure 4.1-12 illustrates the pressureized reflector's apparent quality when viewed from the rear. A slant tube manometer used for pressure measurement can also be seen.

Figure 4.1-13 is a frontal view of the test set-up showing the base roller supports and an adjustable upper roller used for autocollimation. A close-up of a base roller appears in Figure 4.1-14; also shown are air supply and vent lines and a line to a manometer. During the laser ray tracing testing, the reflector was easily rotated on the rollers to different positions. Spacing of the base rollers was determined from a finite element model of the ring; various spacings were analyzed to determine the value that minimized radial ring deflection under gravity loading.

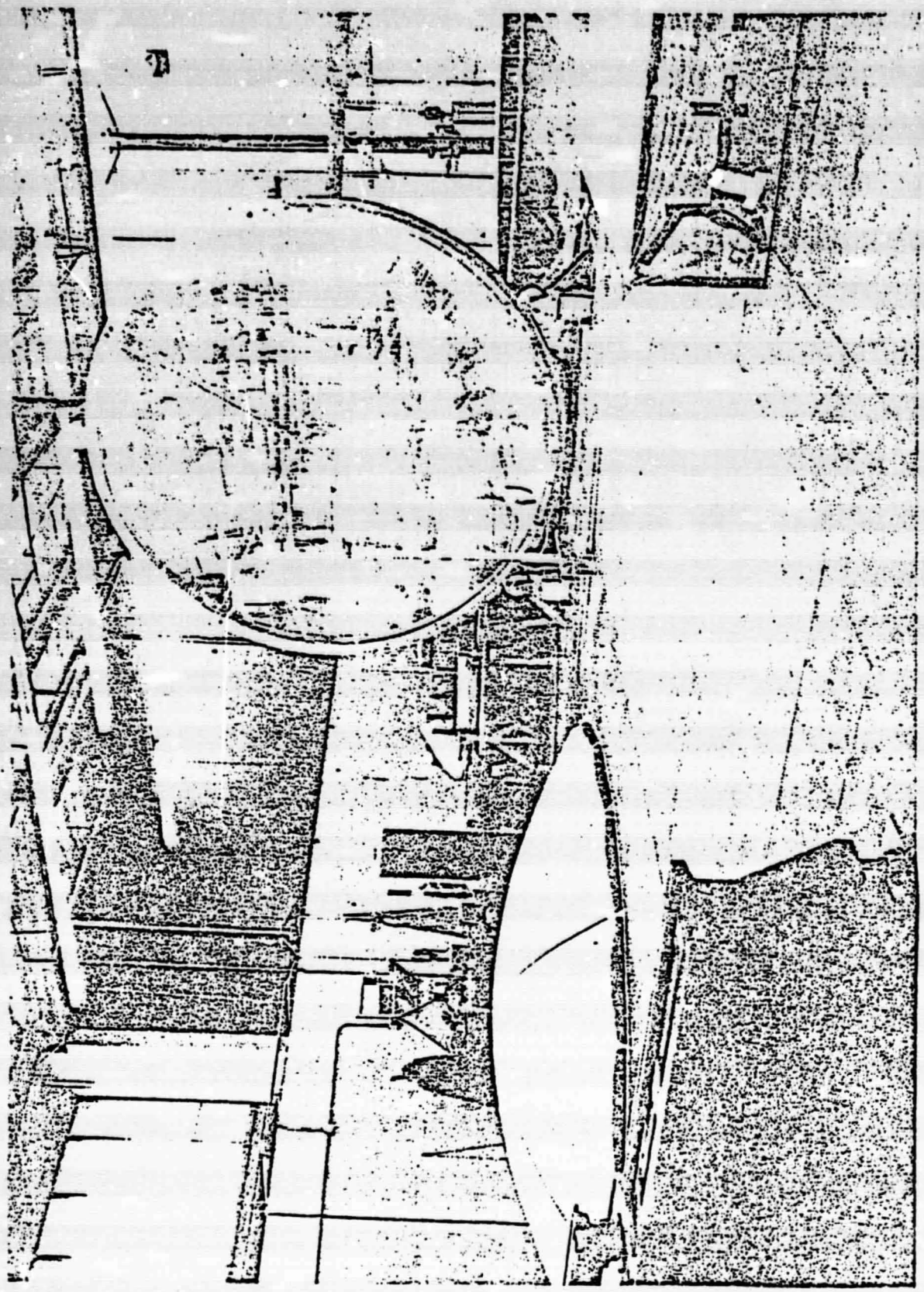

Figure 4.1-10. Overall View of Test and Fabrication Area

85

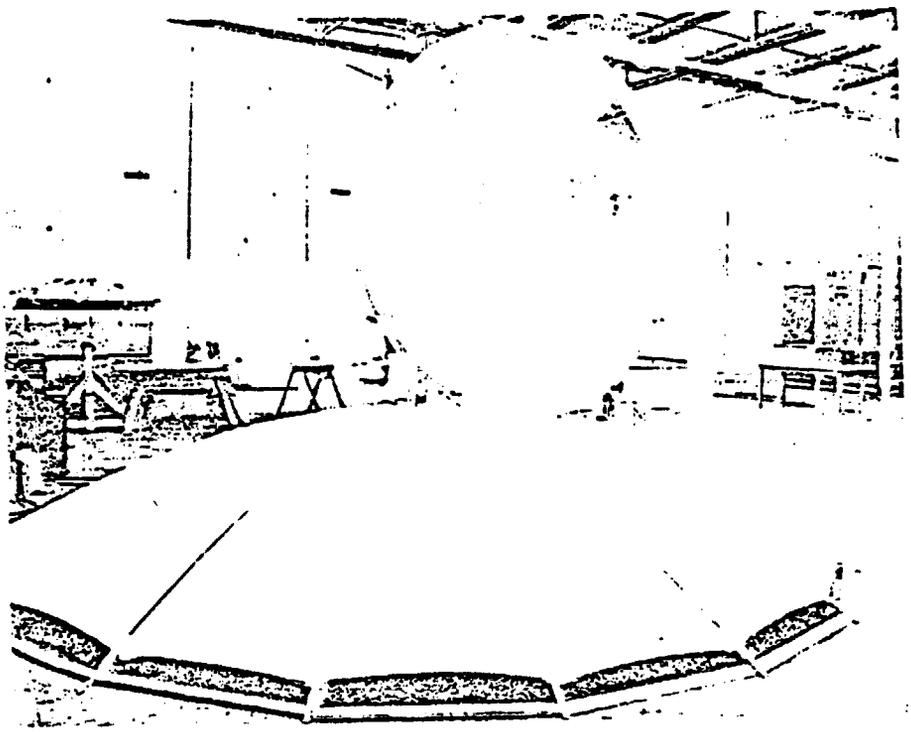

Figure 4.1-11. Lay-up Tool and Inflated Reflector

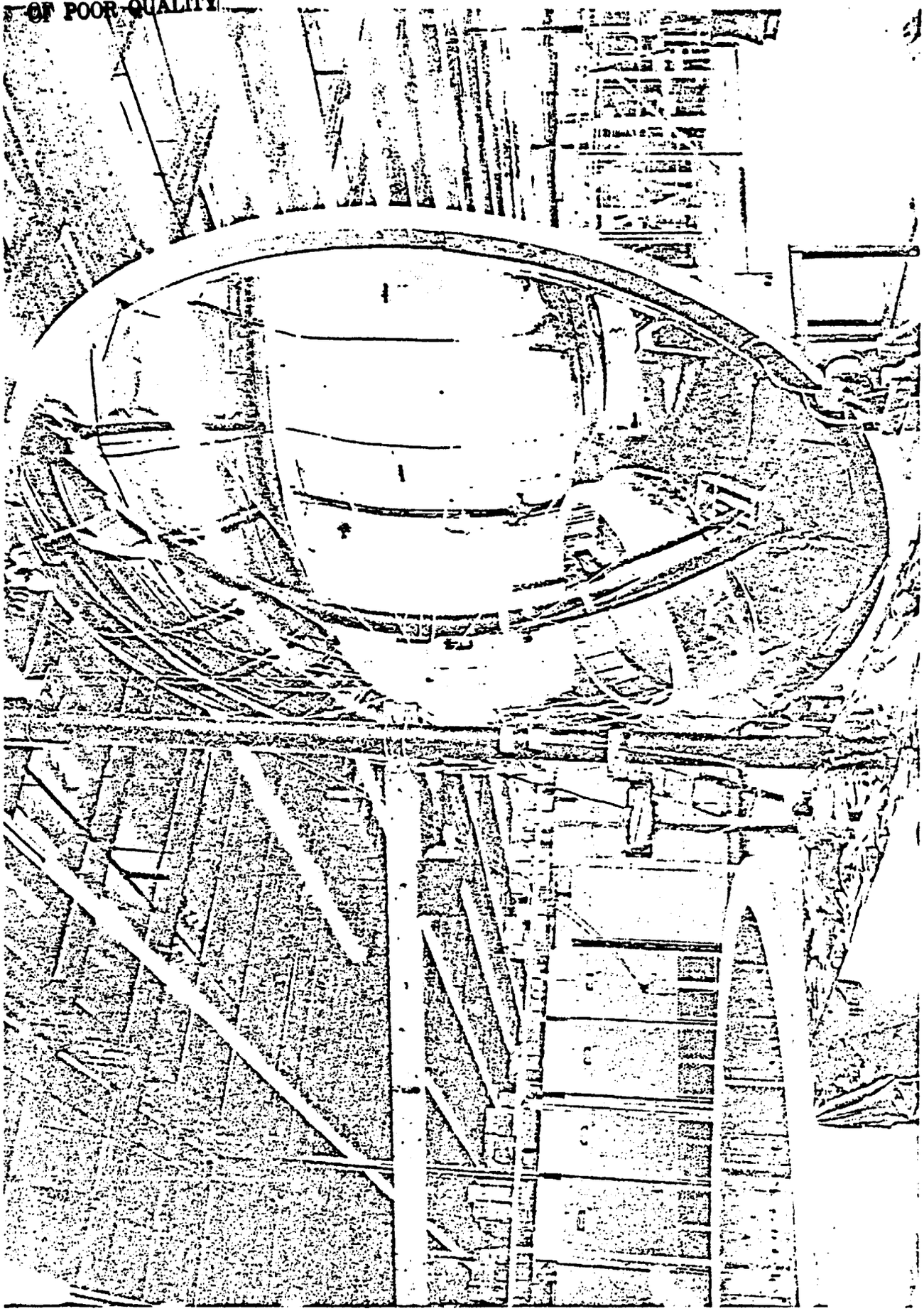

Figure 4.1-12. Backside of Reflector

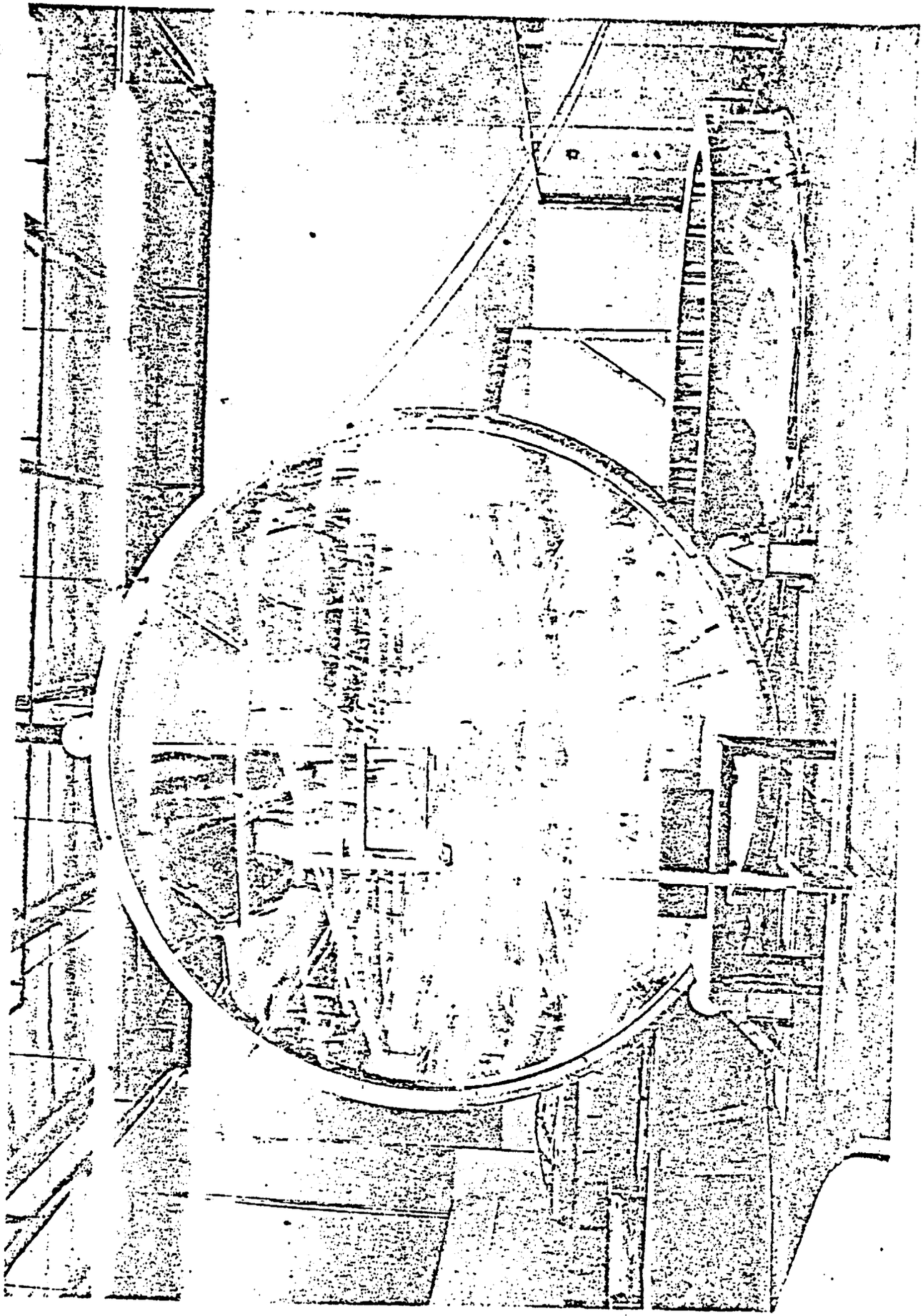

Figure 4.1.13. Test Set-up

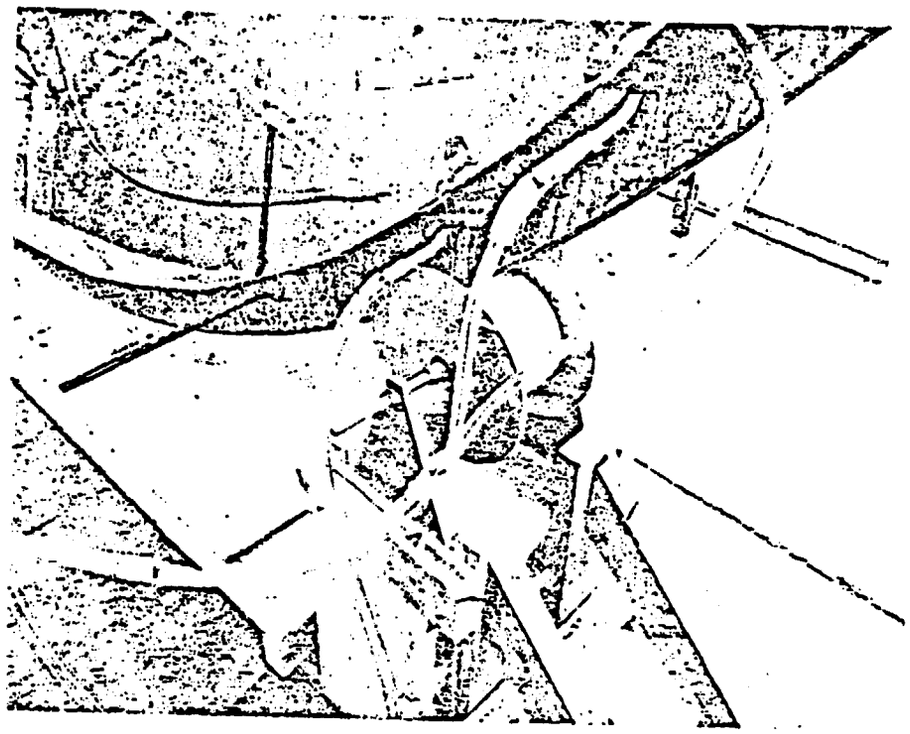

Figure 4.1-14. Reflector Support Roller

4.2 Reflector Testing

The sub-scale reflector was tested to obtain data for surface slope error analysis. This testing was done, as indicated in Figure 4.2-1, by rotating the reflector and laser ray tracing along a horizontal radial line.

Testing was accomplished with a Class I, 1 milliwatt helium-neon laser. The laser was mounted 30 ft. from the reflector ring on a traveling lathe bed as shown in Figure 4.2-2. This set-up allowed the laser to be moved vertically during autocollimation and horizontally along pre-determined radial positions.

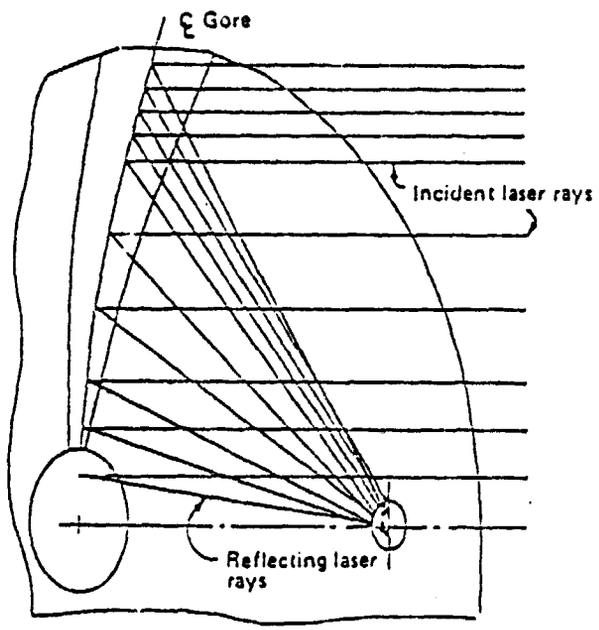

- Purpose
  - Slope deviations
  - Overall surface geometry
- Method
  - Laser on translating optical table, aligned with reflector axis
  - Target at approximate best focal plane
  - Reflected ray intercept at focal plane for several radii and azimuth of incident ray
  - Reflector rotated during testing

Figure 4.2-1. Laser Ray Trace Testing

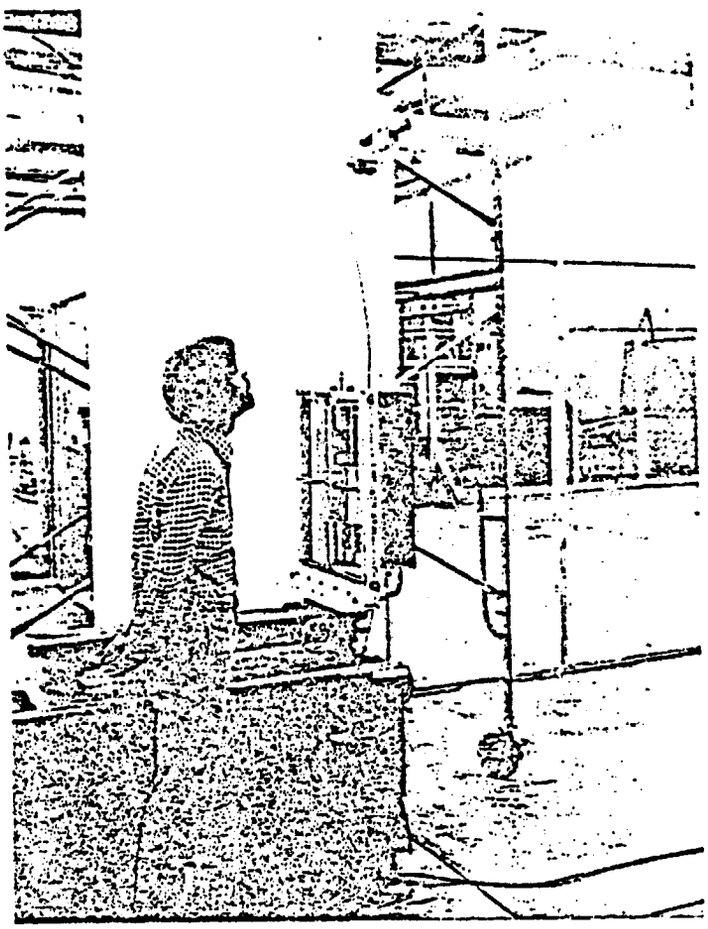

Figure 4.2-2. Laser and Laser Lathe Bed

A general view of the test set-up appears in Figure 4.2-3. Adjustable bolts support the autocollimation framework in front of the reflector. The center of the reflector is 8.5 ft. above the floor. The laser target is supported on a stand a distance close to the reflectors focal point (7.5 ft. out from the reflector center). Actual recording of laser impact points at the target is seen in Figure 4.2-4. Because of a focusing effect, the reflected laser converged to a fine spot on the target which could be accurately recorded with a pen.

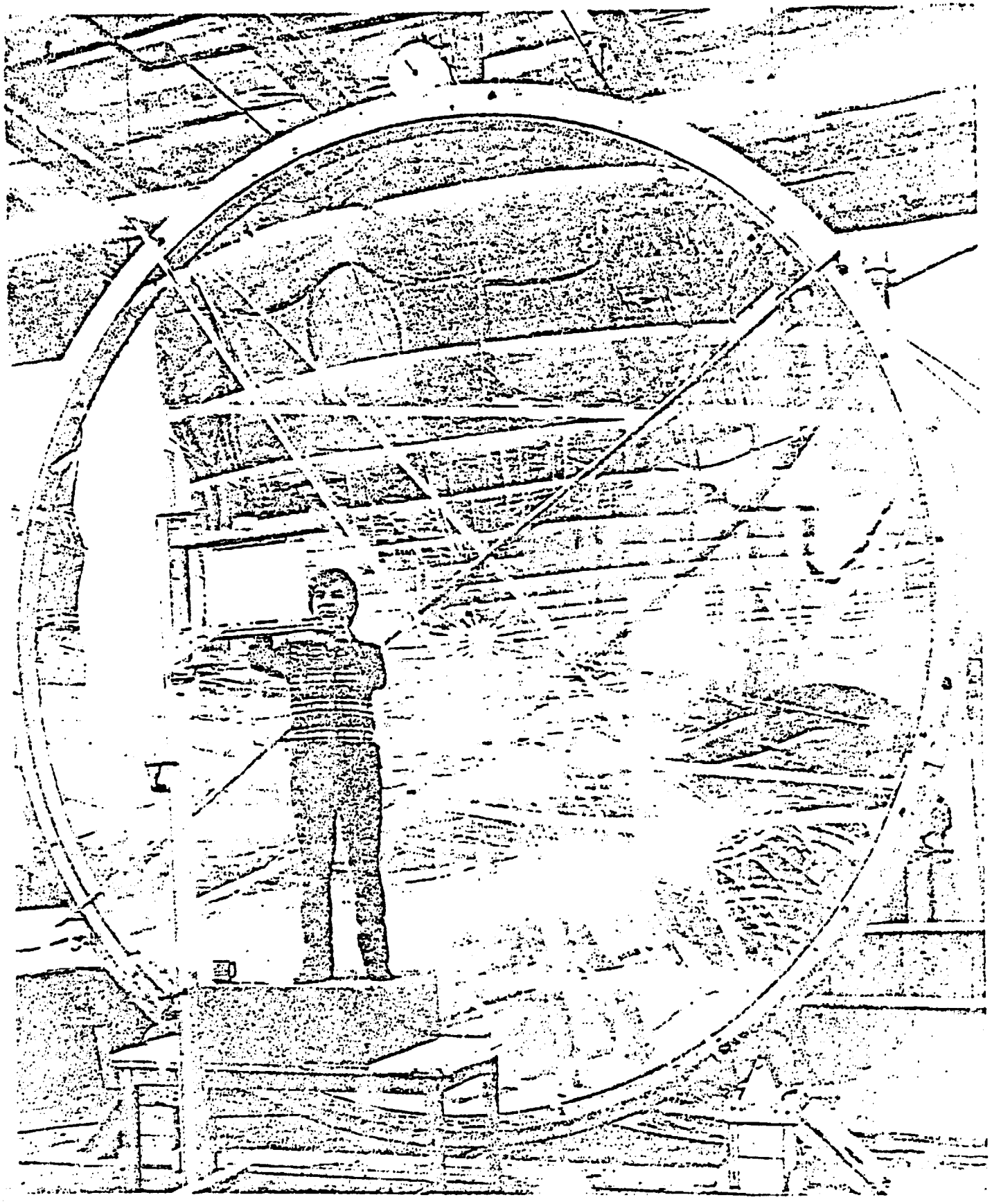

Figure 4.2-3. Overall View of Test Set-up

72

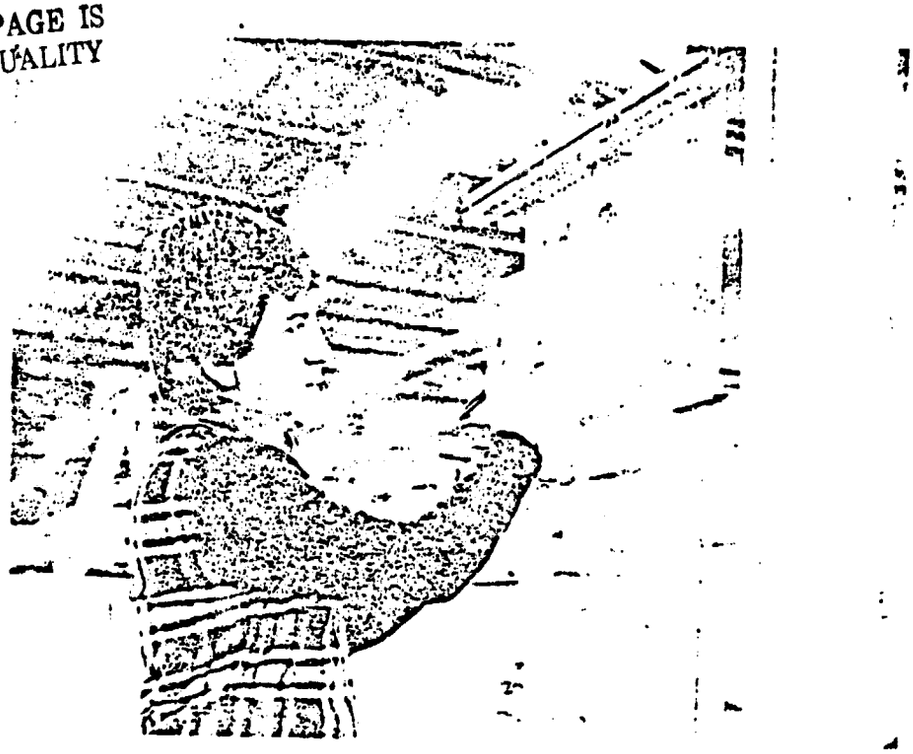

Figure 4.2-4 Recording of Laser Points

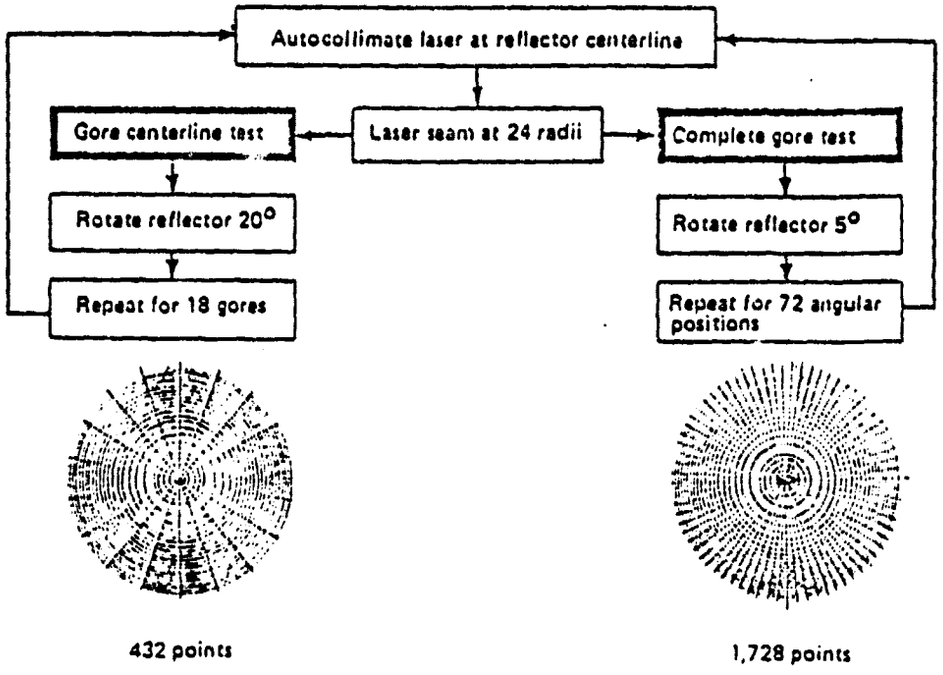

Figure 4.2-5. Laser Test Procedures

Two basic laser test procedures were followed and are summarized in Figure 4.2-5. A series of gore centerline scan tests were first performed followed by a detailed reflector scan at 5° angular increments yielding a total of 1728 data points. The initial centerline gore testing were performed at reflector stabilization pressure levels of 0.44 and 0.66 in. of water. At the 0.66 in. pressure level, the reflector stabilized to a "best fit" paraboloid and was therefore used in all data acquisition tests. Other test conditions were: 65°F ambient room temperature and 75°F internal reflector air temperature.

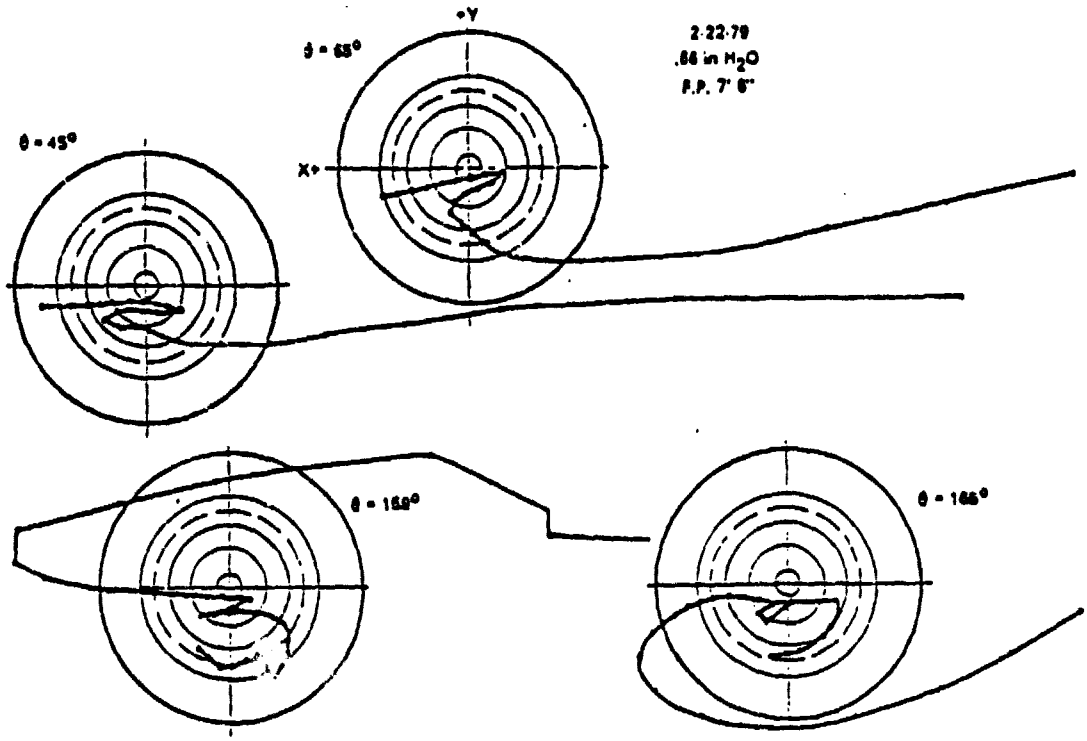

Figure 4.2-6. Laser/Target Intercept Points (Worst)

Typical laser intercept recordings are shown in Figures 4.2-6 to-8 for worst, average and best cases, respectively. The divergence in the data is due primarily to radial surface slope errors which are most severe near the ring. The dotted circles in the recordings represent the concentration ratio associated with the full-scale design (3250:1); the actual dotted circle diameter is 3.15 in.

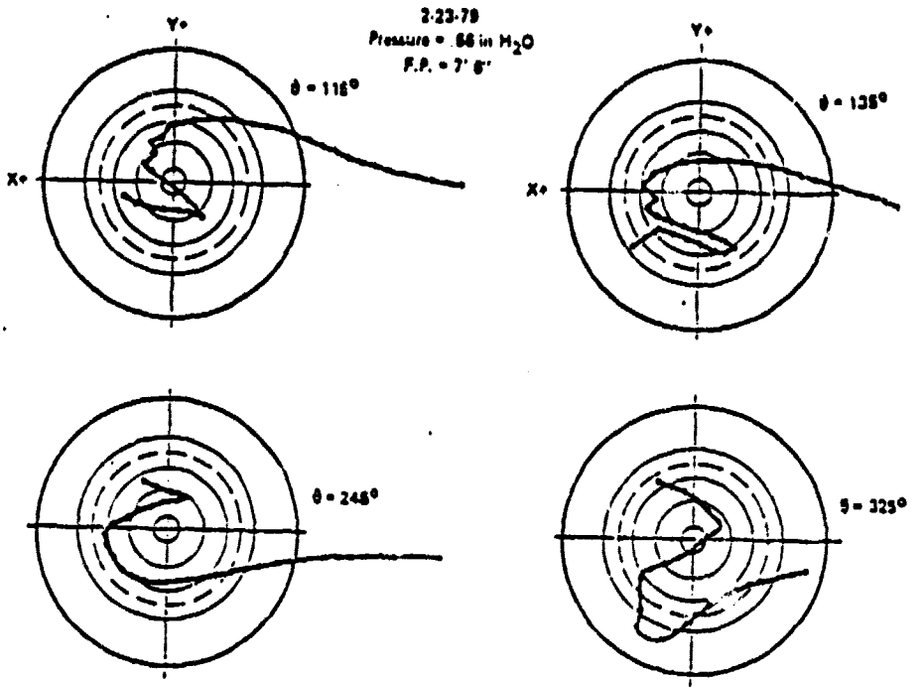

Figure 4.2-7. Laser/Target Intercept Points (Average)

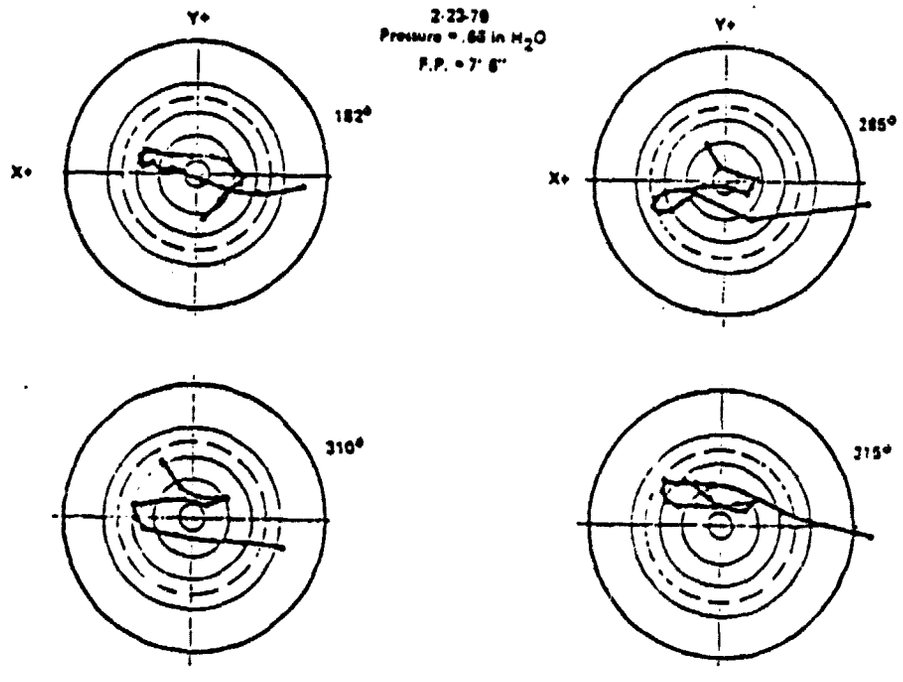

Figure 4.2-8. Laser/Target Intercept (Best)

96

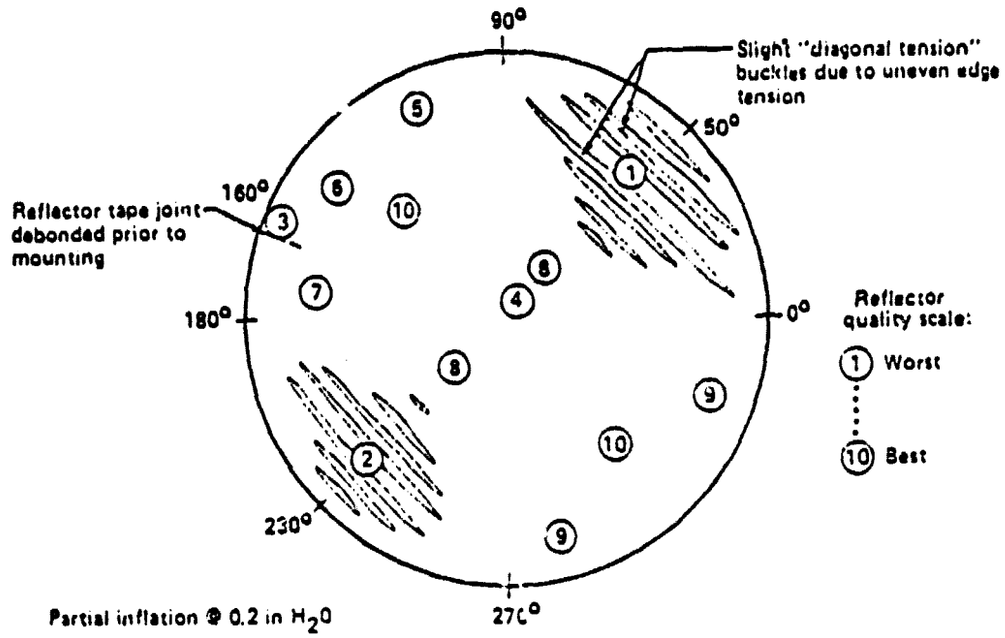

Figure 4.2-9. Comparison of Test Data Quality With Reflector Mounting Imperfections

A review of the laser intercept recordings, together with computerized analysis of the test data, revealed a correlation between surface slope quality and reflector fabrication mishaps as shown in Figure 4.2-9. Four fabrication events seriously degraded the surface quality:

1) During installation of the last gore on the reflector lay-up tool, there was some difficulty in reaching to the center area. Consequently, one tape seam was wrinkled near the pole. It should be noted that the receiver's diameter is 10% of the reflector diameter which would hide polar cap errors.

97

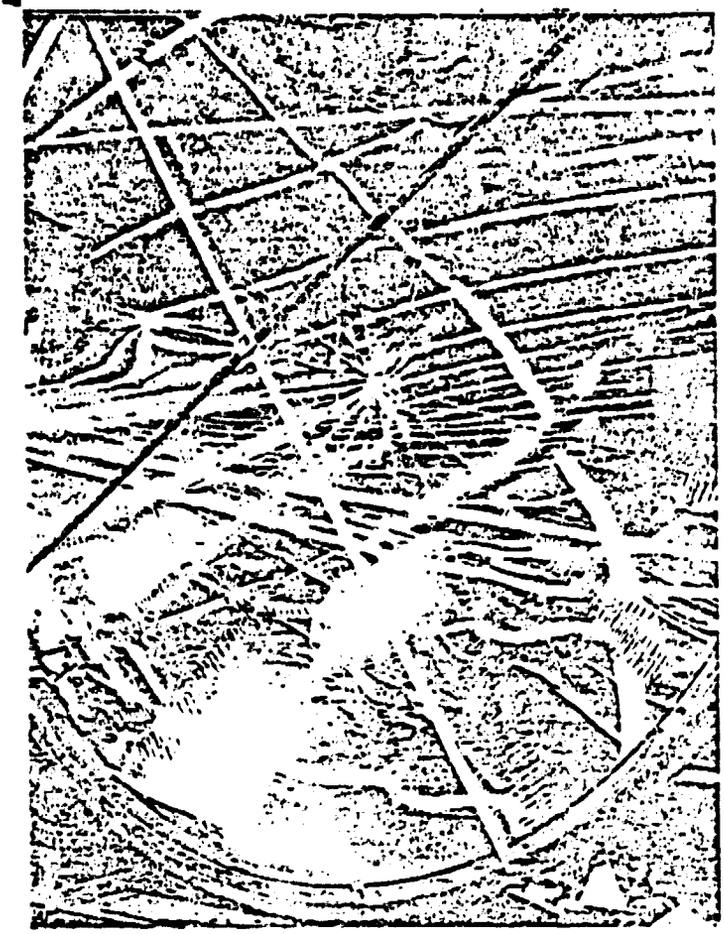

Figure 4.2-10. Tension Wrinkles

2) During mounting of the reflector on the reflector hoisting fixture, four people were tensioning the reflector prior to securing the reflector with tape. Two diametrically opposed individuals pulled harder, causing a slight tension buckling effect. These buckles were seen at pressures less than 0.2 in. of water. While the photograph shown in Figure 4.2-10 does not completely capture this effect, some tension buckles are visible (those that are non-normal to the gore seams).

3) One heavy-handed individual actually tore a gore seam at the 160° edge location during the above reflector mounting process. A defect-free tape repair was not done so the reflector had residual wrinkles in this area as appears in Figure 4.2-11.

4) Hook-and-loop fastening was used to attach the reflector to the ring. This type of fastening has high lateral flexibility and during compaction with a roller, a "bow wave" occurred which caused local gathering of film as shown in Figure 4.2-12.

Figure 4.2-11. Wrinkle Due to Tear

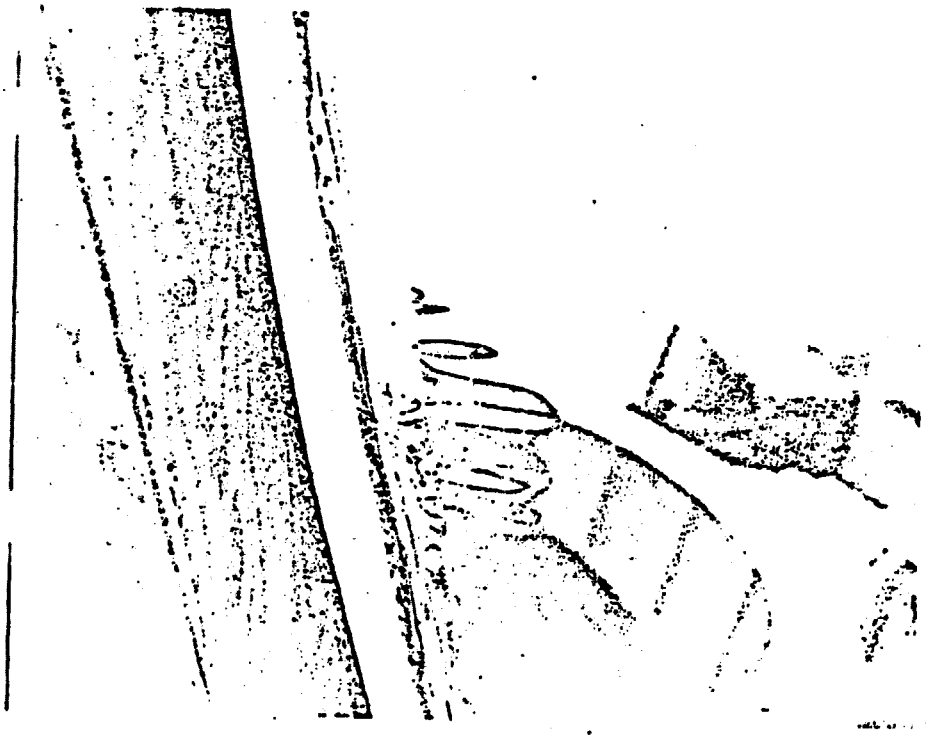

Figure 4.2-12. "Bow Wave" Wrinkle

4.3 Test Data Acquisition

The large amount of test data was acquired, formatted and stored by a computer-aided data management procedure. Each reflector test produced data shown on Figure 4.3-1 and defined as follows:

- o Laser target intercepts X_T, Y_T
- o Target distance Z_T
- o Reflector orientation angle ϕ
- o Radial laser position R_L
- o Stabilization pressure p

The laser target intercepts, X_T and Y_T, were transferred from the recording sheets to a desk-top microcomputer via a digitizer as shown in Figure 4.3-2. This data was directly stored on 8 in. soft-sectored floppy disks. After all of the data for a particular test was digitized, the microcomputer was used to reformat the digitized data into compact files and transmitted the files to a CDC 6600 mainframe computer via a telephone/modem link.

The remaining test data was interactively added to the test data files in the mainframe computer ready for the subsequent data analysis task; a sample test data file is shown in Figure 4.3-3.

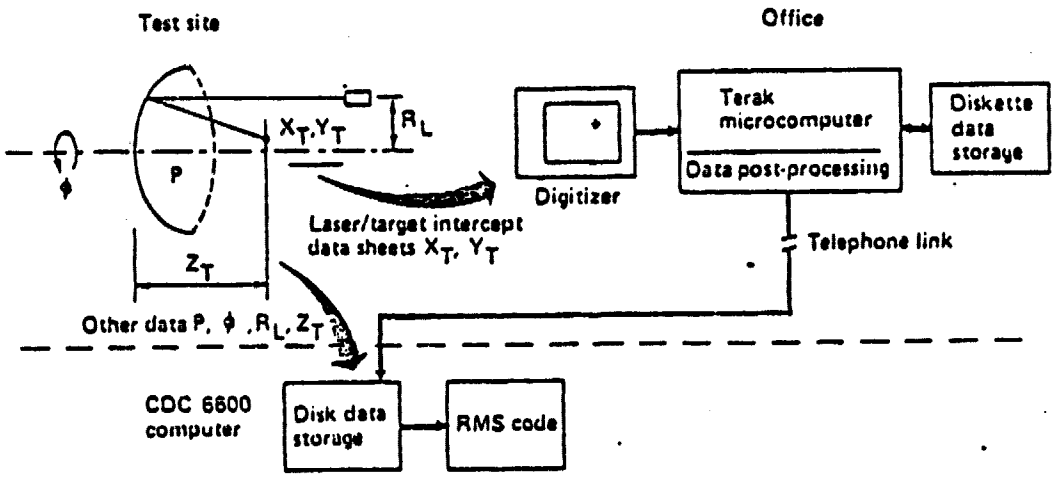

Figure 4.3-1. Test Data Processing

100

Figure 4.3-2. Laser/Target Intercept Data Recording Using a Digitizer

Reflector diameter

Reflector focal distance

```
 4.57        2.2859      3.          .012788     0.          1.
24  72
 0
 0   0   0   0
 0   0   0   0
.133         .203        .31         .414        .51         .723
.895        1.32        1.193       1.29        1.35        1.446
1.53        1.516       1.695       1.77        1.84        1.91
1.98        2.04        2.11        2.17        2.23        2.285
.66
ANGLE         5
-02190 -02030 -01340 -01750 -00350 -01350 -00190 -01250 -00370 -01360
-00920 -00640 -00540 -00750 -00153 -00670 -00820 -00590 -01330 -00110
-00990 -01070 -00758 -00120 -00760 -00140 -00820 -00290 -00840 -00420
-01410 -00640 -00910 -00890 -00550 -01110 -00100 -01250 -00520 -01350
-01450 -01440 -02910 -01520 -05110 -01550 -06540 -01740
ANGLE        10
-02280 -01550 -01370 -01050 -00410 -00790 -00080 -00840 -00310 -00810
-00780 -00660 -00500 -00913 -00140 -00890 -00690 -00930 -00900 -00860
-00750 -00880 -00680 -00630 -00670 -00560 -00610 -00640 -00510 -00160
-00390 -00230 -00210 -00320 -00180 -00210 -00700 -00450 -01210 -00650
-02100 -00920 -01320 -01060 -05240 -01340 -07740 -00510
ANGLE        15
-02510 -00760 -01510 -00320 -00410 -00220 -00120 -00370 -00150 -00
-00490 -00530 -00160 -00750 -00260 -00950 -00830 -00450 -01100
-00730 -00970 -00670 -00540 -00740 -00850 -00740 -00
-00530 -00930 -01150 -00970 -00500 -00970 -01310 -00
-01190 -00270 -04520 -00050 -04640 -00320 -29510
ANGLE        18
  ING -00230 -01390 -00130 -00580
      -00290 -00970 -00290
          -0 -00530
```

Laser/Target Intercept Data Recording Using a Digitizer

No circles, radii

Radial laser positions

in H_2O

Reflector rotation

Laser ray/target intercept coordinates

Figure 4.3-3. Typical Concentrator Test Data File

4.4 Test Data Analysis

Surface errors of the sub-scale reflector were analysed with the aid of a computer model referred to as the RMS code. This code allowed analysis of a large amount of test data to evaluate surface errors with options for consideration of (1) removal of systematic radial surface errors and (2) pertinent test data groups (best quadrant). The main features of the RMS code are shown in Figure 4.4-1; Figure 4.4-2 illustrates the coordinate systems and analytical parameters used in the code. The following discussion describes the analytical methods used in the RMS code.

Initially, the RMS code transforms the test measurements to the reflector coordinate system. A representative reflector projected area is calculated for each measurement. The best optical axis which is the centroid of data at the measurement focal plane is then calculated. To eliminate any test alignment problems the test measurements are corrected to coordinate through the best optical axis.

The angular error (2ε) between the actual and ideal reflected rays as shown in Figure 4.4-2 can be determined from the scalar product of the two reflected ray vectors:

$$\cos 2\varepsilon = \frac{\rho_\varepsilon \cdot \rho_o}{|\rho_\varepsilon|\,|\rho_o|}$$

The reflector surface error, ε, is half the reflected ray deviation. From Figure 4.4-2 we can determine the actual ray,

$$\rho_\varepsilon = \bar{f} + \bar{\varepsilon} - \bar{R}$$

and ideal ray,

$$\rho_o = \bar{f} - \bar{R}$$

Where $\bar{f}$ is the focal distance vector, $\bar{\varepsilon}$ is the error vector, and $\bar{R}$ is the radial vector to the reflector measurement point.

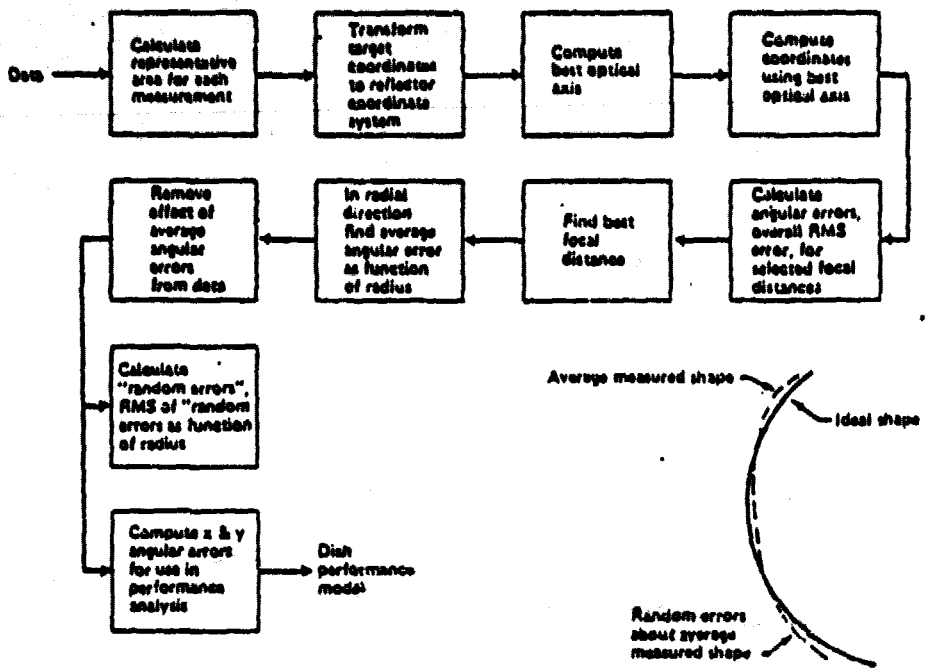

Figure 4.4-1. RMS Code

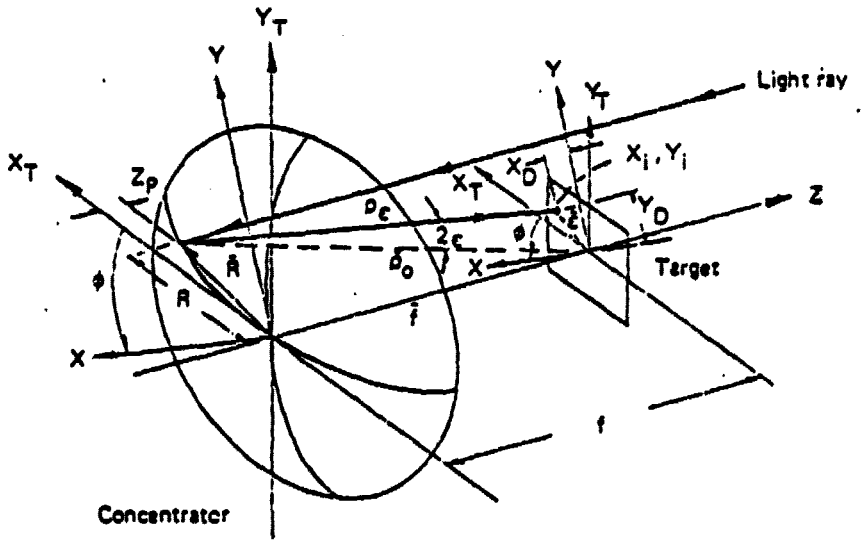

Figure 4.4-2. Coordinate System

Therefore,

$$\varepsilon = 1/2 \cos^{-1}\left(\frac{\rho_\varepsilon \cdot \rho_o}{|\rho_\varepsilon|\ |\rho_o|}\right)$$

$\overline{f}$, $\overline{R}$ and $\overline{\varepsilon}$ can be defined as

$$\overline{f} = f\hat{k}$$
$$\overline{R} = R\cos\phi\,\hat{i} + R\sin\phi\,\hat{j} + Z_p\hat{k}$$
$$\overline{\varepsilon} = X_D\hat{i} + Y_D\hat{j} + 0\cdot\hat{k}$$

Where f is the focal distance, R is the reflector radial distance to measurement, ϕ is the rotation angle of the reflector, Z_p is the Z component of $\overline{R}$. X_D and Y_D are the measurement coordinates that have been transformed into the reflector coordinate system and adjusted to the best optical axis.

Combining the above equations:

$$\varepsilon = 1/2 \cos^{-1}\left\{\frac{-(X_D-R\cos\phi)\,R\cos\phi-(Y_D-R\sin\phi)\,R\sin\phi-(f-Z_p)^2}{\left[(X_D-R\cos\phi)^2+(Y_D-R\sin\phi)^2+(f-Z_p)^2\right]^{1/2}\left[R^2+(f-Z_p)^2\right]^{1/2}}\right\}$$

The surface error angle, ε, is calculated for each measurement. An overall RMS value of the ε angles can be found using

$$\varepsilon_{rms} = \left(\frac{\Sigma\left[\varepsilon^2\ A_\varepsilon\right]}{A_{TOTAL.}}\right)^{1/2}$$

where A_ε is the projected concentrator area corresponding to the measurement from which ε was determined. A_{total} is the total concentrator projected area.

The ideal focal plane is found by calculating ε_{rms} for a series of planes. For each plane the ideal ray is projected to an assumed focal point at the best optical axis intersection with that plane.

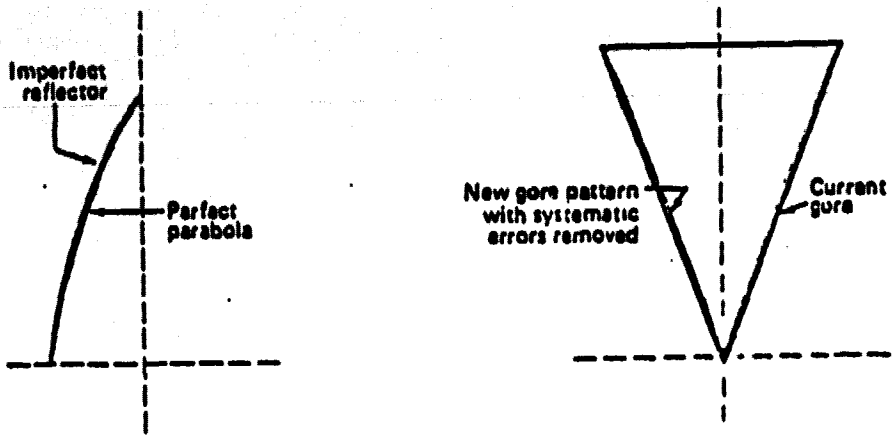

Figure 4.4-3. Removal of Systematic Reflector Errors

The intersection of the actual ray with the focal plane is determined. Individual surface errors and the overall RMS error is calculated at each focal plane, and the lowest value of the RMS error identifies the best focal plane.

The RMS code has the capability to remove radial systematic errors from the test data. This is done by calculating the average angular error in the radial direction and subtracting this error from the data. This is done for each radial section of the concentrator's test data. The result is a corrected random RMS surface error as a function of radius and an overall random RMS value. As part of a full scale reflector fabrication program, the gore template pattern would be modified to remove the first-order systematic errors. This would be accomplished as shown in Figure 4.4-3, by adjusting the gore offsets to correct the reflector's local circumferential distances to those of a perfect parabaloid.

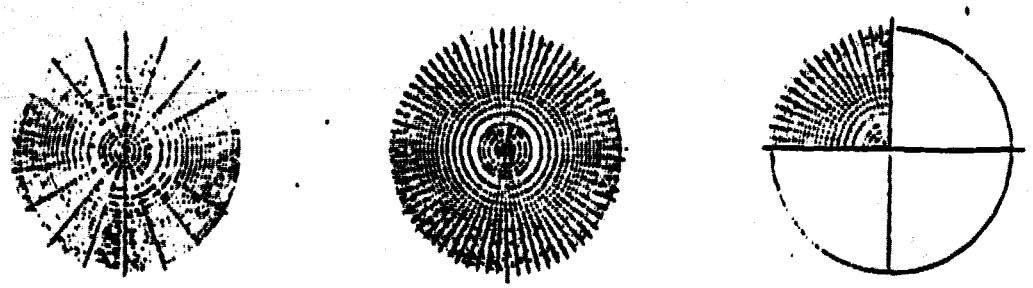

Random RMS = 4.31 mrad
Overall RMS = 5.78 mrad
Gore centerline measurements only

Random RMS = 5.52 mrad
Overall RMS = 7.57 mrad
Measurements for every five degrees around the mirror

Random RMS = 3.54
Overall RMS = 5.32
Best quadrant of 5 degree measurements

Figure 4.4-4. Surface Errors – 15 foot Concentrator

Surface error values are given in Figure 4.4-4, for three different cases: centerlines only, complete data set, and best quadrart. The centerline data is for the gores centerlines only. The complete data set was generated by taking measurements every five degrees. One quadrant seemed to have less error than others (see Fig. 4.2-9) so it was evaluated as a third case. Numbers given in Figure 4.4-3 are for random RMS with the radial systematic error removed, and overall RMS including all errors-systematic and random. Figure 4.4-5 shows the random errors as a function of radius.

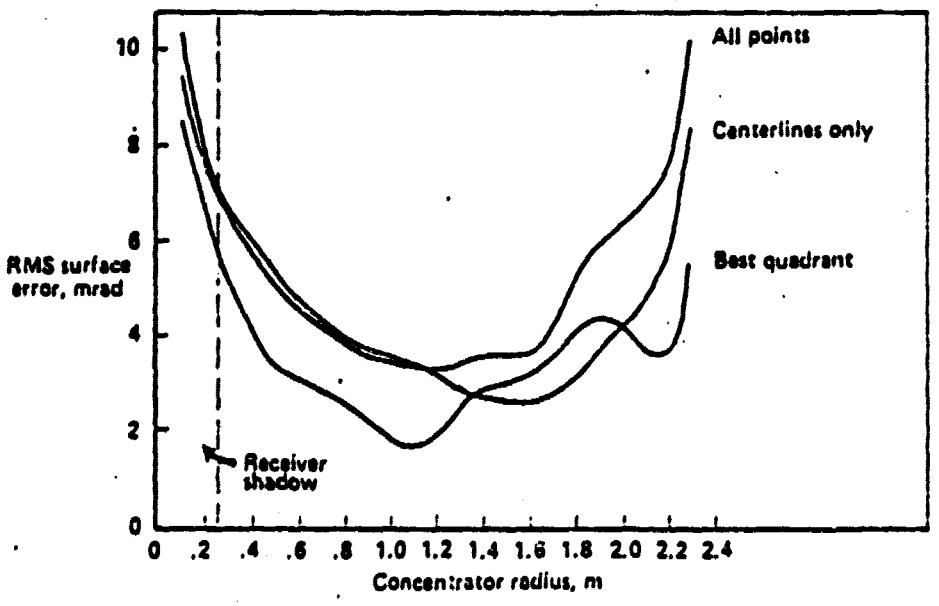

Figure 4.4-5. Surface Errors

The RMS code also creates a file of test data, with the radial systematic errors removed, which is an input to the performance model for performance predictions. This analysis is discussed in Section 5.2.

Table 4.4-6. Laser Ray Trace Uncertainty Analysis

Error source	Measurement	Estimated measurement error		Reflector surface error uncertainty	
		Average	Maximum	Average	Maximum
Laser/mirror angular misalignment	Laser reflection from mirror back to laser	0.1"	0.5"	0.33 mr	1.66 mr
Laser/mirror translational misalignment	Laser spot on mirror	0.03"	0.1"	0.15 mr	0.66 mr
Target/reflector misalignment	Laser reflection from target back to laser	2.0"	5.0"	0.04 mr	0.1 mr
Mirror/reflector misalignment	(Removed by RMS code)	–	–	–	–
Focal distance	Focal distance	0.02"	0.05"	0.05 mr	0.20 mr
Marking laser intercept on target	Visual center of laser spot	–	0.01"	–	0.05 mr
Coordinate matching on digitizer	Visual alignment	–	0.01"	–	0.05 mr
Positioning of digitizer cross hairs	Visual center of dot	–	0.002"	–	–
Internal accuracy of digitizer	–	–	0.015"	–	0.1 mr
			Root sum square =	± 0.4 mr	± 1.8 mr

An analysis was performed to evaluate the significance of test data uncertainties; the results of this analysis are summarized in Table 4.4-5. Nine sources of surface slope error were studied in terms of measurement errors, misalignment errors and equipment tolerances. An average root sum square value for surface slope error uncertainty is estimated to be +0.4 mrad; which is on the order of less than 10% of the computed surface slope error values given in test data analysis section (Section 4.4). An estimated upper bound on uncertainty is +1.8 mrad which is believed to be unlikely to have occurred.

5.0 CONCENTRATOR PERFORMANCE ANALYSIS

5.1 Performance Analysis Model

Performance, as measured by net energy into the receiver aperture, is predicted with the aid of a discrete ray tracing computer model. The model treats the various geometrical, optical, and system parameters that are important to performance. Basic model considerations are shown in Figure 5.1-1. A list of modeled parameters is given in Figure 5.1-2. Note that the model can use actual data for surface errors or a representative RMS value associated with a theoretical Gaussian error distribution of the surface slope.

A comparison with literature data indicates that the BEC performance model gives results that are comparable with those of other investigators. Comparison with a model developed by Dr. George Schrenk is shown in Figure 5.1-3 (Ref. 2). In the figure, the interception factors shown represent the amount of energy which goes into the receiver with respect to the amount of energy that is incident on the concentrator.

The performance model is based on a discrete idealization of the reflector, outlined in Figure 5.1-4 a,b,c,d. A grid is projected onto the parabolic reflector dividing it into elements. If actual surface error test data is being input, each element represents a test data point. The unit normal for each element is rotated according to surface slope and tracking errors. A cone of light representing a uniform intensity solar disk, is simulated by equal energy rays clustered around the unit normal. The amount of energy in the cone is determined by the solar intensity and the element area. The cone of light is reflected about the rotated unit normal and projected onto the receiver aperture grid at the focal plane. The computer model prints the resulting energy distribution map at the aperture, and computes the ratio of energy captured by the aperture to energy into the concentrator (interception factor).

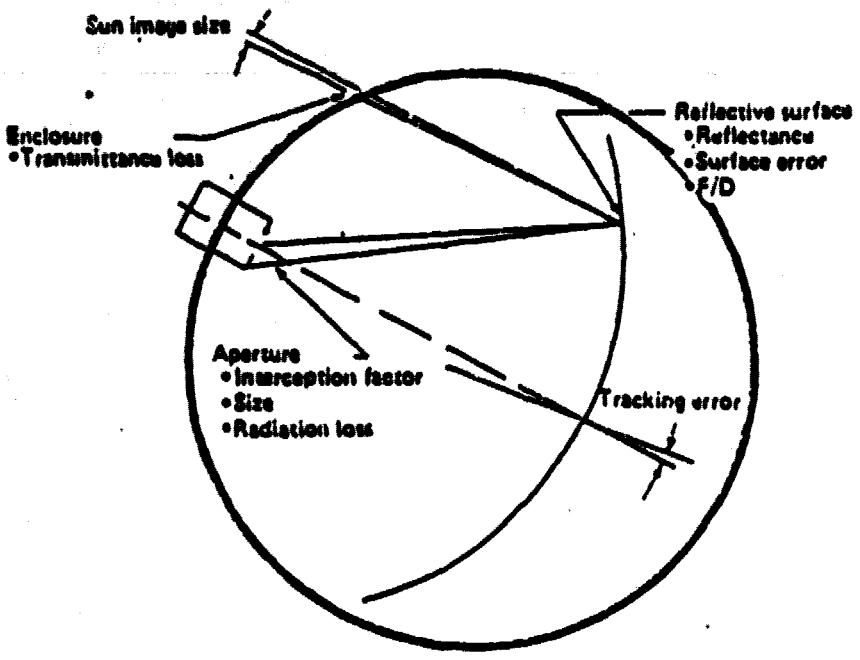

Figure 5.1-1. Performance Model Basic Considerations

- Reflective surface properties
- Reflective surface error
- Solar tracking error
- Focal length/diameter ratio
- Concentrator diameter
- Enclosure transmittance properties including dust effects on the external surface
- Enclosure size and location
- Aperture size and location
- Structural blockage
- Program option to accept test data

Figure 5.1-2. Performance Parameters Modeled

Figure 5.1-3. Comparison of Theoretical Interception Factors

r/R	BEC $\sigma_c = .002$ $\sigma_r = .002$	SCHRENK $\sigma_c = .002$ $\sigma_r = .002$
0	0	0
.001	.0148	.012
.002	.0625	.048
.003	.1185	.089
.004	.2024	.170
.005	.2898	.252
.006	.3868	.341
.007	.4757	.433
.008	.5582	.522
.009	.6333	.604
.010	.6962	.679
.011	.7518	.744
.012	.7936	.799
.013	.8272	.845
.014	.8527	.881

- σ_c = Circumference standard deviation
- σ_r = Radial standard deviation
- r/R = Aperture radius/concentrator radius
- Rim angle = 45°
- Tracking error = 0

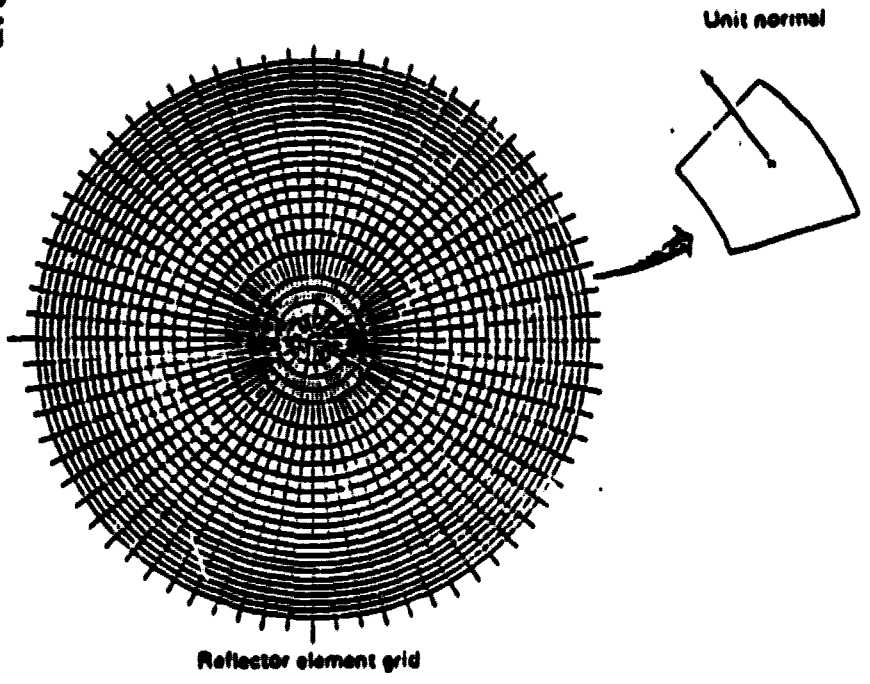

Figure 5.1-4a. Parabolic Reflector

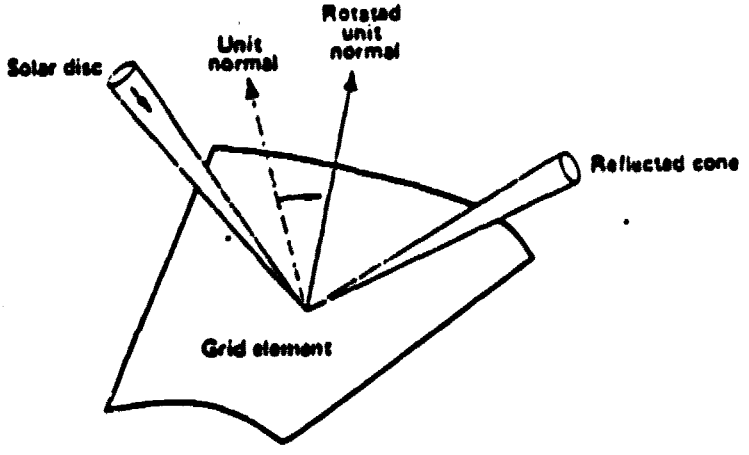

Figure 5.1-4b. Rotating Unit Normal

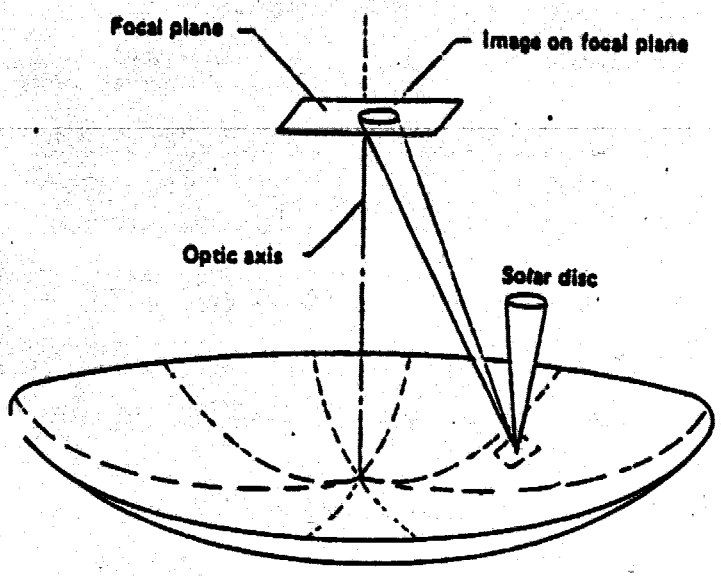

Figure 5.1-4c. Projecting Cone on to Focal Plane

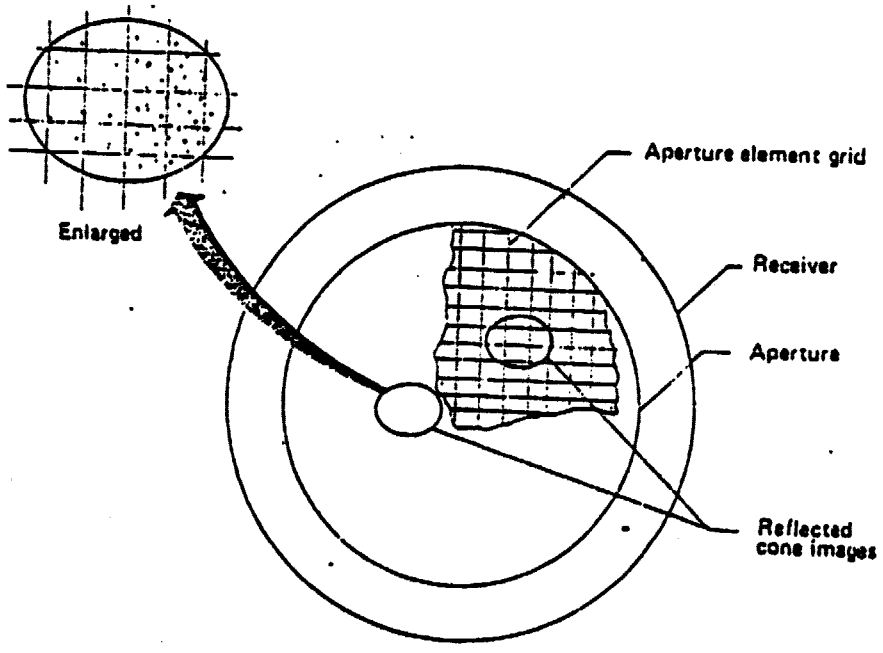

Figure 5.1-4d. Receiver and Aperture Details

113

Normally, performance is predicted assuming equal cone angles for incoming and reflected light. A study was done to determine the effect of an increase in reflected cone angle on performance predictions due to non-specular reflections. Figure 5.1-5 shows performance comparisons for various cases of reflectance and cone angles. The reflectance and added cone angles correspond to actual measurements of an aluminized polyester film made with the Boeing bi-directional reflectometer. For each case, one curve was generated using the performance model with a sun cone angle only; the other curves were generated with the reflectance cone angle increment added to the sun cone angle. These two cases should provide the lower and upper limits of the beam spreading effect. As indicated in Figure 5.1-5, the effect of beam spreading performance is minimal. A comparison was also made between actual surface error data and the representative theoretical RMS surface error value. Net energy is plotted versus the aperture radius/concentrator radius ratio for each case as shown in Figure 5.1-6. The differences that resulted are primarily due to the assumption of a Gaussian normal distribution for the theoretical surface errors. The actual surface errors are dominated by the periodic gore seams and edge mounting in perfections which should be accounted for in future theoretical modeling.

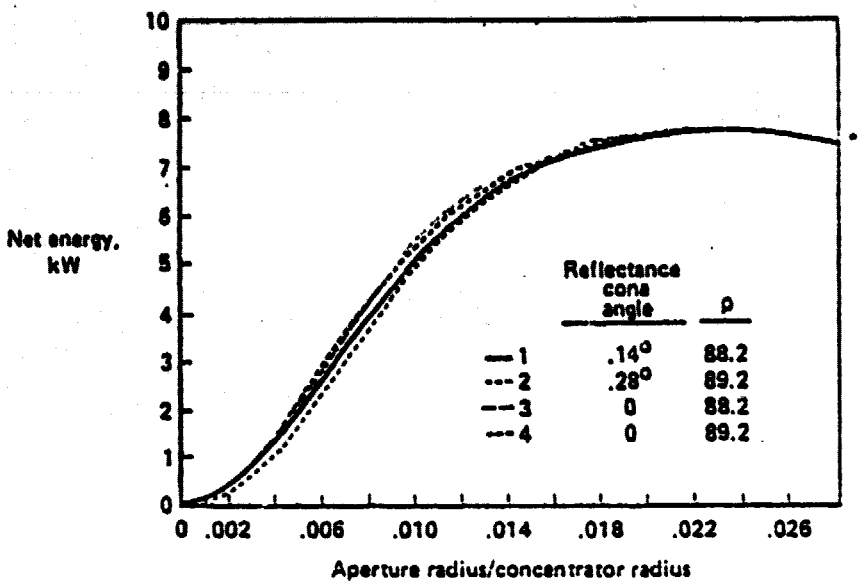

Figure 5.1-5. Reflectance - Cone Angle

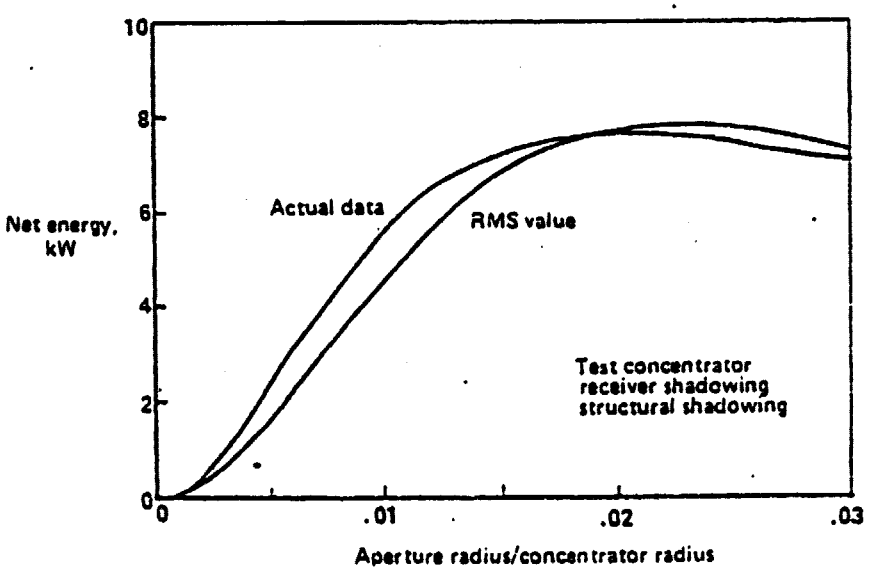

Figure 5.1-6. Actual Data with RMS Value

5.2 Performance Analysis Results

The following paragraphs describe the results of the performance analyses. The effects of several parameters are studied before discussing the final performance predictions.

Performance of the concentrator is influenced by the enclosure transmittance and reflector reflectance. The production design choices are Kynar for the enclosure, and aluminized Melinex 0 for the reflector. The effect of transmittance on performance is shown in Figure 5.2-1. The specular transmittance of Kynar is 0.91; based on other studies, the average long-term effects of soiling could reduce this to about 0.86. The range of performance for different reflector film candidates is shown in Figure 5.2-2. Since the relative effect on performance is minimal, the choice of reflector material is based primarily on other film characteristics, such as availability and durability.

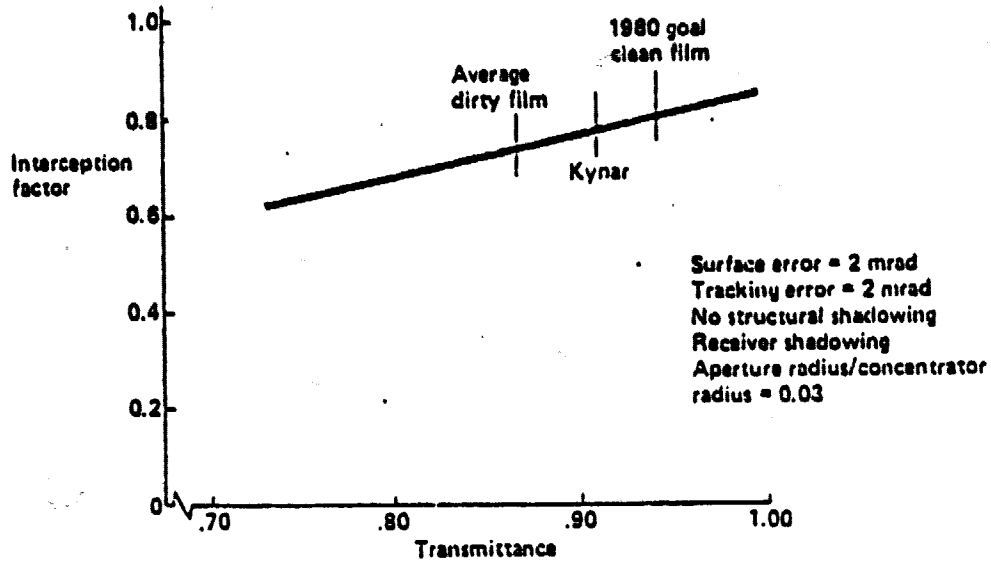

Figure 5.2-1. Enclosure Transmittance Effects

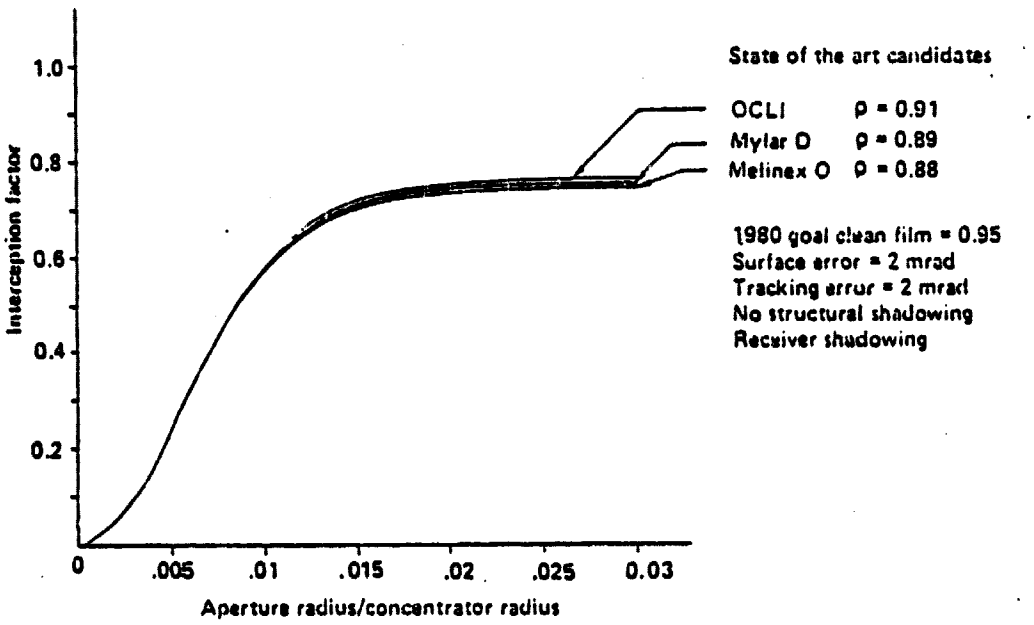

Figure 5.2-2 Reflective Surface Reflectance Effects

During Task I, two types of enclosure were considersd. Performance was affected by the type of enclosure (fixed or rotating), due to differing enclosure diameters. The incidence angle of the incoming light rays to the enclosure vary over the enclosure. Enclosure incidence angles are higher at the periphery of the reflector. The performance model treats the transmittance losses by a table look up procedure that relates transmittance to local incidence angle. Interception factors for the preliminary design enclosure size relative to the reflector diameter is shown in Figure 5.2-3.

Results from a sensitivity analysis of aperture axial location, Figure 5.2-4, indicate that the receiver can be supported by conventional steel truss structure without performance degradation due to thermal expansion.

Structural shadowing has a noticeable effect on concentrator performance, Figure 5.2-5. Shadowing for the production design is estimated to be 5%. This includes structural members, enclosure seams, reflector seams, and Brayton unit air supply lines.

The reflector focal length to diameter was optimized in Task I, as shown in Figure 5.2-6. The figure is the result of an aperture optimization procedure. Net energy into the aperture, incident energy minus the reradiated energy, was optimized for each F/D configuration. The optimum F/D data plot shows that performance reaches a plateau at about F/D=0.4 and reaches a maximum value at about F/D=0.5. The production design is selected to have F/D=0.5.

Predicted performance using actual test data is shown in Figure 5.2-7. Curves are shown for the complete test data set, and the best quadrant data as described previously in Section 4.4. The performance prediction for the production design goals of 2 mrad surface error and 2 mrad tracking error is in Figure 5.2-8. Figure 5.2-9 gives net energy versus surface and tracking errors. This data was developed by an optimization procedure similar to that used in the F/D optimization study. Concentrator performance fall-off due to surface and tracking errors is predicted to be small up to respective values of 2 mrad.

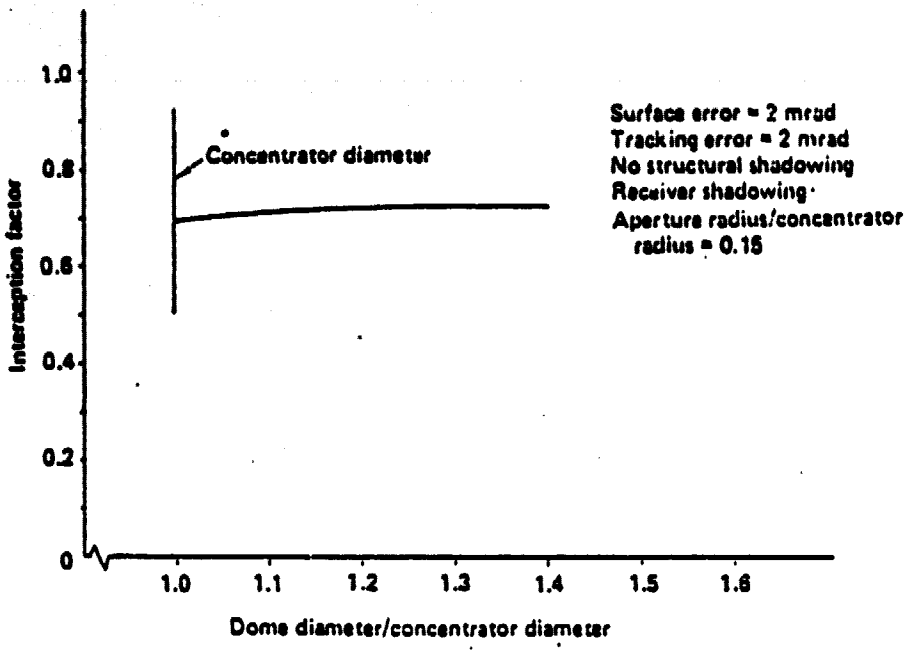

Figure 5.2-3. Effect of Enclosure Reflector Diameter Ratio

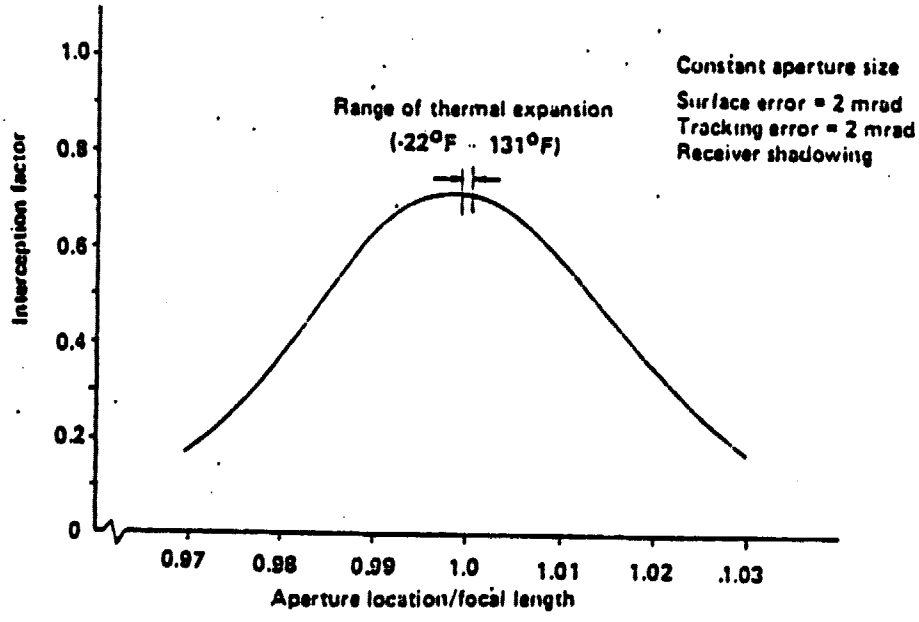

Figure 5.2-4. Effect of Aperture Location

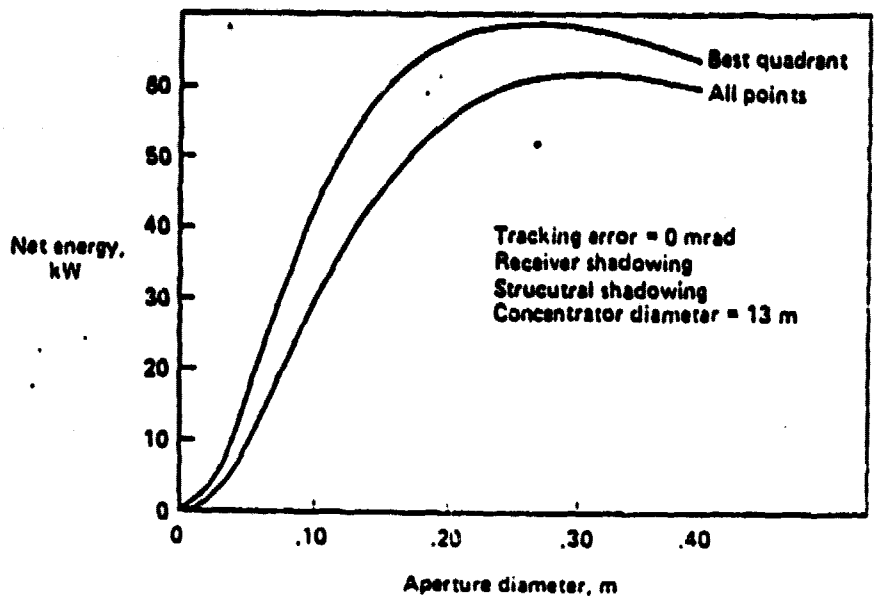

Figure 5.2-7. Predicted Performance Using Test Data

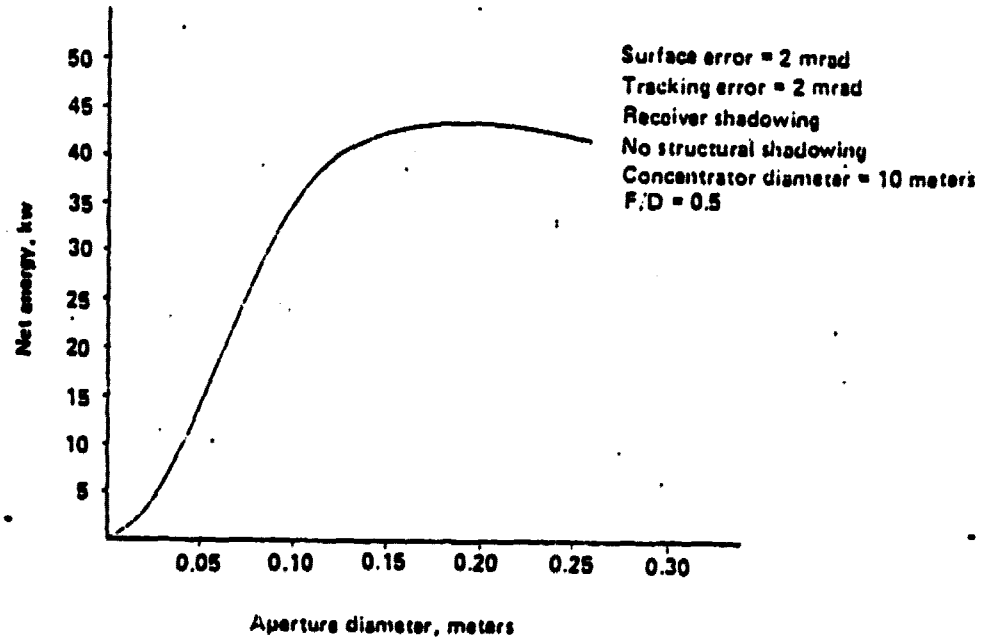

Figure 5.2-8. Net Energy Into Aperture Versus Aperture Diameter

120

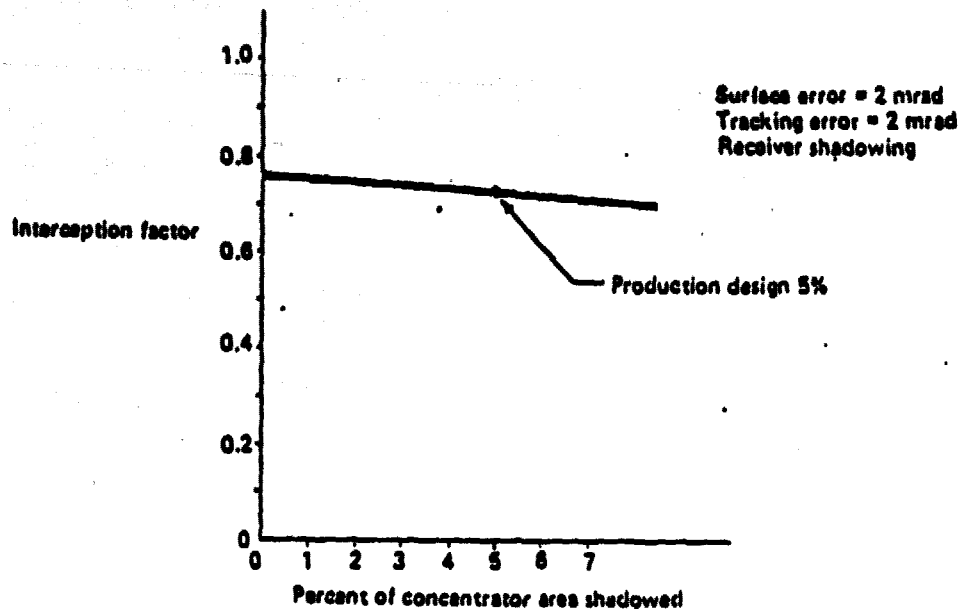

Figure 5.2-5. Effect of Structural Shadowing

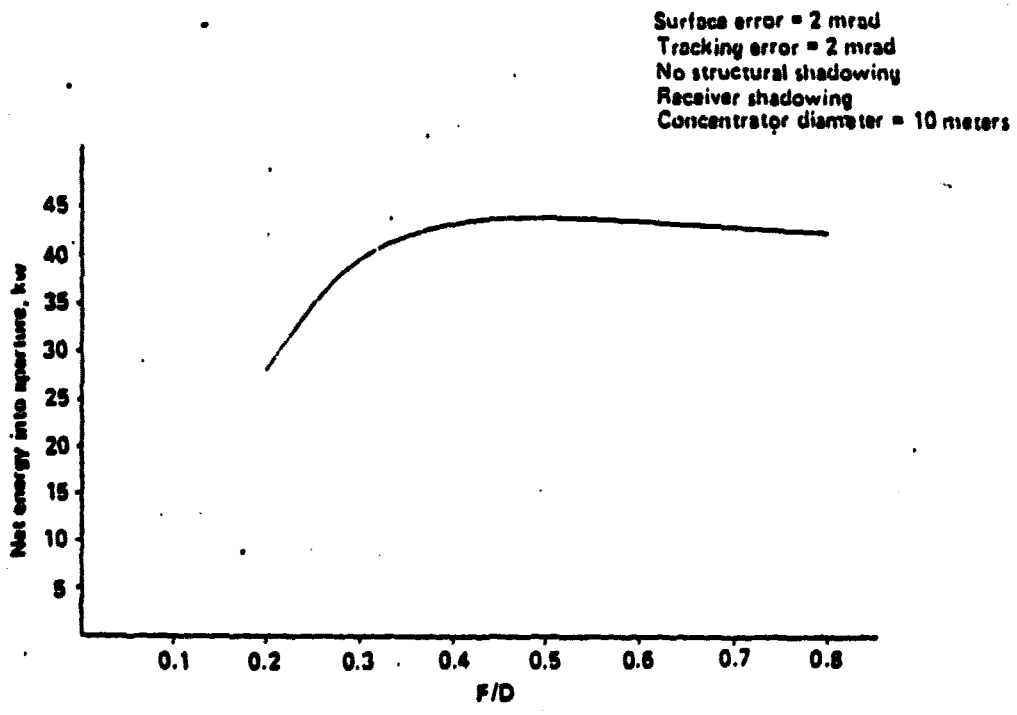

Figure 5.2-6. Net Energy into Aperture Versus F/D

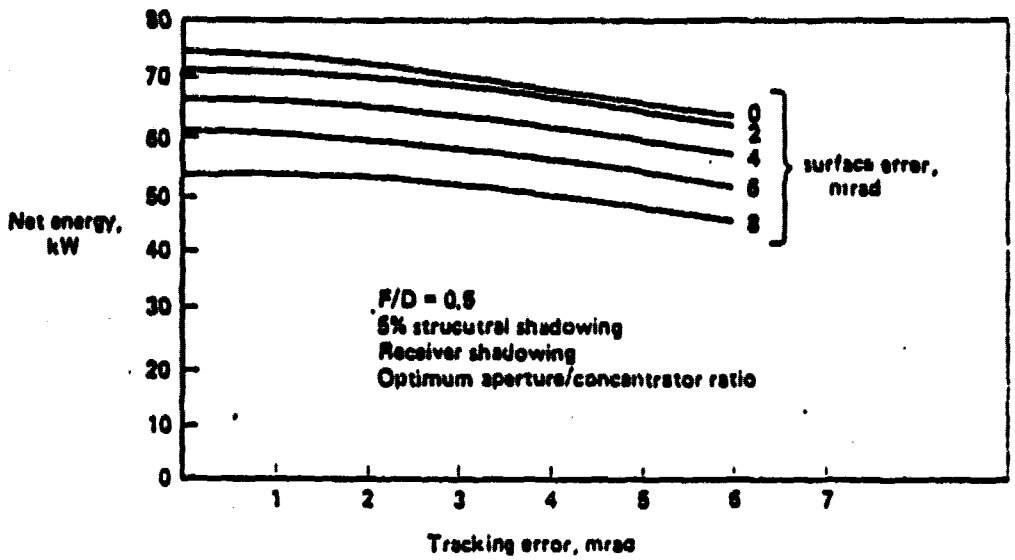

Figure 5.2-9. Net Energy Versus Surface and Tracking Errors

6.0 CONCENTRATOR ECONOMIC EVALUATION

Conceptual design, planning and economic studies were performed to determine mass-production costs, life cycle costs and performance/cost ratings for the preliminary concentrator design. These studies, described in this section, involved conceptual design of a plant for producing 100,000 units annually, production cost estimates, field installation and maintenance cost estimates, and economic parameter evaluations.

6.1 Production Plant

The steps followed in the production plant design are illustrated in Figure 6.1-1; these steps are discussed in the following sections.

The design approach for the physical plant consisted of developing design objectives for the building and then relating those objectives to the physical plant design required to produce 100,000 solar concentrators per year. These design objectives are listed in Figure 6.1-2.

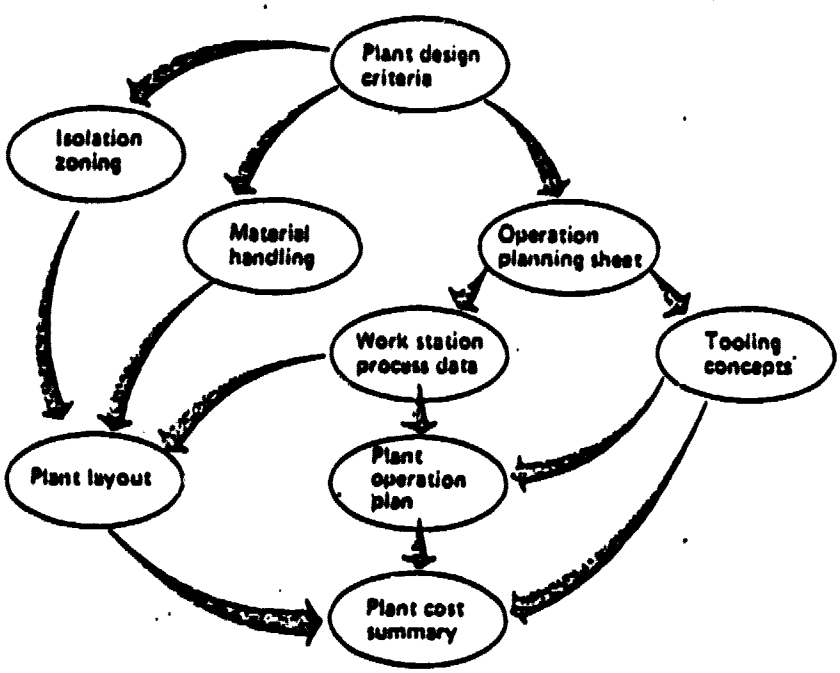

Figure 6.1-1. Plant Design Approach

- High production rate goal: 2.1 min/unit
  - 100,000 concentrators/year
  - Computer controlled automation
  - Inprocess quality control
  - Linear flow production
  - Uniform containerization

Figure 6.1-2. Plant Requirements

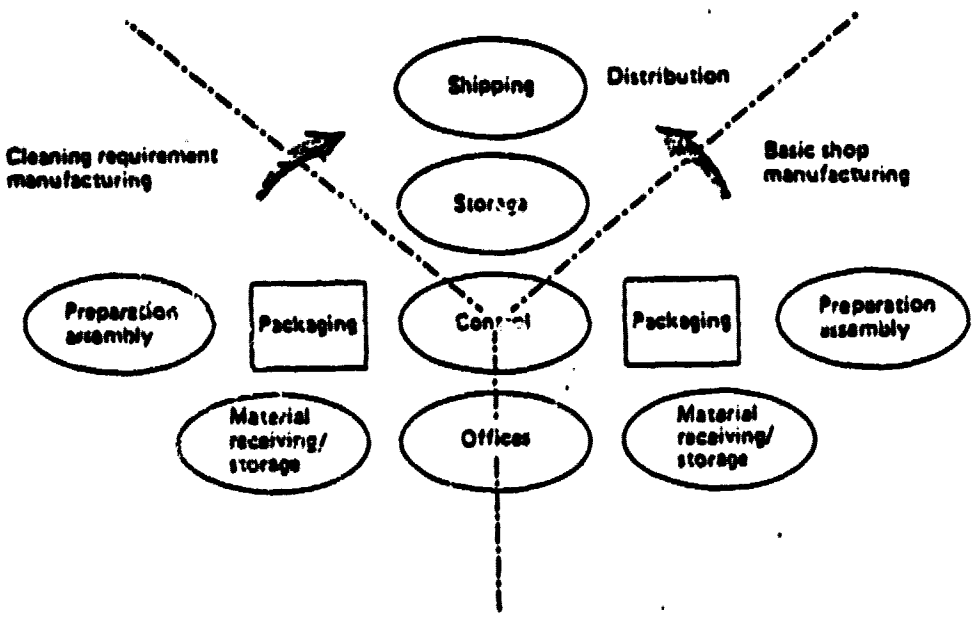

Figure 6.1.1-1. Isolating Zoning

6.1.1 Isolation Zoning

As shown in Figure 6.1.1-1. the plant was divided into two manufacturing areas of differing cleanliness requirements and a distribution area. The three areas have support activities of administration, computer control, final storage, and shipping. In this zoning concept, material receiving/ storage, material preparation, manufacturing assembly, and packaging for the plastic concentrator components with clean manufacturing requirements were on one side of the common support activities while the conventional manufacturing activities for the other structural, mechanical and electrical components were located on the opposite side of the building.

This would allow a separation of activities that would meet the different levels of cleanliness and allow the raw materials to flow into the factory on one side, become assembled within the building, and finally exit the other side of the factory as a solar concentrator ready for shipping.

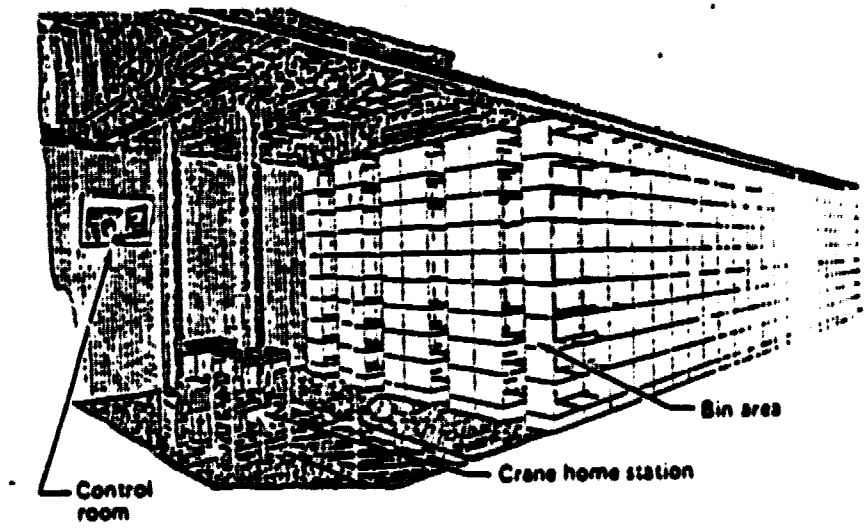

Figure 6.1.2-1. Related Automated Material Handling Equipment Application

6.1.2 Material Handling

Cook-Newhouse and Associates, Inc. conducted a preliminary analysis of the material handling requirements. Their analysis included the square footage, manloading, and equipment costs needed to support a high speed production rate. In order to have a 100,000 concentrators per year production rate, a computer-controlled material handling inventory system was conceptually designed. This type of system exists and is being used successfully throughout the manufacturing industry as illustrated in Figure 6.1.2-1.

After selecting the equipment based on the nature of the items being handled, the system would be programmed to synchronize the receiving/inventory/ distribution of the raw materials and parts with the production requirements of each manufacturing line all the way through to packaging and distribution of a solar concentrator.

The receiving/inventory/distribution building area for raw materials is designed for a 30 day inventory of materials and parts. Another 15 days of material and parts would be in transit from suppliers or in production. While only trucking delivery is illustrated in our conceptual layout, it is recommended that the factory be located on a rail siding.

The same material handling equipment that distributes the material and parts to the manufacturing lines will also pick-up the waste material from the manufacturing areas and dump them in respective waste hoppers. Waste materials can then be recycled for their salvage value although the volume of waste material is expected to be very small.

The final height of the building in this area would be based on a study to optimize vertical storage costs versus horizontal building costs as they relate to material handling equipment cost.

Building areas associated with the containers are stacked container storage areas, cleaning and maintenance area, and along the packaging lines. Externally, on the receiving and distribution sides of the building, container storage and handling areas are provided on the loading and unloading docks.

Containerized shipping, as illustrated in Figure 6.1.2-2, provides a concept for packaging that will facilitate the required high production rate as well as provide weather tight transportation and field storage benefits. Therefore the development of uniform containers that will fit on a standard 45 foot-long trailer will be essential to the manufacturing process. One container would pass down one side of the factory and the clean manufactured items would be placed in it while a second one would pass down the other side of the factory and the shop manufactured items would be placed in it. The containers can be color coded for easy identification as to their correct side of the factory. The flow of the containers would also be part of the material handling program so that they would phase in with each manufacturing line. At the distribution end of the building a container from each side of the factory would be stacked together and then placed on a truck trailer. With the activation of quick hold-down devices, the trailer, holding two containers that are housing the components for one solar concentrator, would be ready for shipping. From the dock the trailer would be towed to a staging line ready for connecting to a truck tractor and transported to a field site. With one solar concentrator per truck/trailer, logistic inventorying and monitoring of the concentrator while in transit is very simple.

The frequency of truck/trailer departures would be 28 per hour, for 14 hours of plant production hours. Since the trailers depart from a staging line, the truck departures could be spread over a 24 hour period, thereby reducing the frequency of departures to 16 per hour. With the high level of truck traffic, the demand for punctual departures will require a dedicated truck/trailer transportation system. With the diversity and remoteness of the site locations, rail shipments of the concentrators do not seem practical.

A returning truck will pick up two empty containers and return the trailer and containers to a staging line on the receiving side of the factory. From there the trailer is towed over to the building where the containers are off loaded by an over-head travel lift, then they are deposited onto a chain-drive, live roller conveyor and sent into the building for storage. From stacked storage the containers are called out as needed for production.

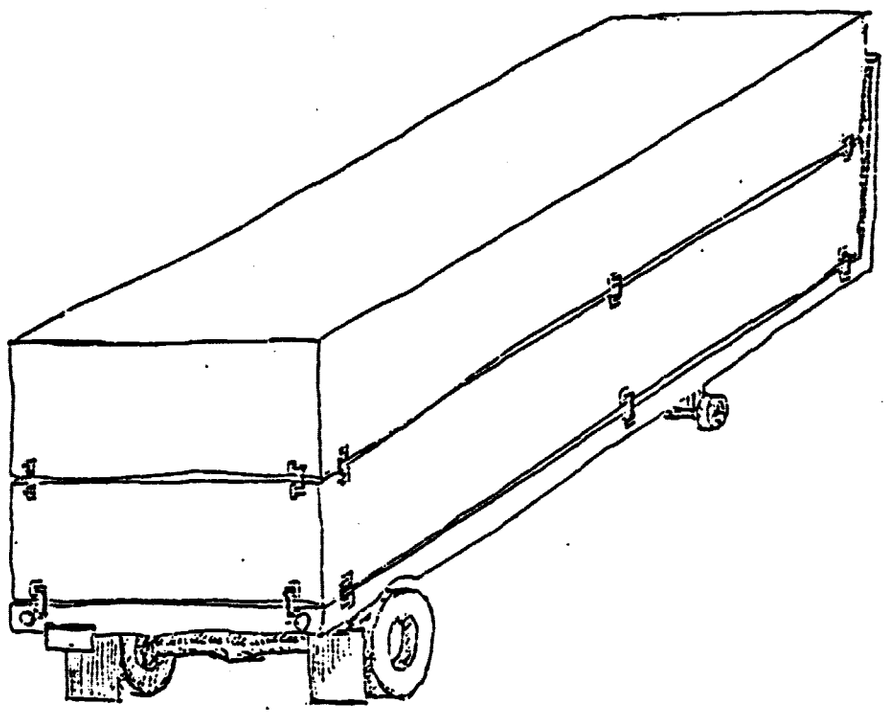

Figure 6.1.2-2 Shipping Containers

Before entering the manufacturing area the containers pass through a car wash type, cleaning environment and then inspected for necessary repairs.

6.1.3 Operation Planning

A basic work sheet was developed and is shown in Figure 6.1.3-1; this sheet allowed the association of all items and components of the solar concentrator with the required manufacturing processes of each item or component.

On the left hand side of the worksheet parts were quantified and identified. Next the parts were analyzed as relating to activity flows. This was broken down into a receiving column that identified if the part/component was a make or buy item. Secondly if the item required quality control before being assembled or after being assembled. Next, cleaning requirements were identified.

Following that, subassembly activities were identified. The last three considerations of part flow identified packaging, storage, and shipping requirements. Next the worksheet listed part sizes and weights which inter-relate with the equipment size and the number of work stations to determine the building area required.

The production rates per work station were estimated from the tooling design and dictated the number of work stations needed to meet the 100,000 unit/yr. quota. Plant production days for a five day work week are 250 days, this allows for ten holidays per year. Assuming 14 hours of production per day that will require the completion of a solar concentrator every 2.1 minutes. The manloading is divided into three categories; process, maintenance, and material handling. The required process manpower includes personnel for tooling, small part assembly, container recycling, and computer control. Maintenance manpower will overlap between different tools and will include vehicle mechanics, electricians, and metal workers. The manpower needed for material handling was estimated by Cook-Newhouse and Associates. A basic factory concept was then developed from the part requirements as listed on this worksheet.

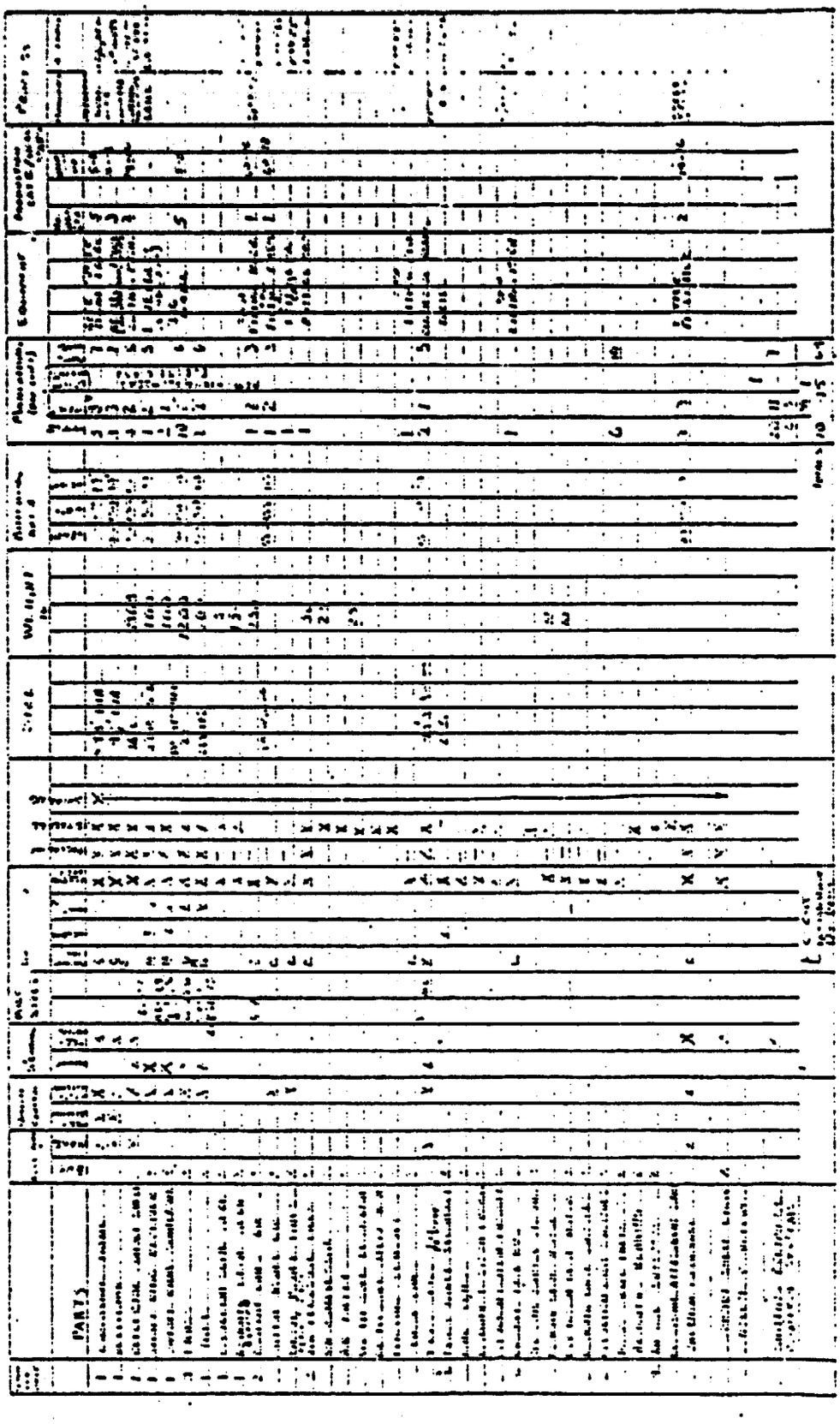

Figure G.1.3.1. Production Work Sheet

Key part	Production rate/work station (units/hr)	No. of work stations	Manloading per work station	Work area sq. ft.
Enclosure dome Fabrication & test	6-8	6	1	100,000
Reflector Cutting Fabrication & test	10-15	3	1	15,000
Vacuum membrane Cutting Fabrication & test	14-16	2	1	15,000
Reflector support shell Material construction	14-16	2	1	15,000
Misc fabrication				587,500
Total building area				732,500

Figure 6.1.3-2. Plant Operations Plan for Unique Parts

Figure 6.1.3-2 summarizes the key parts to be manufactured within the factory and their plant operational factors. From this operational planning, the building area and volume requirement for the manufacturing activities were determined along with tooling requirements.

6.1.4 Tooling Concepts and Costs

The operation planning study identified three work stations that can be classified as unique, important to production rate, and requiring tooling development.

These fabrication areas are: reflector film, reflector support shell and enclosure. A brief design study was then conducted to define the respective tooling concepts and related costs.

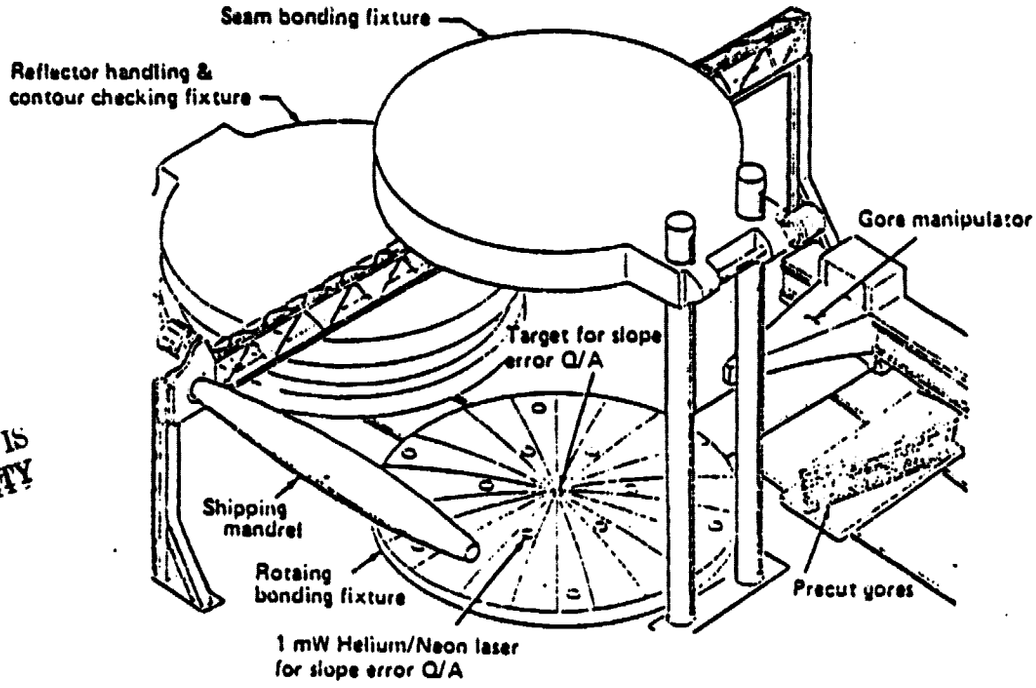

Figure 6.1.4-1. Reflector Fabrication Tooling

The reflector fabrication workstation concept is illustrated in Figure 6.1.4-1. and has the following features. Pre-cut gores (cut elsewhere on high-speed roller die equipment) would be placed on a rotating bonding mandrel by a computer-controlled gore manipulator arm. After all gores are placed on the mandrel and held by vacuum, a seam bonding tool would be lowered onto the reflector; this tool would apply tape to the reflector seams. A handling fixture would then be used to (1) lift the reflector, (2) apply a vacuum to the rear side and (3) hold the reflector for a quick laser surface quality check. The completed reflector would then be rolled on a collapsable shipping mandrel.

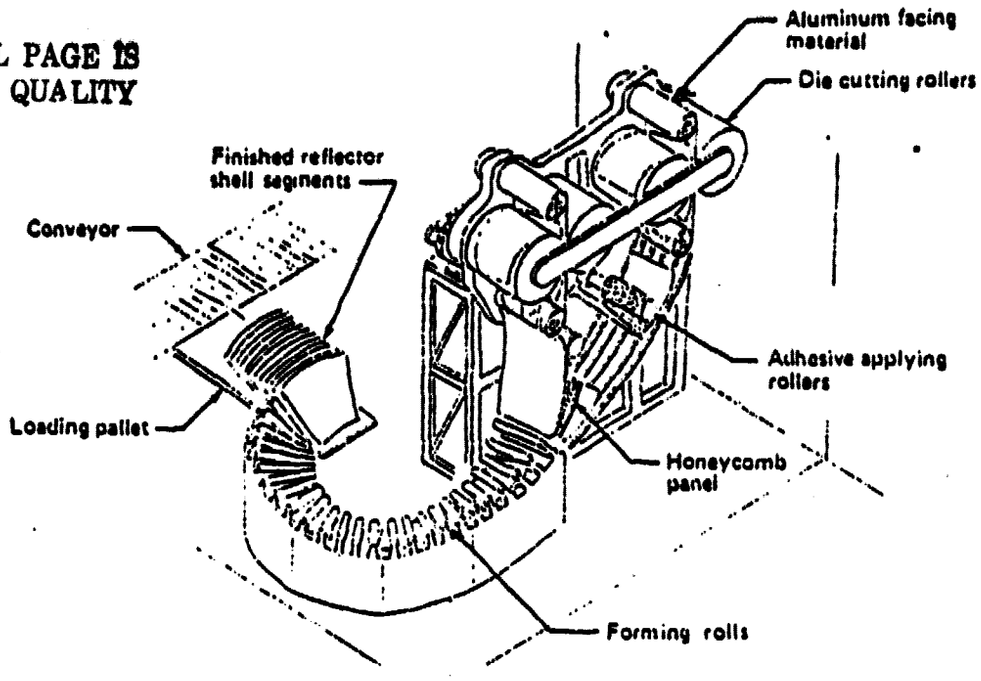

Figure 6.1.4-2. Reflector Shell Segment Fabrication

The honeycomb panels for the reflector support shell would be fabricated in an automated workstation as illustrated in Figure 6.1.4-2. The process is envisioned to be continuous, starting with aluminum coil stock and kraft paper hobes and ending with bonded and trimmed panels. Forming rollers would shape the panels during adhesive bonding and also feed the panels past edge trimming routers.

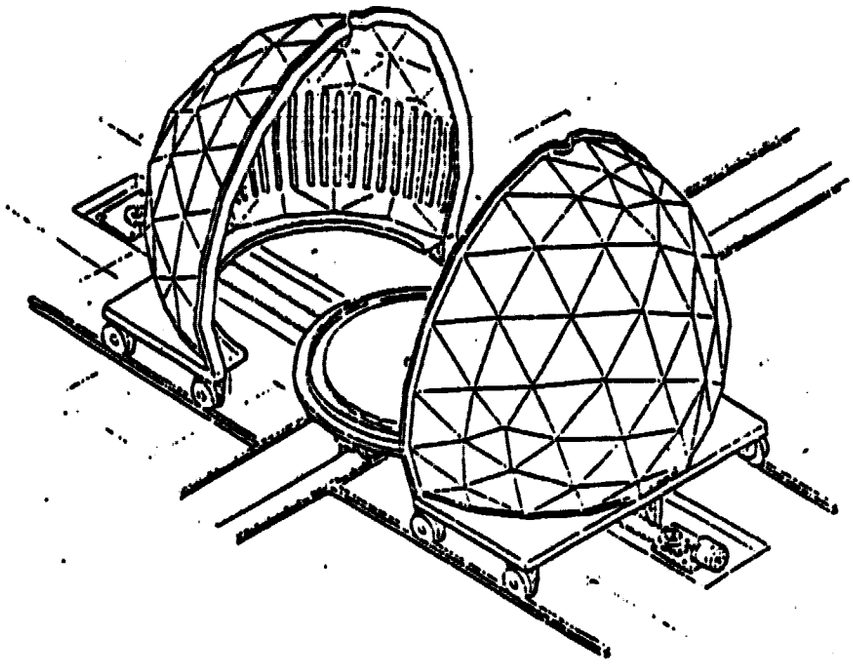

Figure 6.1.4-3 Heating/Blowing Chamber

Two methods of enclosure fabrication were studied: thermoforming and gore-forming. In the thermoforming method, which is being researched in a current Sandia Laboratories Contract for heliostat enclosures (Ref. 4), flat plastic sheets would be heated and blown into spherical shape. Figures 6.1.4-3 and -4 show a split heating chamber tooling concept for enclosure thermoforming that was identified in previous preliminary heliostat studies (Ref.5). The current thermoforming research is directed at the development of a process involving blank pre-heating and transfer to a heating chamber as illustrated in Figure 6.1.4-5 . After blowing, the required side seam and edge and door retention beads would be applied in a separate heat sealing process and then the completed enclosure would be packaged for shipment. In this process, material moves through the workstation in an essentially continuous manner. Results from this program will be published in a future report.

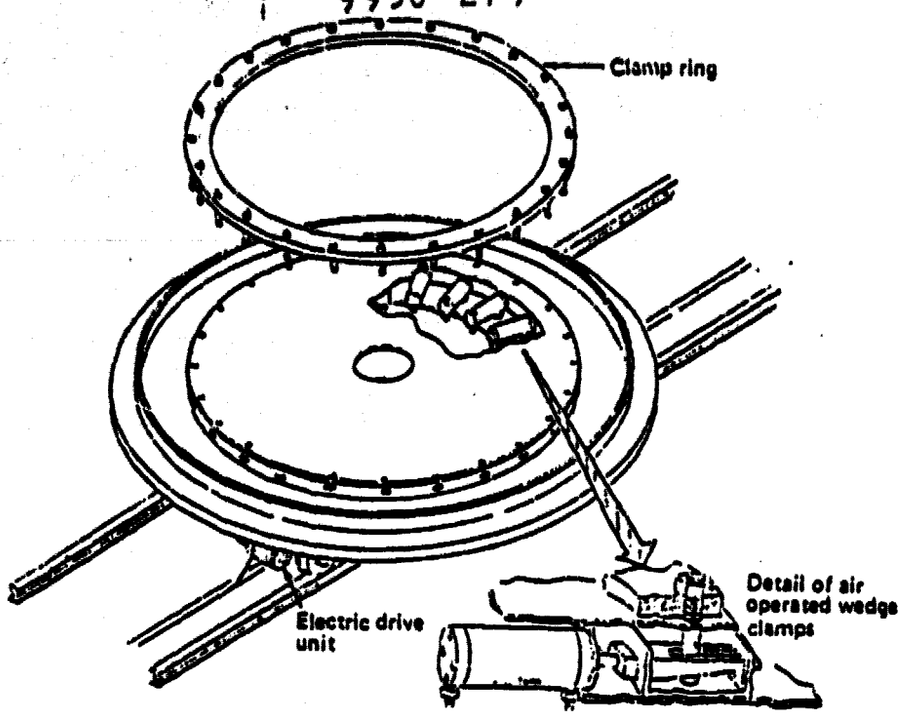

Figure 6.1.4-4. Thermoform Blank Holding Fixture

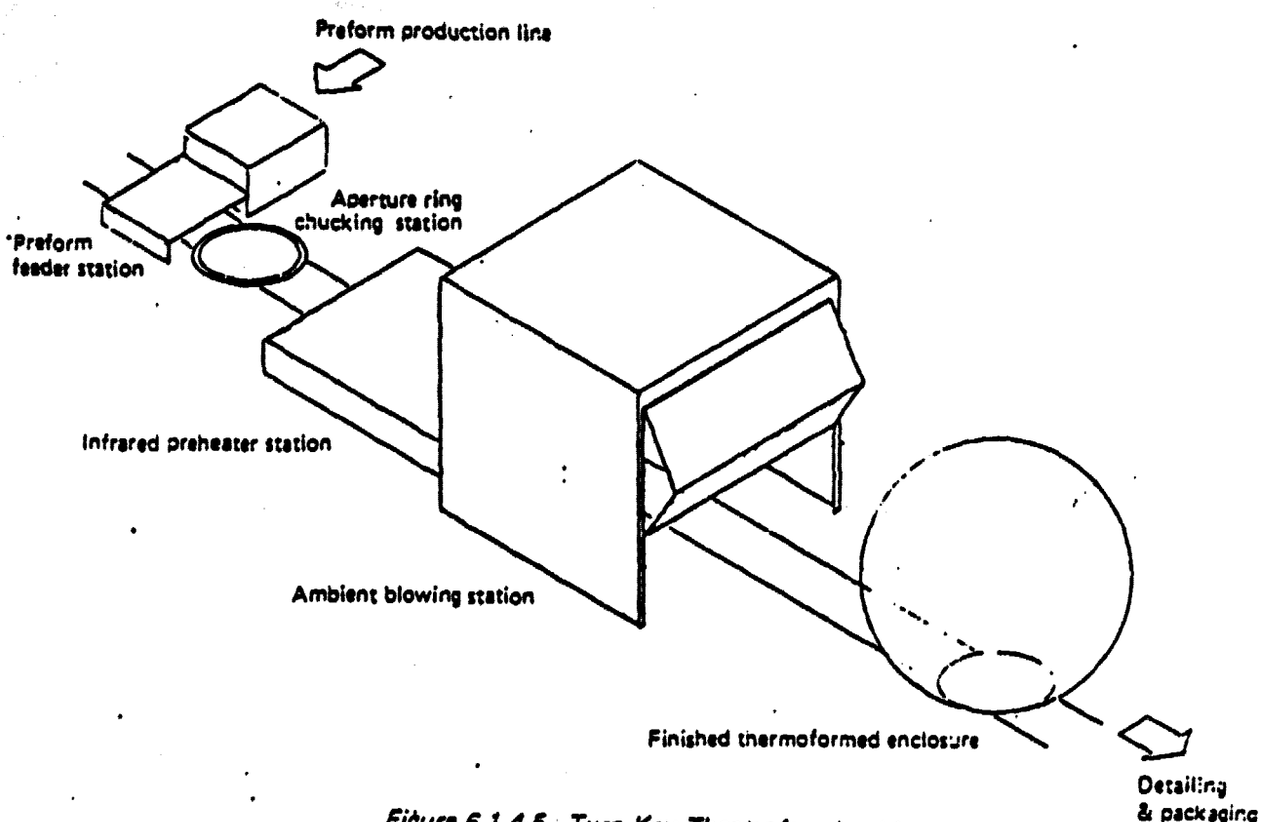

Figure 6.1.4-5. Turn-Key Thermoforming Line

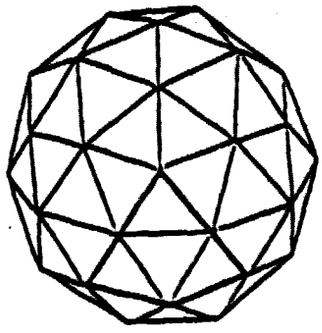

Figure 6.1.4-6. Enclosure Gore Icosahedron Configuration

In the gore-forming method, the enclosure would be built up from a number of geometric panels. One configuration that results in minimal trim scrap is called an icosahedron (from the Greek word for a twenty sided regular polygon) and is illustrated in Figure 6.1.4-6. This type of enclosure would be fabricated on a rigid rotating mandrel using dual material manipulator arms such as shown in Figure 6.1.4-7. The computer-controlled arms would cut the gore pieces, position the gores on the mandrel and perform seam heat-sealing in a smooth sequence of operations. While on the mandrel, automated tooling would also apply side seams and edge bead reinforcements on the enclosure prior to packaging for shipment.

Based on prototype heliostat domes delivered to Boeing by Sheldahl, no difficulties are anticipated in packaging the enclosure for shipping. Figure 6.1.4-8 shows a concept for removal of a completed dome from a fabrication mandrel; as the enclosure is pulled into a shipping container, rollers would promote gentle folding.

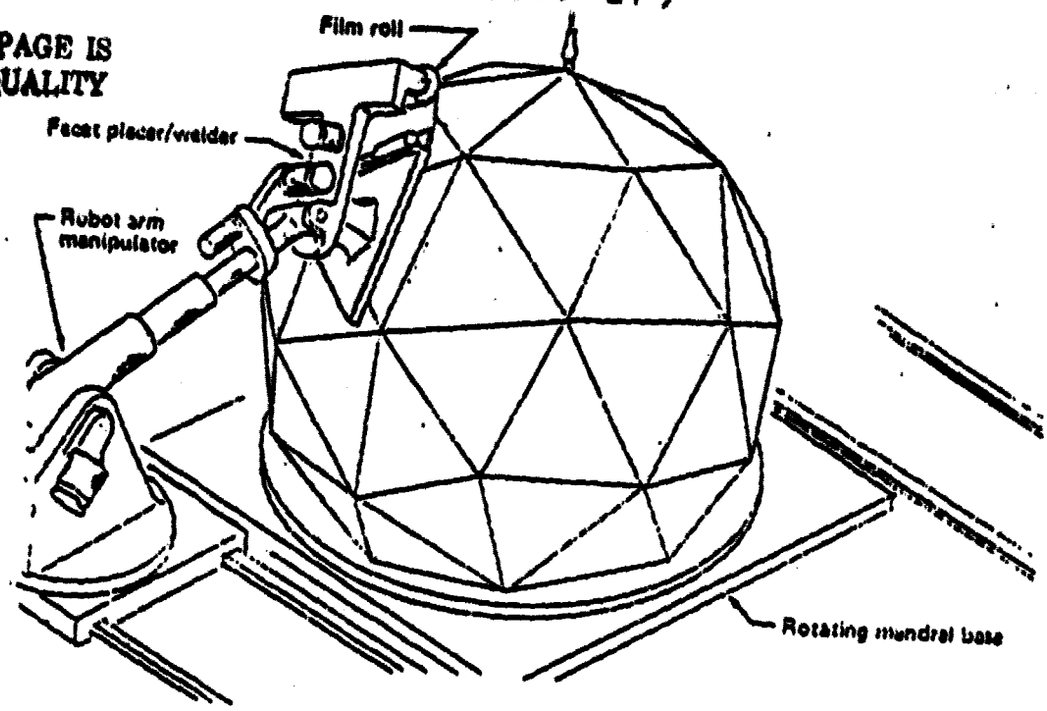

Figure 6.1.4-7. Enclosure Fabrication Tooling

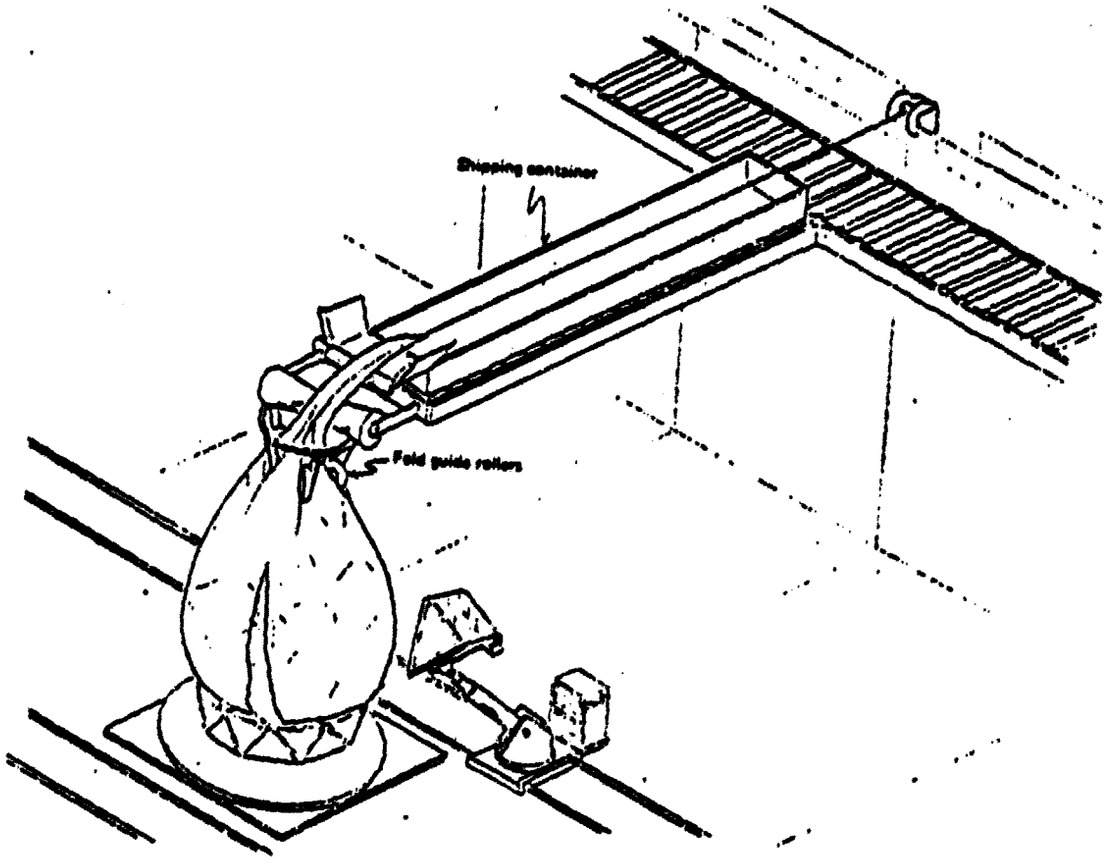

Figure 6.1.4-8. Enclosure Packaging

Table 6.1.4-1 presents a summary of costs for the two candidate enclosure fabrication methods. The main cost driver is material cost which is significantly different between the two methods. The thermoformed method has higher cost because of thickness variation. In a current Sandia Contract (Ref. 4) BEC has blown small Kynar and polyester domes. Thickness variation observed in these small experimental domes was used for this cost comparison study. On this basis, the thermoformed production enclosures were assumed to have thicknesses of 21 mil at the base and 7 mil at the top (where the maximum film loads occur). Consequently, the thermoforming process shows higher material cost due to excess material near the base. This material excess is expected to be reduced in future research in which techniques such as variable-thickness blanks, controlled local heating and variable blowing operations will be studied to achieve uniform enclosure thickness.

The material costs shown in Table 6.1.4-1 are based on material quantities of 741 lbs. for thermoforming and 460 lbs. for gore-forming. Material unit costs were obtained from Westlake Plastics and are $6.00/lb. for thermoforming blanks and $5.00/lb. for gore-forming film stock (7 mil); the higher unit cost is due to special extrusion equipment needed for the large, thick thermoforming blanks. Workstation labor and production rates were determined from operation planning, as discussed in Section 6.1.3, and the equipment costs resulted from tooling cost estimates similar to those described in the following pages. Based on the large difference in total unit costs shown in Table 6.1.4-1, the gore-formed fabrication method was selected for the production enclosure and the method assumed for the following tooling and part cost analysis (Sections 6.1.4 and 6.4.1).

Table 6.1.4-1. Thermoforming Versus Gore Forming Comparisons

	Material cost ($/unit)	Manloading (man/work station)	No. of work stations	Production rate (units/hr/sta)	Total labor cost ($/unit)	Equipment cost $/unit (w/design hrs)	Total unit cost ($/unit)
Thermoforming							
Total mat'l incl. Trim waste credit	4,447 4,257	1	4	7.00	4.29	8.78	$4,301
Gore forming							
No trim waste	2,300	1	5	6.00	5.00	18.92	$2,324

Notes: No rejects
100,000 units/year for 7 years
$30 labor cost

The selection of gore forming for the enclosure fabrication method results from several considerations:

- Near-term enclosures would have to be gore-formed since it will be some time before facilities for thermoforming 15 m enclosures will be available.
- Several vendors have indicated they have existing capabilities to fabricate enclosures by gore-forming.
- Kynar, with its high material unit cost, governs the total enclosure fabrication cost if thermoforming thickness variations are assumed to occur.

The selection of the thermoforming process could occur as a result of:

- Progress in current thermoforming process research to achieve uniform enclosure thickness.
- Further study of tooling concepts and costs.
- Availability of a low cost, inherently stable polyester film material.

The tool fabrication and installation hours were estimated from the preceding sketches by a Boeing tooling estimator. A "wrap-around" cost rate of $30/hr. was used to convert the estimated hours into fabrication and installation dollars. The material costs were based on a varying % of the total fabrication cost. To establish these individual percentages, the amount and type of raw material required for a tool, as well as the tool sophistication was considered.

The miscellaneous details listed in the item column include electrical and hydraulic equipment. As stated the tool design cost was calculated as 33% of the total fabrication cost.

Cook-Newhouse and Associates, a materials handling consultant, analyzed the material handling requirements for a production rate of 100,000 concentrators/year. The cost estimate submitted by Cook-Newhouse and Associates was added to the total tooling cost.

Table 6.1.4-2. Tooling and Plant Material Handling Equipment

Item	Tool fab & install. hrs	No. of lines	Rate ($/hr)	Total fab cost ($)	Mat'l cost ($)	Total cost
Enclosure	42,400	8	30.00	6,510,000	124,000	6,634,000
Reflector	30,000	3	30.00	2,700,000	150,000	2,850,000
Reflector support shell	15,000	2	30.00	900,000	60,000	960,000
Truss/yoke fab	18,000	6	30.00	1,800,000	100,000	1,900,000
Laser cutter	2,000	1	30.00	60,000	10,000	70,000
Electrical & air line fab	1,000	2	30.00	96,000	15,000	111,000
Vacuum membrane	4,000	2	30.00	240,000	40,000	280,000
Misc details	10,000	1	30.00	300,000	100,000	400,000
				12,606,000		13,206,000
Tool design (@ 33% of fab)				4,158,980		4,158,980
				16,706,980	600,000	
Total tooling						17,364,980
Automatic plant material handling system						7,571,380
Total cost						$24,936,360

Tooling and plant material handling equipment costs are summarized in Table 6.1.4-2. The tool fabrication and installation hours were estimated from the preceding sketches by a Boeing Aerospace Company tooling estimator. A "wrap-around" cost rate of $30/hr, was used to convert the estimated hours into fabrication and installation dollars. The material costs were based on a varying percent of the total fabrication cost. To establish these individual percentages, the amount and type of raw material required, tooling complexity, and degree of automation were considered.

The miscellaneous details item includes electrical and hydraulic equipment needed for the "conventional" metal working workstations. (such as yoke fabrication). A factor of 33% was used to cover tool design and installation supervision costs. Material handling equipment was a major cost item as discussed in Section 6.1.2. The cost total shown in Table 6.1.4-2 is the figure for tooling and equipment used in the cost analysis discussed in Section 6.4.

6.1.5 Plant Layout

The conceptual plant layout shown in Figure 6.1.5-1 is the culmination of the preceding activities and it brings together the interplay of the different processes as they relate to the manufacturing production rates. The original objective of isolating the manufacturing requiring a clean environment from standard shop manufacturing is achieved in the conceptual layout by the packaging container flow through the plant. On either side of the container storage and cleaning area are the material receiving/distributions area required for their associated manufacturing areas. The small parts storage and distribution area is conceived as less automated than the other material handling areas and also functions as the tool room activity for the manufacturing areas.

The clean manufacturing area is divided up into a low bay area of about 30 feet and a high bay area of 70 feet. In the high bay area the enclosure dome is manufactured in five lines. Adjacent to the enclosure dome area is the low bay area where the reflector is produced in three lines and the vacuum membrane is produced in two lines. Also cable bundling and the pneumatic hoses are assembled on this side of the factory. Additional area is reserved here for equipment repair, circulaiton, and expansion.

The conventional shop manufacturing area is a low bay area also 30 foot high. This side of the factory will handle the yoke, truss, and reflector shell fabrication. Additional area is also reserved on this side of the factory for circulation, damaged part repair, and expansion.

The control area is combined with the office area and located adjacent to the shop manufacturing area. From this position there can be visual control as well as electronic control of the manufacturing process. The offices are intended to be a two story area housing supervision, administration, and engineering functions.

With the quantity of truck and trailer traffic required for the distribution of the solar concentrators, area on the property is provided for minor truck/trailer repairs, servicing, and cleaning.

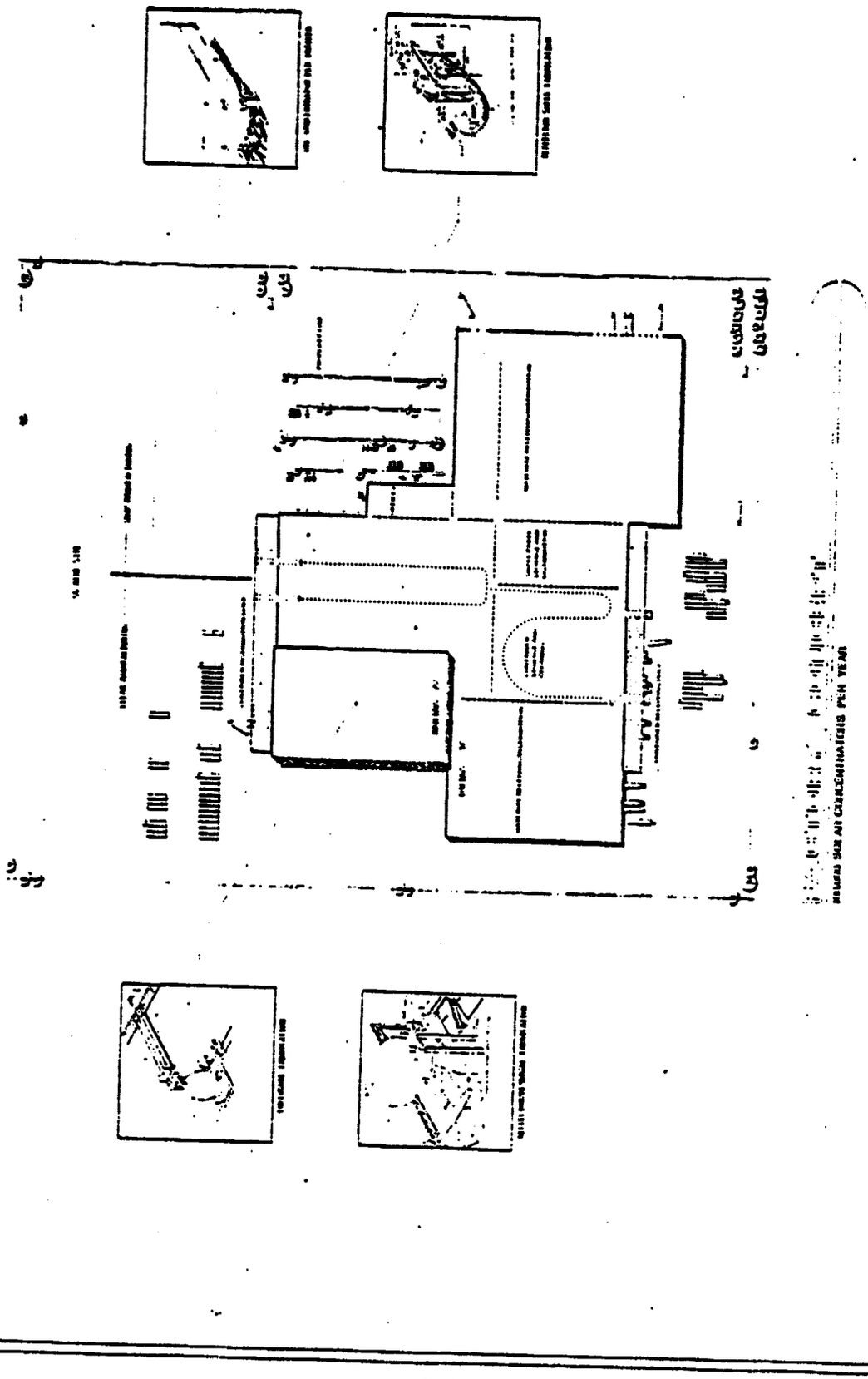

Figure 6.1.5-1. Factory Concept – 100,000 Solar Concentrators Per Year

142

6.1.6 Building Cost Summary

Costs for building, land and site improvements are summarized in Table 6.1.6-1. It should be noted that costs do not include tooling and equipment costs which are used along with the building costs, in the cost analysis section (Section 6.4).

For a representative site, the plant was assumed to be located in Tucson, Arizona. Industrial land in Tucson, is currently costing $85,000 to $110,000 per acre depending on how close it is located to the new IBM plant in the south-east portion of the city. North-west of the city there is desert land that could be developed into a 55 acre site for the factory. This land is undeveloped and is priced at approximately $85,000 per acre.

The size of the site is a function of the factory building area, required truck and auto parking, and circulation roadways. It is planned for the trailer parking area to also serve as a temporary water run-off retention area. In the conceptual site layout, trailer parking on the receiving side of the building is based on 150 trailers, which allows a five hour shut-down of the receiving line. On the distribution side of the building, the trailer parking is based on handling 14 hours of production without any shipments. Including roadways, a rectanglar parcel of land for site development would be required.

The site improvement cost shown in Table 6.1.6-1 was determined by estimating parking and roadway areas, security fencing, guard houses, and utility installations.

Table 6.1.6-1. Building Cost Summary

Item	Area	Cost
Site land	55 ac	$4,675,000
Site improvements		1,642,000
Building		
High bays	100,000 sf	8,250,000
Low bays	632,500 sf	24,114,000
Subtotal		38,681,000
Engineer/design (@6%)		2,320,860
Total cost		$41,001,860

Building costs are based on the cubic foot costs of two somewhat similar factory buildings currently being constructed by Boeing in the Seattle area. The construction cost index for Tucson and Seattle are relatively close with Seattle being a little higher, so that no adjustment was made to the Seattle based cost factors.

Architectural and engineering design fees for this type of project could range from 4% to 6%; 6% was assumed in the building cost analysis.

6.2 Field Installation

Installation of the concentrators was studied for a typical field of 50 units. In order to have low field installation costs, the following ground rules were assumed:

- Field installation will be done by specialty contractors with a minimum of personnel.
- On-site temporary storage will be provided by the concentrator shipping containers.
- The concentrator electrical and mechanical components will be pre-assembled to the truss and yoke members.
- The equipment skid will be pre-packaged.
- Critical reflector assembly operations will be done under temporary, clean shelter using special portable fixtures.
- Temporary shelters will be needed for reflector and enclosure installations in windy conditions.
- Concentrator functional checkout and controller tracking corrections will be done with portable service equipment.

The planned sequence of installation operations are illustrated in Figure 6.2-1. These operations as well as field preparation and clean-up are itemized in Tables 6.4-2 and 6.4-3 of the cost analysis section (Section 6.4).

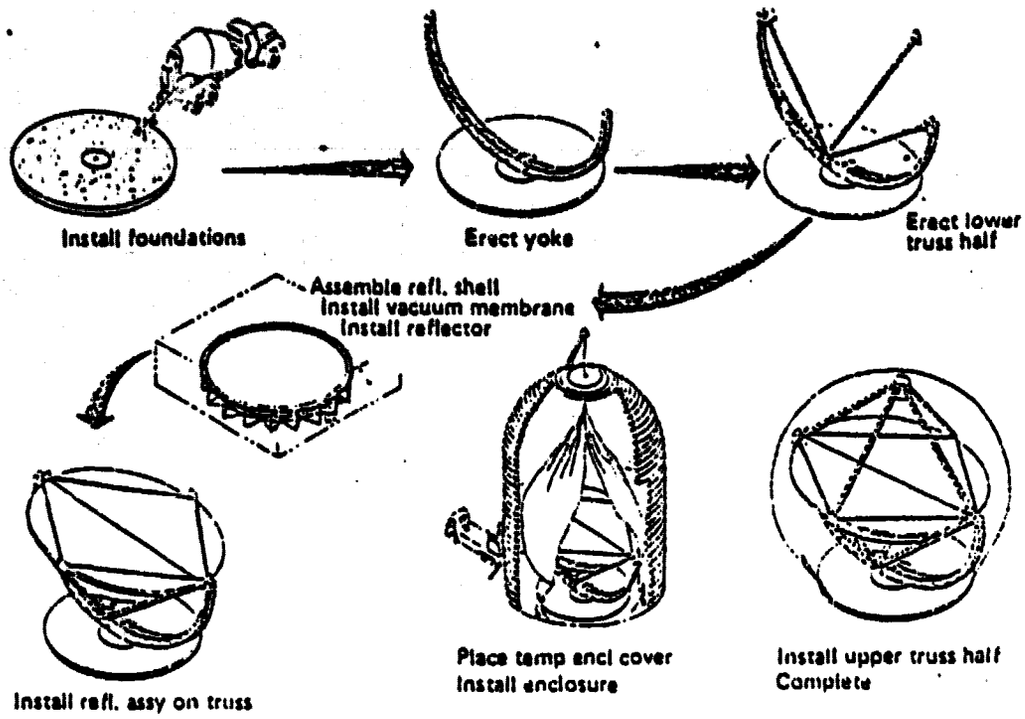

Figure 6.2-1. Field Installation Events

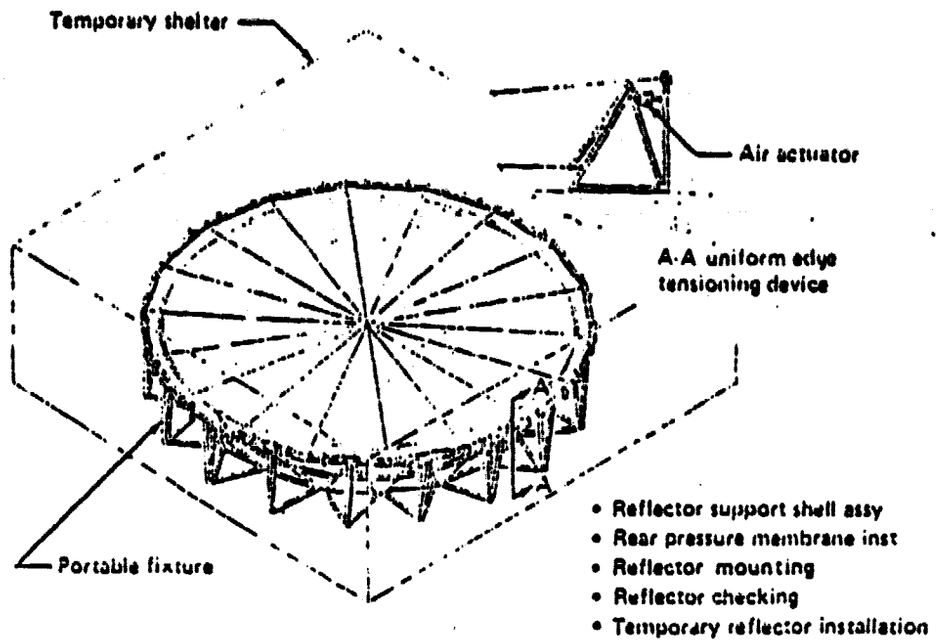

Figure 6.2-2. Reflector Field Assembly Fixture

A critical field operation is assembly of the reflector. Figure 6.2-2 shows a concept for a portable fixture that will be used for:

- o Reflector support shell assembly
- o Rear vacuum membrane installation
- o Reflector film installation
- o Reflector checkout

The reflector film is installed by first unrolling the part from a shipping mandrel onto vacuum hold-downs. Air actuated grips would then hold the reflector in proper position while a vacuum is drawn behind the reflector.

Portable laser ray trace equipment would be used to quickly check surface quality. The reflector would then be fastened to the support shell with a heat-sealing adhesive. A temporary cover can then be used to protect the reflector during movement from the assembly shelter to concentrator installation site.

Because clean and calm conditions are needed for installation of the reflector assembly and enclosure, a pneumatically stabilized portable shelter is included in the field installation plans. The shelter would be light and would be guyed to adjacent foundation pads for stabilization against wind.

147

6.3 Maintenance

Table 6.3-1 shows the maintenance requirements, frequency, and cost, for a concentrator during its 30-year life. This includes one enclosure replacement, and an average washing frequency of once every 3 weeks. The annual maintenance cost of one concentrator is $263. The following three figures show the major maintenance requirements being carried out.

Table 6.3-1. Concentrator Maintenance Costs

Function	Service	Repair	Replace	Unit labor		Unit mat'l cost	Equip and supplies	Cost subtotal	Freq years	% of units	Total cost/yr
				Hrs	Cost						
Air supply system											
Blower			X	1	12	125	–	137	8	100	$13.7
Prefilter			X	.25	3	3	–	6	1	100	6
Final filter			X	.25	3	30	–	33	2	100	15.4
Diff press controls (2)			X	2	24	75	–	99	10	100	6.6
Solenoid valves (2)			X	2	24	60	–	84	10	100	5.6
Check valves	X			.5	6	–	–	6	10	100	.4
Exhaust valves	X			.5	6	–	–	6	10	100	.4
Flexible ducting			X	3	36	60	–	96	15	100	3.2
Truss & yoke system											
Bearings (3)	X			1	12	2	–	14	1	100	14
Gear reducers (2)	X			1	12	5	–	17	5	100	2.8
Enclosure		X		4	48	5	–	53	10	5	.27
Enclosure			X	8	96	2,211	19.5	2,326.5	15	100	77.8
Reflector alignment check	X			.2	24	–	15	39	10	100	2.6
Update controller	X			.5	6	–	–	6	3	100	1.8
Washing enclosure	X			.33	4	1.07	1.42	6.49	3 wks	100	112.5
									Total yearly maintenance cost/unit		262.9

- 50 units/field
- Labor rate $12/hr
- 30 year operational life

148

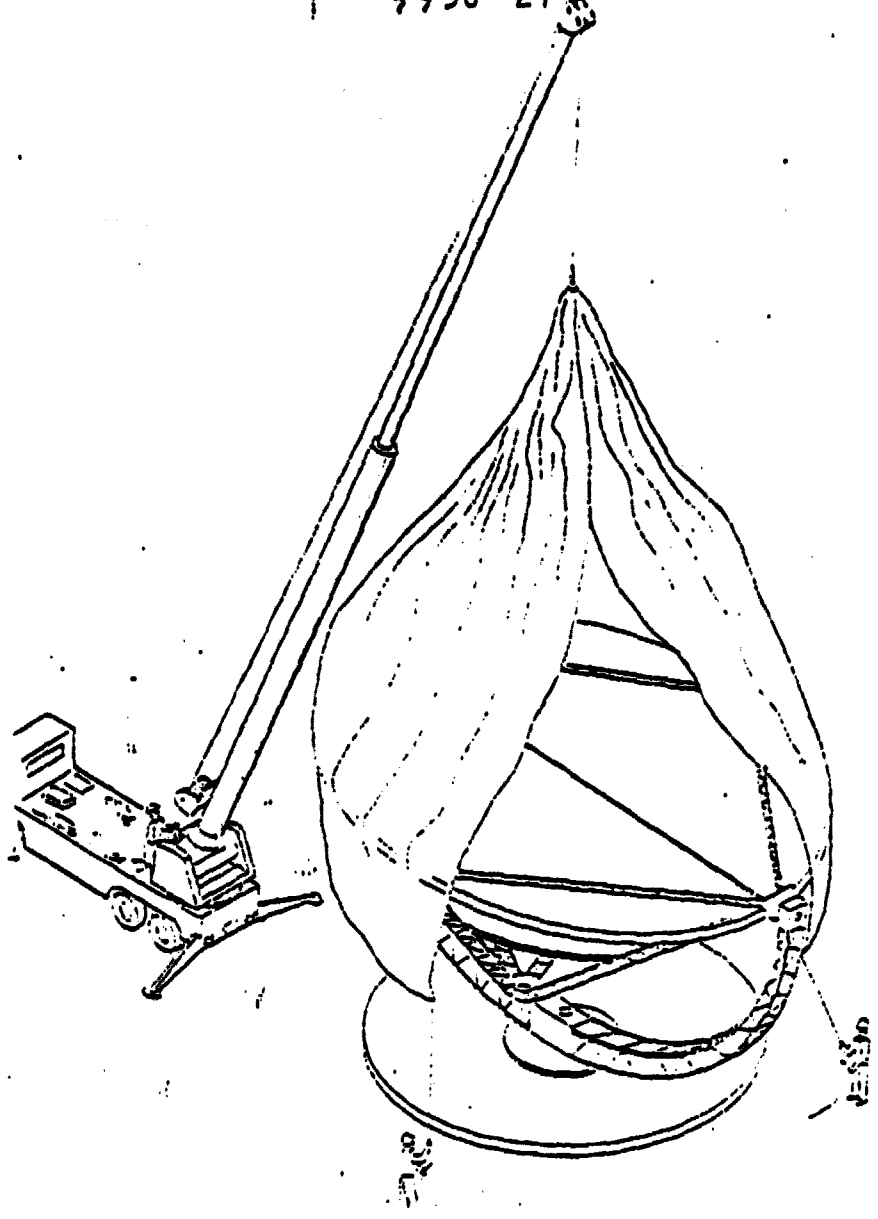

Figure 6.3-1. Enclosure Replacement

Figure 6.3-1 shows the concept of installing a new enclosure which will be done after 15 years. The replacement can be carried out without a protective shelter during periods of calm, dry weather.

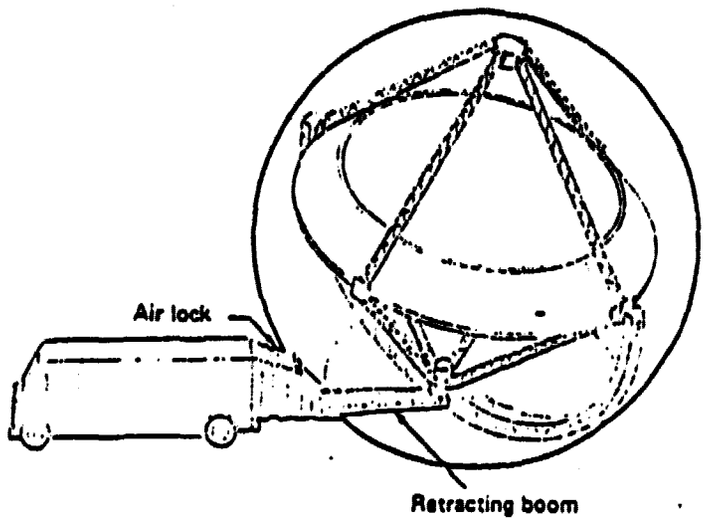

Figure 6.3-2 Brayton Unit Servicing

Figure 6.3-2 shows the Brayton unit being removed from the concentrator. Once the maintenance van has pulled up to the enclosure and the air lock seal has been made, the access door can be removed. Work can now be carried on without loss of pressurization. Work can be carried out during periods of inclement weather since workers and equipment are protected from the environment.

Before the Brayton unit is removed from the concentrator, a cable will be placed between the receiver support ring and yoke to prevent the concentrator from rotating 180°.

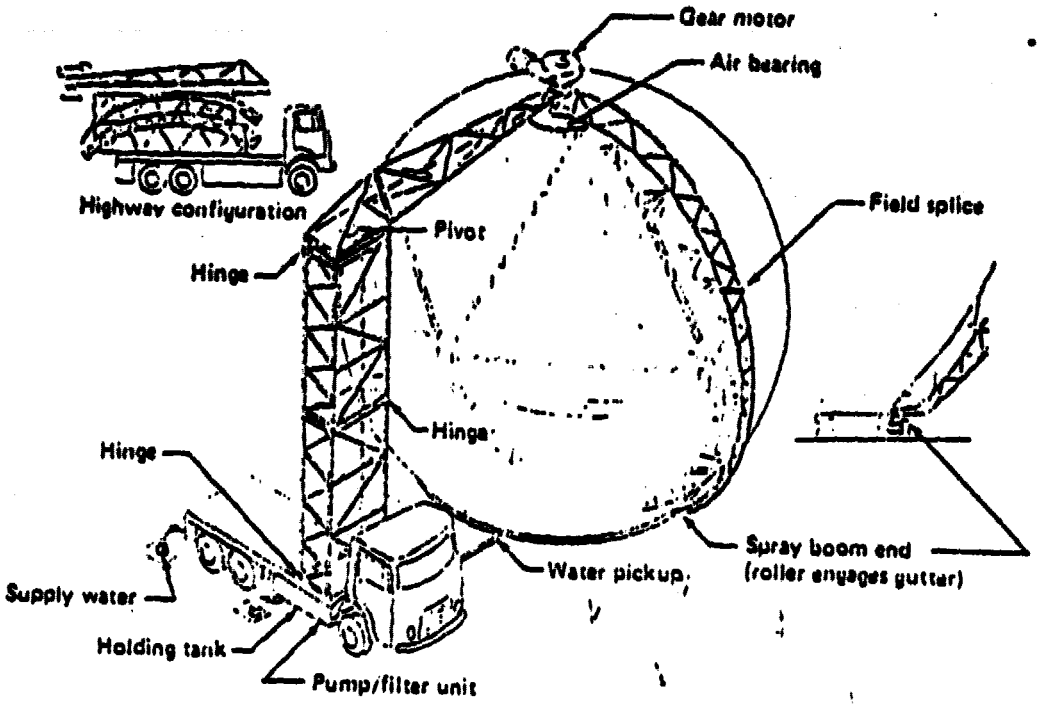

Figure 6.3-3. Highway Configuration

Figure 6.3-3 shows the concept for washing of the enclosure that was used for the cost analysis. The water recovery system is also shown. The spray boom is pivoted around the enclosure by the gear motor at the top.

151

Table 6.3-2 Washing Costs/Unit

Enclosure area	6,500 ft^2	
Required water*	.0132 gal/ft^2	
Cost of water*	5¢/gal, 75% recovery	$1.07
Washing cycle	20 min	
Washing frequency	3 weeks	
Labor	1 person @ $12/hr	$4.00
Equipment	$60,000 for washing truck	$1.42
	Total washing cost/unit	$6.49
	Total yearly washing cost/unit	$112.50

*Sandia cost analysis model

Using the preceding washing concept, the cost of washing one enclosure for a year is $112.50 as shown in Table 6.3-2. The frequency of washing would vary according to weather conditions and the related amount of degradation in the enclosure transmittance.

6.4 Cost Analysis

The production cost estimate was divided into three categories: part inventory, field installation, and site preparation. An itemized part list was then prepared for each category and programmed into the microcomputer. Use of the microcomputer facilitated the cost analysis by giving print-outs with the updated cost totals after changes had been made to the programs. Figure 6.4-1 shows the approach that was taken.

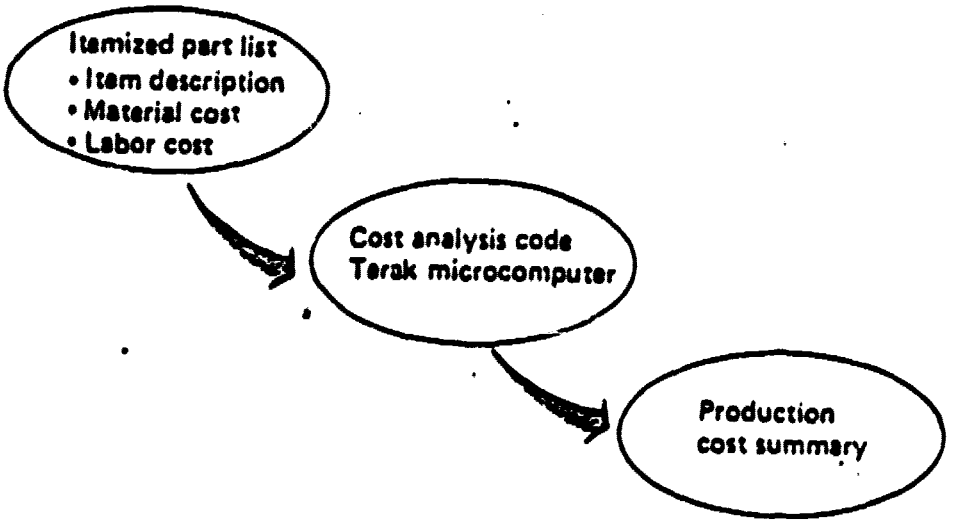

Figure 6.4-1. Production Cost Estimate

153

Baseline direct cost analysis

- **100,000 units/year dedicated factory**
- **Late 1978 dollars**
- **Direct factory labor at $8/hour plus 40% fringe**
- **Installation and maintenance labor at $12/hour plus 40% fringe**
- **Material costs based on vendor budgetary quotes and comparison to similar catalog items**

Figure 6.4-2. Costing Ground Rules

A baseline production rate of 100,000 units/year was used in the detailed study of direct and indirect costs. The direct labor rate of $8/hr was an average of factory labor rates in the Tucson area. Installation and maintenance labor were placed at $12/hr representative of construction craft labor rates. Costs were either vendor quotes or taken from similar catalog items produced at high rates. Figure 6.4-2 summarizes the costing ground rules.

Table 6.4-1a. Parts Inventory

	MATERIAL	CATEGORY	UNIT	LB/UNIT	$/UNIT
	1.0 ENCLOSURE DOME				
1.1	FILM	F	6700 SF	0.065	0.33
1.2	INSTALL. SEAM	F	1 EA	4.00	2.00
1.3	ROPE BEAD	F	90 FT	0.50	0.05
1.4	ACCESS DR. & FITTINGS	F	1 EA	110.00	110.00
	2.0 REFLECTOR				
2.1	ALUM. POLYESTER	R	1400 SF	0.015	0.057
2.2	TAPE JOINTS	R	378 FT	0.01	0.01
	3.0 VACUUM MEMBRANE				
3.1	COATED POLYESTER	R	699 SF	0.015	0.04
3.2	TAPE JOINTS	R	50 FT	0.01	0.01
	4.0 REFLECTOR SUPPORT SHELL				
4.1	UPPER RING	R	1 EA	80.68	100.35
4.2	LOWER RING	R	1 EA	56.00	70.00
4.3	SHELL PANELS	R	1055 SF	0.57	0.49
4.4	PANEL JOINTS	R	12 EA	5.00	1.00
4.5	TRUSS JOINTS	R	8 EA	3.00	1.00
4.6	REFLECTOR MTG.	R	0 SF	5.00	0.05
	5.0 TRUSS				
5.1	TRUSS MMBRS. & JOINTS	T	242 FT	2.06	1.55
5.2	TRUSS MMBRS. & JOINTS	T	112 FT	1.23	0.92
5.3	CROSS-TIE & TENSILE.	T	50 FT	0.20	0.25

Table 6.4-1 a, b, and c show the parts and material costs. The 48 ft enclosure made of 7 mil Kynar is by far the largest cost driver of the concentrator. It is 37% of the overall part inventory cost. The tracking system at $790 is a little over 12% of the overall cost. The reflector support shell, yoke, and truss are the remaining large cost drivers. The total cost of all parts and materials is $6,351.

Table 6.4-1b. Parts Inventory (Cont)

	6.0 RECEIVER SUPPORT RING				
6.1	RING FRAME & FITTINGS	T	1 EA	60.00	60.00
	7.0 COUNTERWEIGHT SUPPORT RING				
7.1	RING FRAME & FITTINGS	T	1 EA	65.00	65.00
	8.0 CONCRETE COUNTERWEIGHT				
8.1	CONCRETE & REBAR	C	5.5CF	148.00	1.50
	9.0 YOKE				
9.1	PORT ARM	Y	24 FT	10.50	7.88
9.2	STARBD. ARM	Y	24 FT	10.50	7.88
9.3	CENTER SECTION	Y	24 FT	14.85	11.14
	10.0 TRACKING DRIVE SYSTEM				
10.1	UNIT CONTROLLER	G	1 EA	5.00	225.00
10.2	SYSTEM CONTROLLER	G	1 EA	0.10	50.00
10.2	ELEV. BEARINGS	Y	2 EA	4.00	20.00
10.3	AZIMUTH BEARINGS	G	1 EA	68.00	200.00
10.4	SUN SENSOR	Y	1 EA	10.00	25.00
10.5	ELEV. GEAR REDUCER	Y	1 EA	26.00	60.00
10.6	AZIMUTH GEAR	Y	1 EA	20.00	5.00
10.7	ELEVATION MOTOR	Y	1 EA	8.00	75.00
10.8	AZIMUTH MOTOR	Y	1 EA	8.00	75.00
10.9	SENSOR LINES	Y	30 FT	0.10	0.15
10.10	SENSOR LINE	Y	40 FT	0.10	0.15
10.11	ELEV. ENCODER	Y	1 EA	0.50	10.00
10.12	AZIMUTH ENCODER	G	1 EA	0.50	10.00
10.13	ELEV. LIMIT SW.	Y	1 EA	0.20	1.50
10.14	AZ. LIMIT SW.	G	1 EA	0.20	1.50

Table 6.4-1c. Parts Inventory (Cont)

	11.0 ENCLOSURE AIR SYSTEM				
11.1	AIR BLOWER	G	1 EA	43.00	125.00
11.2	AIR FILTER SYSTEM	G	1 EA	10.00	40.00
11.3	EXHAUST VALVE	G	1 EA	2.00	5.00
11.4	DIFF. PRES. CONTROL	G	1 EA	2.00	15.00
11.5	CHECK VALVE	G	1 EA	2.00	5.00
11.6	INLET LINE	G	10 FT	0.10	1.00
11.7	EXHAUST LINE	G	10 FT	0.10	1.00
	12.0 REFLECTOR AIR PRESSURE SYSTEM				
12.1	VENT LINE	Y	60 FT	0.05	0.50
12.2	SOLENOID VALVE	Y	2 EA	1.00	30.00
12.3	DIFF. PRES. CONTROL	Y	1 EA	2.00	60.00
	13.0 BRAYTON SYSTEM LINE				
13.1	SUPPLY AIR	T	40 FT	0.10	1.00
13.2	SUPPLY AIR	Y	30 FT	0.10	1.50
13.3	SUPPLY AIR	G	14 FT	0.10	2.00
13.4	INSUL. EXHAUST AIR	T	48 FT	0.10	1.75
13.5	INSUL. EXHAUST AIR	Y	36 FT	0.10	2.25
13.6	FLEXIBLE DUCTING	Y	6 FT	0.10	5.00
13.7	SWIVEL JOINT	G	1 EA	5.00	25.00
13.8	FITTING SET	Y	2 EA	5.00	25.00
	14.0 FOUNDATION PARTS				
14.1	EDGE RING	G	1 EA	465.00	350.00
14.2	FILM CLAMPS	G	1 EA	50.00	50.00
	15.0 BRAYTON RECEIVER (SUPPLIED BY JPL)				
15.1	BRAYTON UNIT	R	1 EA	825.00	0.00
15.2	POWER BUS	Y	1 FT	0.00	0.00

Total cost = $6,338

Table 6.4-2. Field Installation Costs/Unit

OPERATION	CATEGORY	CREW	TIME	MATL. COST
SHIPPING FROM FACTORY	M	4.0	2.5	0.0
OFFLOAD MATERIALS	M	2.0	1.0	0.0
INSTALL FOUNDATION	C	4.0	2.5	$12.0
INSTALL YOKE BEARING PLATE	C	1.0	0.5	2.0
ERECT YOKE	C	3.0	1.0	0.0
ERECT LOWER TRUSS HALF	C	3.0	1.0	0.0
INSTALL AIR LINES	C	2.0	2.0	0.0
MECH/ELECT. HOOK-UPS	C	2.0	1.0	0.0
ASSEMBLE REFL. SHELL	C	3.0	2.0	5.0
INSTALL VACUUM MEMBRANE	C	2.0	0.5	0.0
INSTALL REFLECTOR	C	2.0	1.0	0.0
INSTALL REFL. COVER	C	2.0	0.25	0.0
MOVE REFL. ASSY. TO SITE	C	1.0	0.25	0.0
INSTALL REFL. ASSY. ON TRUSS	C	3.0	0.25	0.0
INSTALL TEMP. TRUSS COVER	C	2.0	0.25	0.0
PLACE TEMP. ENCLOSURE COVER	C	2.0	0.5	0.0
INSTALL ENCLOSURE	C	3.0	0.5	0.0
INFLATE ENCLOSURE	C	1.0	2.5	0.0
REMOVE ENCLOSURE COVER	C	2.0	0.25	0.0
PURGE ENCLOSURE AIR	C	1.0	1.0	0.0
REMOVE TRUSS COVER	C	2.0	0.5	0.0
INSTALL UPPER TRUSS HALF	C	2.0	2.0	0.0
INSTALL COUNTERWEIGHT	C	2.0	1.0	0.0
INSTALL TRUSS AIR LINES	C	2.0	1.0	0.0
MECH/ELEC. HOOK-UP	C	2.0	2.0	0.0
PURGE ENCLOSURE AIR	C	1.0	1.0	0.0
REMOVE TEMP. REFL COVER	C	2.0	0.25	0.0
CONTROL SYSTEM HOOK-UP	C	1.0	0.5	0.0
ALIGN TRACKING SYSTEM	C	1.0	1.0	0.0
FUNCTIONAL TESTING	C	1.0	1.0	0.0

Total labor = 67 hours = $1,126

Total material cost = $519

The results of a study of the necessary operations for installation of a concentrator in the field and the corresponding crew time are shown in Table 6.4-2. The study starts with shipment of a concentrator in a single container from the factory and goes through reflector assembly, enclosure attachment, and ends with functional testing of the concentrator. Total labor time for installing a concentrator is 67 hours.

157

Table 6.4-3. Site Preparation Costs

FIELD SITE COSTS..50 CONCENTRATORS. 40 DAYS

OPERATION	CATEGORY	CREW	TIME	MATL. COST
SET-UP FIELD ASSY. AREA	S	6.0	4.0	0.0
REFLECTOR SHELTER	S	0.0	0.0	240.0
ENCLOSURE SHELTER	S	0.0	0.0	952.0
TRUSS SHELTER	S	0.0	0.0	475.0
ERECT ASSY. SHELTERS (3)	S	6.0	12.0	0.0
CRANE RENTAL (14 TON)	S	0.0	0.0	2000.0
PICK-UP TRUCKS (2)	S	0.0	0.0	150.0
SANI-CANS (2)	S	0.0	0.0	90.0
TELEPHONE (2)	S	0.0	0.0	100.0
DISMANTEL ASSY. SHELTERS (3)	S	6.0	12.0	0.0
CLEAN UP SITE	S	6.0	4.0	0.0

Total labor/unit = 3.84 hrs = $64.50
Total material cost/unit = $79.40

Shown in Table 6.4-3 are the site preparation costs. The field size is approximately 600 ft. x 600 ft. per 50 concentrators. The necessary shelters and facilities are brought in and set up in the field. After the field of concentrators has been completed, these facilities are dismantled and shipped to another installation site. The itemized costs are for 50 units while the final labor and material costs are for 1 unit.

Table 6.4-4. Estimated Production Costs — 100,000 Units/Year

Direct labor	70
Materials	6,351
Utilities	15
Direct production costs	6,436
Indirect production costs	1,328
Total production cost	7,764
Profit (20% return on investment)	71
Selling price (FOB factory)	7,835

Table 6.4-4 shows the estimated production costs. The factory produces one unit every 2.1 minutes based on 2 shifts per day. The first shift has 64 people for material handling, 45 people for maintenance, and 70 people for the assembly line. The second shift has a lower requirement for material handling and maintenance personnel, but the same amount of personnel are needed for the assembly line, where each work station requires one person for processing. Adding 40% of the labor cost for fringe benefits, the total direct labor cost is $70/unit. The utility cost of $15 was arrived at by dividing the annual utility cost by the factory output. The direct production cost which is the summation of utility, factory labor, and material costs amounts to $6436. The indirect cost of $1328 takes into account the following: taxes, insurance, interest, depreciation on capital investments, and operating expenses. With $71 added for profit, which is obtained by taking 20% equity on capital investments, an estimated selling price of $7,835 is reached for a production rate of 100,000 units/year.

Table 6.4-5. Life Cycle Costs

FOB factory	7,835
Field installation	1,645
Site preparation	144
Installed cost	9,624
Maintanance for 30 years	7,886
Life cycle cost	17,510

$kW_{th}/\$ = .0041$

The life cycle cost not only depends on the selling price but also the planned maintenance of the concentrator over 30 years and the installation costs. Table 6.4-5 sums up the costs arrived at in the preceding pages. To arrive at the $kW_{th}/\$$ value of .0041 the average net power into the receiver aperture of 71 kW_{th} was divided by the life cycle cost of $17,510.

6.5 Economic Analysis Summary

Several studies were performed to determine the estimated selling price at varying annual production rates. The results are shown in Figure 6.5-1.

A study of factory, land, tooling, utilities and labor costs was performed at the production rate of 100 per year using a labor intensive factory. At this production rate, it was estimated to take 70 people on the first shift and 58 people working the second shift to produce a concentrator at the rate of one every two and a half days. Using the same cost analysis that was explained in Table 6.4-4, an estimated selling price of $87,400 was arrived at for a production rate of 100 unit/year.

Costs at higher production rates for the labor intensive factory were estimated by applying an improvement curve of 85% to direct labor rates, 98% to material costs, and keeping the same labor intensive factory but increasing the number of lines required.

Another study was done to determine the selling price of a concentrator at a production rate of 10,000/year using an automated factory. The results are shown in Figure 6.5-1.

A third study was performed to approximate the costs of a unit at various production rates using the manufacturing concept that was explained in detail in Section 5.1. The number of assembly lines were reduced and because of this the square footage of factory area was also reduced. The result of this study is on the second dotted line in Figure 6.5-1.

The final curve using the preceding three studies as guidelines shows an estimated selling price of a low production model to be eleven times that of a high production model.

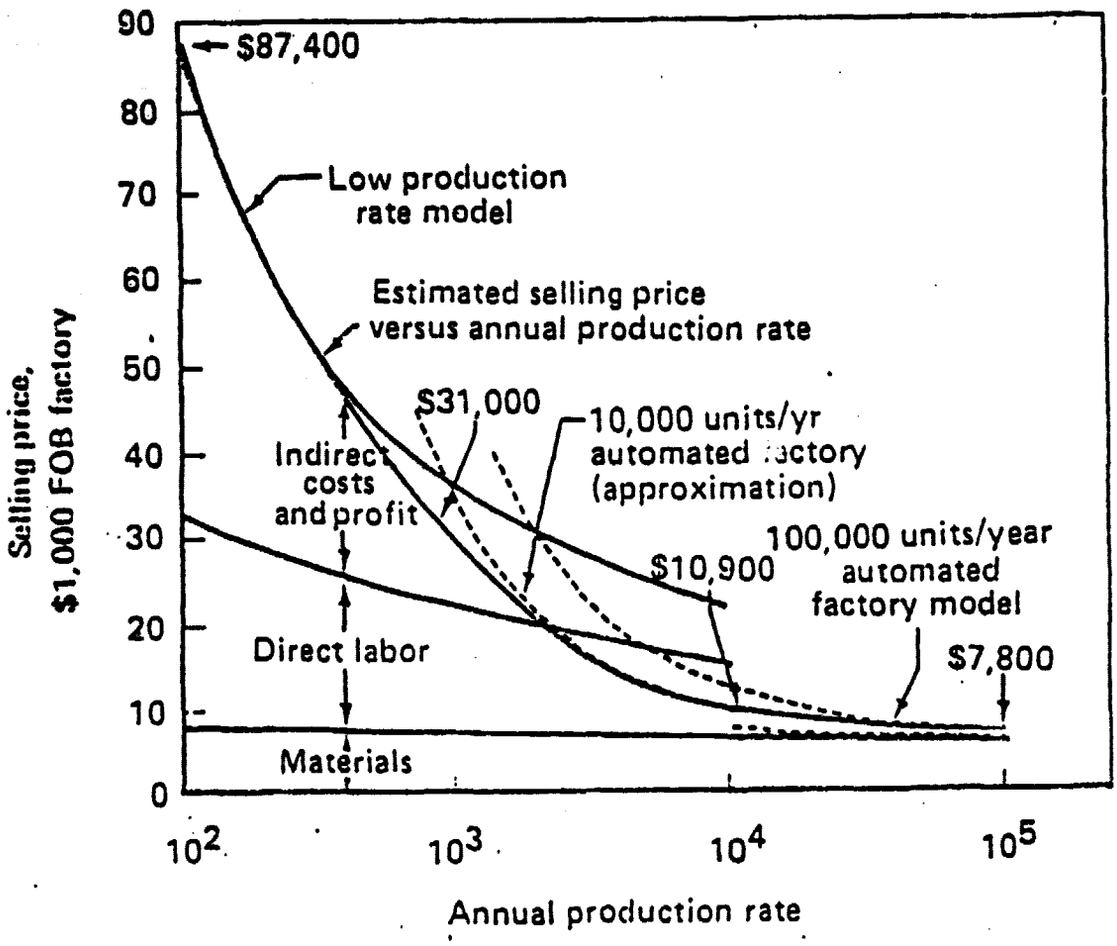

Figure 6.5-1. Estimated Selling Price

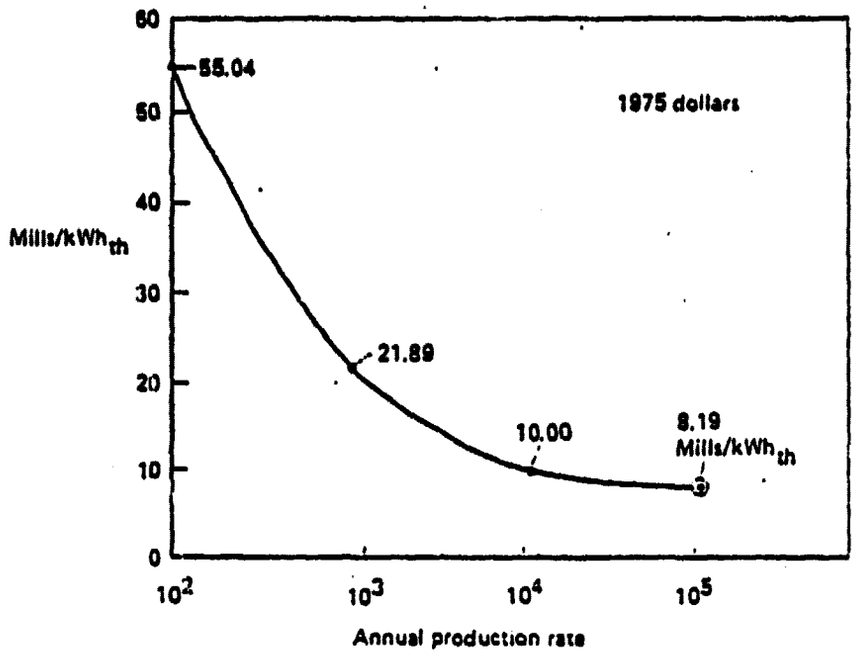

Figure 6.5-2. Levelized Energy Costs

Figure 6.5-2 shows the levelized busbar energy costs using 1975 dollars. These values were derived from the computer program provided by JPL. The imput variables used in the program are:

- Plant capacity= .071 MW
- Annual operation charges= 0
- Annual maintenance charge= $ 156.2
- Fuel cost= 0
- Capital Costs at
  - 100 units/yr=$76,000
  - 1000 units/yr=$29,037
  - 10,000 units/yr=$12,000
  - 100,000 units/yr=$ 9,400

Capital costs were arrived at by taking the installed cost of the concentrator and adding on the present value of an enclosure replacement. The costs which were originally in 1978 dollars were computed to mid 1975 dollars. All other inputs to the program were provided by JPL.

1.3

The BEC design offers a very low cost per unit area of concentrator. However, the efficiency is also reduced, primarily due to the enclosure transmittance loss. The ratio of cost to efficiency is suggested as a reasonable measure of the overall cost effectiveness. Using the installed concentrator cost (1978 dollars) and performance based on the sub-scale reflector test with systematic errors removed, the computed unit cost/efficiency parameters for the preliminary design concentrator are:

Table 6.5-1. Unit Costs/Efficiency for BEC Concentrator

Reflector Quality Classification	Surface Error RMS mrad	Net Power kW	Efficiency	Unit Cost/Efficiency $/M^2
Same as Subscale Test	5.52	61.2	0.576	125.50
Design Goal	2.0	71.0	0.669	108.17

These unit cost/efficiency values compare favorably with the goals given by JPL in Ref. 7 for point focus concentrators. JPL goals and the unit/cost/efficiency ratio from the JPL goals are:

Table 6.5-2. JPL Goals for Concentrator Unit Cost/Efficiency

Year	Efficiency	Unit Cost $/M^2	Unit Cost/Efficiency $/M^2
1982	0.90	100-150	111-167
1985	0.92	70-100	75-109

From a comparison of the computed BEC concentrator performance and the JPL goals it is evident that the BEC design meets the 1982 goals using the full set of data obtained in the laser ray trace test. Using the design goal for mass production units of 2 mrad surface error further improves the cost effectiveness to just within the range of the JPL 1985 goals.

7.0 DESIGN SENSIVITY STUDY

Studies were made to determine effects on weight and cost of the following design variations:

- Different Brayton unit weights
- Kynar versus UV stabilized polyester enclosures
- Reduced Receiver temperature
- Concentrator size optimization

The above design variations are reviewed in the remainder of this section. Other design options were also studied but were found to have a small influence on performance and cost; these options are:

- Yoke bracing with outriggers having rollers on the foundation
- Elevation axis shifted forward allowing self-balancing without use of a counterweight.

7.1 Brayton Unit Weight Variation

A variation of Brayton unit weight results in proportional changes in counterweight and nearly proportional changes in truss and yoke weights. The reflector assembly and remaining miscellaneous moving weight will be essentially unchanged. A summary of weight and cost changes relative to the baseline preliminary design are shown in Table 7.1-1.

Table 7.1-1. Weight/Cost Sensitivity to Brayton Unit Weight

Relative engine/ receiver weight	0.1	1.0	1.21	2.0
Engine/receiver	82.5 lb	825	1,000	1,650
Counterweight	82.5	825	1,000	1,650
Reflector assy	808	808	808	808
Truss	375	658	773	1,272
Yoke	518	908	1,044	1,568
Misc	336	336	336	336
Total moving weight	2,202 lb	4,360	4,961	7,284
Structural weight change	−673 lb	0	+251	1,274
Structural cost change @ $0.75/lb	−$505	0	+188	+956

166

Table 7.2-1. Cost Sensitivity to Enclosure Materials

	Kynar	UV stable polyester
Initial fabrication		
Enclosure material cost	2,211	578
Discounted		
Replacement material cost	1,408	368
Total capital investment present value	$3,619	$946
Cost difference	$2,673	

7.2 Enclosure Materials

Table 7.2-1 lists Kynar and UV stabilized polyester enclosure costs based on current material prices and discounted material costs for a common field replacement period of 15 years. The cost advantage of stabilized polyester film is significant. This advantage has motivated at least one major producer, ICI Americas, to have an on-going R&D program with the goal of producing an inherently stable polyester film. BEC currently has polyester film samples from ICI undergoing testing at the Desert Sunshine Test Facility in Arizona. Results from this testing, if favorable, may have an impact on future selection of enclosure material.

7.3 Reduced Receiver Temperature

With a decrease in receiver temperature the net energy to the receiver is increased along with the optimum aperture diameter as shown in Figure 7.3-1. Alternately, for the same net energy into the aperture, the reflector surface error could be allowed to increase. As shown in Table 7.3-1 the surface error of the production design concentrator could increase about 1 mrad, and still have the same net energy with the lower receiver temperature.

The effect on economics of the lower receiver temperature could be examined in several ways:

- The higher allowable concentrator surface error for the 1200°F receiver could permit lower cost fabrication of the reflective surface. At present, the production cost variation with surface quality cannot be defined. However, with automated mass production, impact of surface quality on cost of the reflective surface is expected to be very small.
- With the same surface error, the concentrator size could be reduced for the lower receiver temperature, to produce the same net energy. From the cases analyzed (Figure 7.3-1), the concentrator area is reduced 7.4 percent with the 1200°F temperature. The concentrator diameter would decrease from 13 m to 12.5 m, and the life cycle cost would decrease from $17,500 to $16,200. These reductions increase the energy cost parameter from .0041 $kW_{th}/\$$ to .0044 $kW_{th}/\$$, and reduce the Bus Bar Energy Cost from 9.63 mills/kW_{th} to 8.87 mills/kW_{th}.

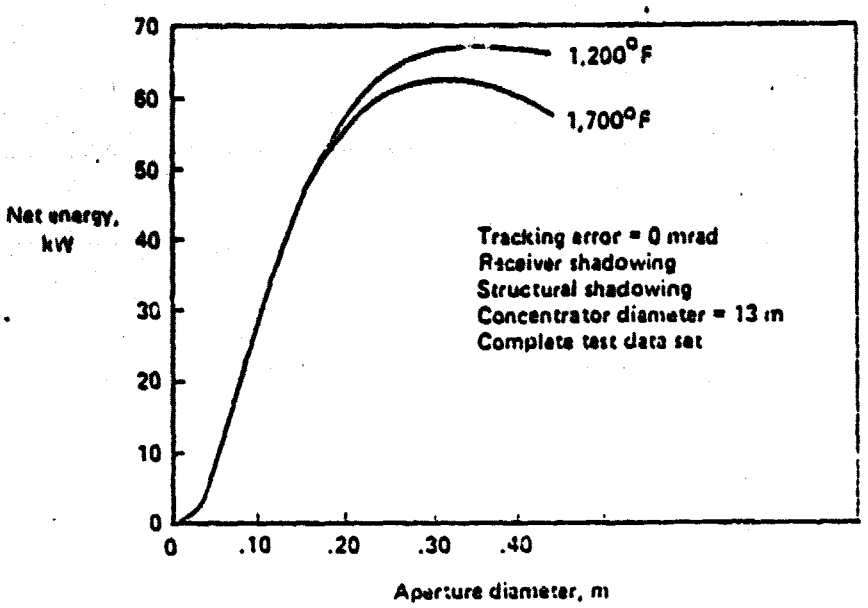

Figure 7.3-1. Reduced Receiver Temperature

Table 7.3-1. Reduced Receiver Temperature

Receiver temp (°F)	1,700	1,200
Surface error (mrad)	2	3
Optimum aperture diameter (m)	.2002	.2496
Net energy (kW)	73,968	74,100

13m concentrator (15 m dome)
No tracking error
Receiver and structural shadowing included

7.4 Concentrator Size Optimization

The cost data base developed for the preliminary concentrator design was used, together with cost trade data from Task I, in a concentrator size optimization study. Data from Task I for 7.6, 11, 14 and 17 m (25, 36, 46, and 56 ft.) diameter reflectors were related to the baseline preliminary designs. Updated selling prices, installation costs, maintenance costs and life cycle costs were then computed. For performance predicted for concentrators having 2 mrad surface and tracking errors, the performance/unit life cycle cost perameter (kW_{th}/S) is maximized over a range of diameters from 9.7 to 14 m (32 to 46 ft.) as shown in Figure 7.4-1. The corresponding levelized bus bar energy cost becomes a minimum for a reflector diameter of about 13 m (42.7 ft.). It is interesting to note that the 13 m diameter is less than the optimum size determined in Task I which was 15 m (without shipping constraint imposed). This reduction in optimum size is primarily due to the increased cost of the Kynar enclosure compared to the polyester enclosure specified earlier. Thus it was found that the optimum concentrator diameter is sensitive to material costs and its final value depends on the outcome of subsequent detail design features and vendor developments.

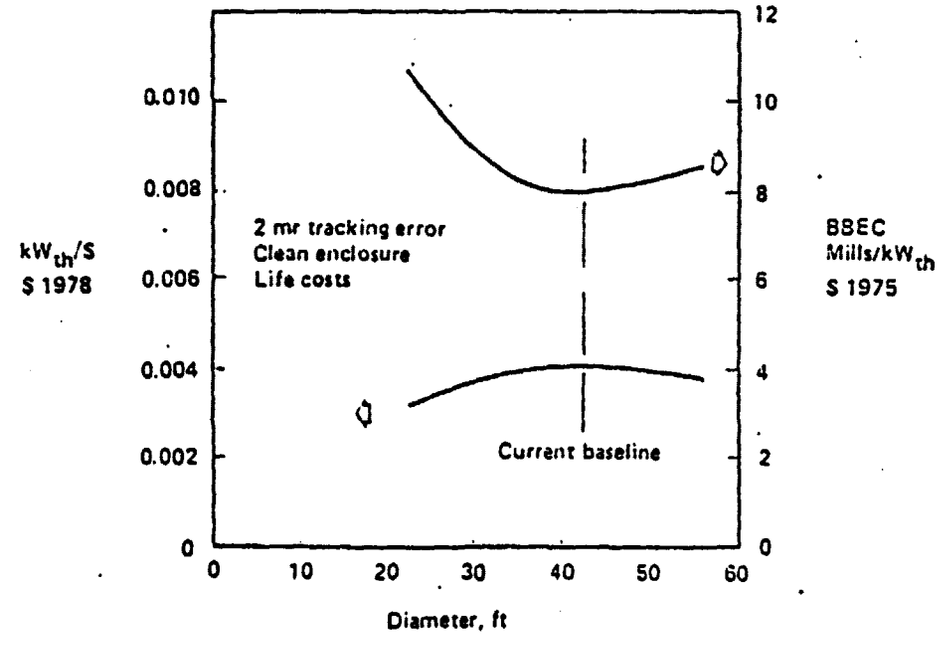

Figure 7.4-1. Concentrator Size Optimization

8.0 CONCLUSIONS

The objectives of this program were to:

- Optimize the concentrator design parameters for maximum solar energy collected per concentrator unit cost
- Develop a preliminary design
- Investigate the manufacturing, installation, and maintenance of the concentrator
- Predict the costs for mass production

In fulfilling these objectives, a preliminary design was developed for a low cost point focus solar concentrator having an ultra-light 13 m diameter pneumatically stabilized plastic film reflector. Conclusions from the program are summarized below:

The pneumatically stabilized concentrator design concept is mass-producible at low cost and offers high energy collection per unit concentrator cost. Low cost is achieved by overall low concentrator weight made possible by use of a clear plastic film enclosure that shields the concentrator from wind, dust and other environmental stresses.

Technical viability and prototype fabrication methods for the thin paraboloidal aluminized polyester film reflector were demonstrated by the building and testing of a subscale 4.57 m diameter reflector. Techniques for forming and mounting the reflector using inexpensive tooling were developed. The results of laser ray trace testing, involving a scan of 1723 reflector points, show that a surface slope quality of 5.52 mrad RMS with systematic errors removed was achieved with this first large scale trial reflector. Based on previous experience in a Sandia Laboratories program (Ref.3) an evaluation of the test reflector, improved performance would be obtained in further fabrication and testing at this reflector size. With production tooling, reflectors having installed surface slope errors of 2 mrad RMS are feasible.

A plant design was conceived for mass production of 100,000 concentrator units per year at a rate of 2.1 units per hour, operating at 2 shifts per day. The plant design study resulted in a facility having 732,500 sq. ft. floor area, $41 million building and site cost and $25 million tooling and equipment cost for a total capital investment of $66 million.

Highly automated tooling and material handling concepts are needed to realize high plant production rates. Sophisticated tooling concepts were identified for the critical reflector and enclosure fabrication workstations; these tooling require development before high production rates can be achieved. Enclosure fabrication must be studied in detail considering forming technique, film selection, polymer costs and automated tooling trade-offs. While a gore-formed Kynar enclosure concept was selected to determine enclosure part costs in this program, developments in current research in thermoforming of enclosures are expected to reduce enclosure costs.

The concentrator can be quickly erected in the field from containerized pre-assembled concentrator parts. A critical field operation is reflector assembly which would be done on portable precision fixtures under shelter. Temporary shelter will be required during reflector and enclosure installation in windy conditions.

An analysis of maintenance requirements over a 30 year lifetime indicates washing of the enclosure will be a major life-cycle cost component followed by enclosure replacement programmed at 15 years. Washing could be done with a mobile washing truck traveling from field to field. Maintenance of the concentrator in the inflated enclosures would be done using portable service equipment having air locks.

Based on analysis of production, field installation and maintenance costs, the concentrator's estimated selling price based on 1978 dollars is $7835 ($59/m^2) FOB factory at an annual production of 100,000 units. Installed concentrator cost, including related construction site and equipment costs, is $9624 ($73/m^2). With life cycle costs considered, including maintenance, the concentrator cost is $17,510 ($132/m^2).

Optimum mass-produced concentrator size was determined to be a reflector diameter of 13 m with an optimized aperture diameter of 0.228 m and F/D of 0.5. At this size, the concentrator design is predicted to have a net energy collection of 71 kW_{th} for an insolation of 800 W/m^2, 2 mrad RMS surface slope error and 2 mrad RMS tracking error.

In terms of concentrator unit cost/efficiency, the concentrator has an installed cost/efficiency ratio of $125.50/$m^2$ for a reflector surface quality of 5.52 mrad RMS (representing the full subscale test reflector with systematic errors removed) and $108.17/$m^2$ for the 2 mrad RMS surface design goal. These ratings compare favorably with JPL's goals for concentrator costs of $100 to 150/$m^2$ ($111 to 167/$m^2$ when factored for efficiency) for 1982.

The concentrator's performance/cost rating can be improved in several ways. Success in current vendor research on inherently stabilized polyester film would result in large initial concentrator cost savings. Also, reduction in enclosure film cost and/or washing costs would significantly reduce life cycle maintenance costs.

REFERENCES

1. Boeing Document BCS-G0166-1, Thermal Analyses-Beta, Users Manual, TES-176, February 1969.

2. Mathematical Theory and Methodology for Simulation of Real Reflectors, Final Report-Analysis of Solar Reflectors, G. L. Schrenk, Allison Report EDR3693, 16 December 1973.

3. Plastic Parabolic Concentrator Feasibility Study, Sandia Report SAND 79-7004, prepared by Boeing Engineering and Construction Company January 1979.

4. One Piece Dome Fabrication Study, being performed by Boeing Engineering and Construction under Sandia Contract 18-7830.

5. Solar Central Receiver Prototype Heliostat Final Technical Report, Report No. SAN/1604-1, Boeing Engineering and Construction Company, June 30, 1978.

6. The Sun-Tracking Control of Solar Collectors Using High-Performance Step Motors, R.O. Hughes, presented at the Sixth Annual Symposium on Incremental Motors Control Systems and Devices, Champaign, Ill., May 1977.

7. JPL Report 5104-26, Point Focusing Distributed Receiver Technology Project--Executive Summary, Annual Technical Report, Fiscal Year 1978, prepared by Jet Propulsion Laboratory, Pasadena California.

APPENDIX

Preliminary Design Drawings

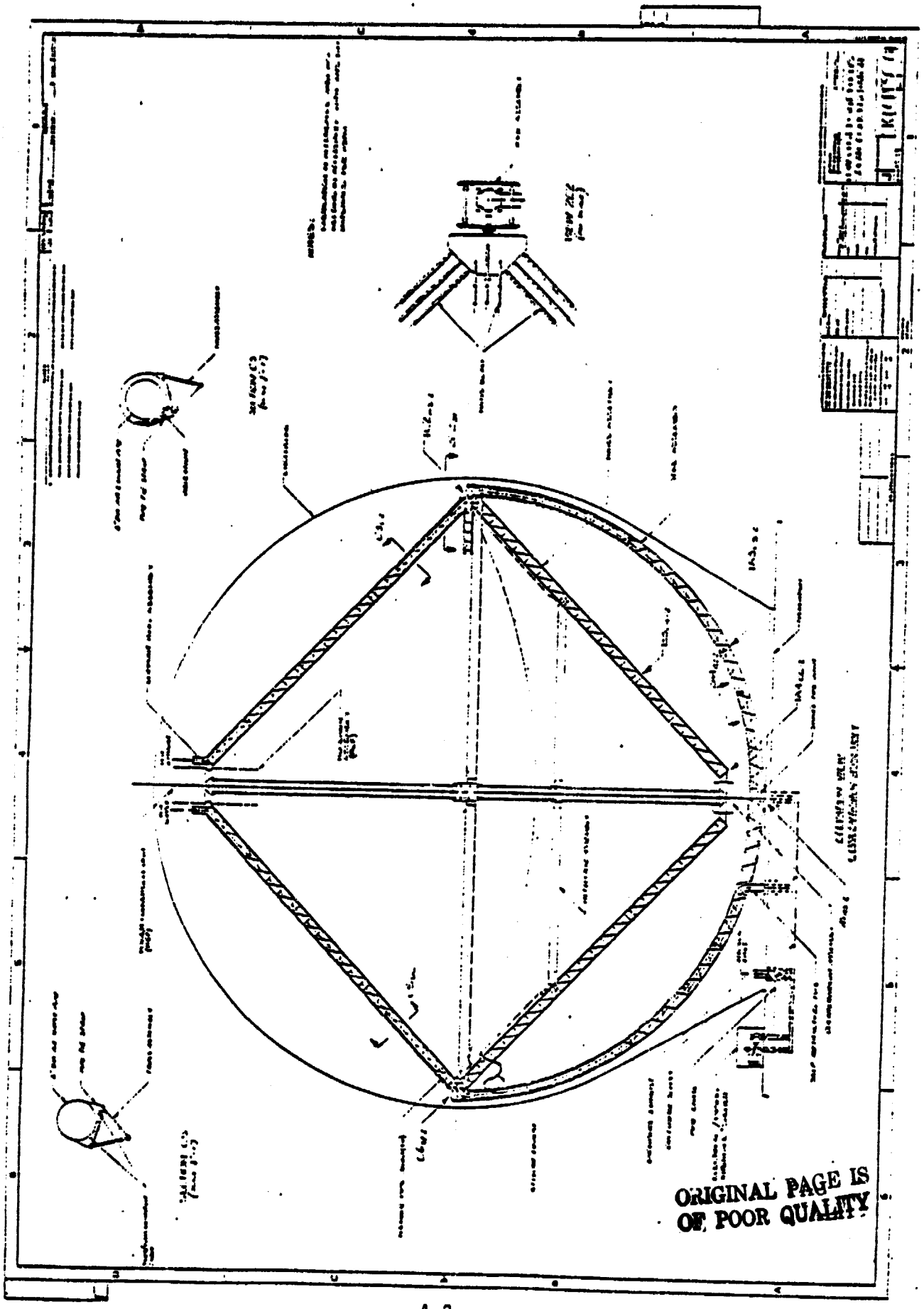

ORIGINAL PAGE IS
OF POOR QUALITY

177

ORIGINAL PAGE IS
OF POOR QUALITY

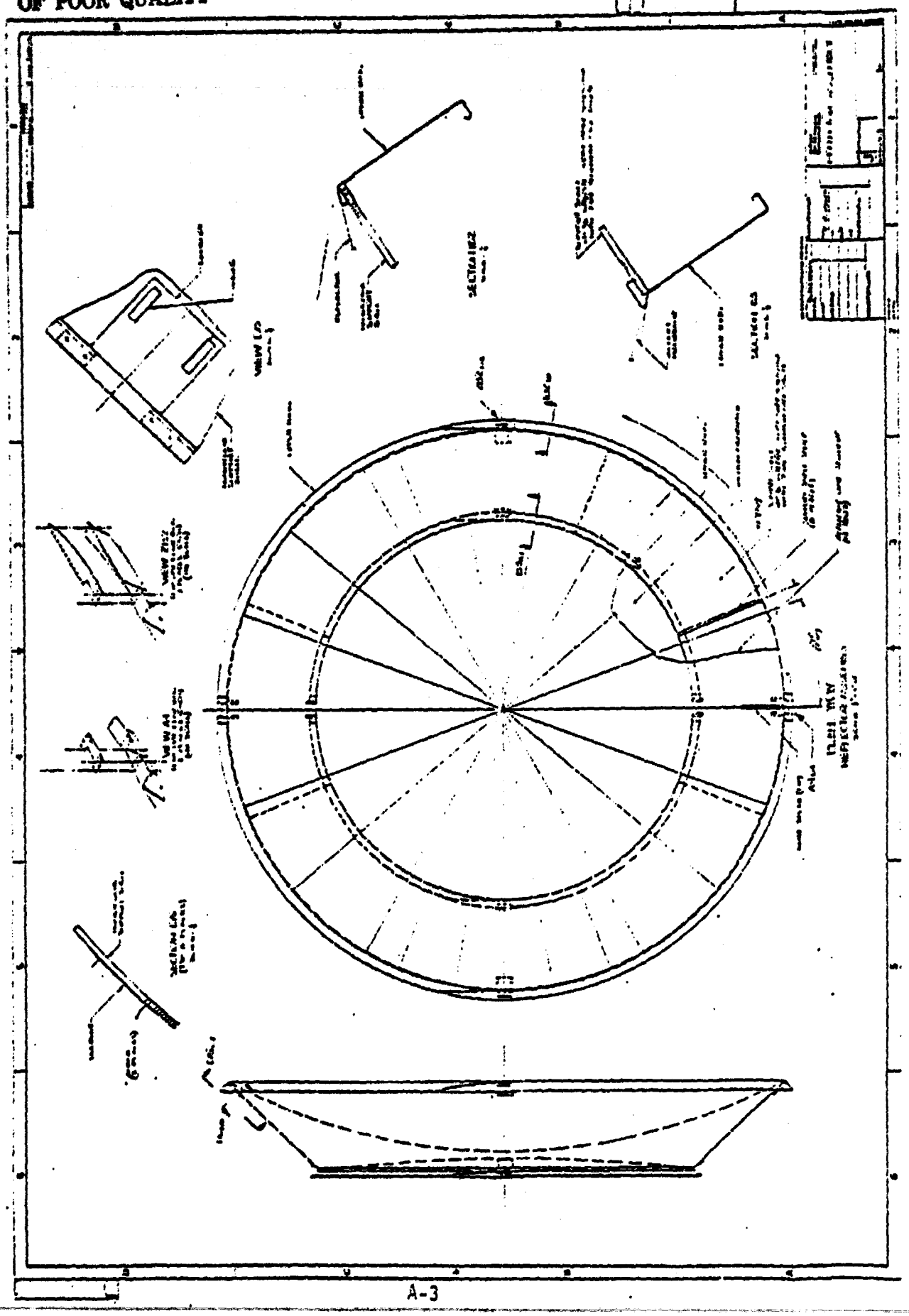

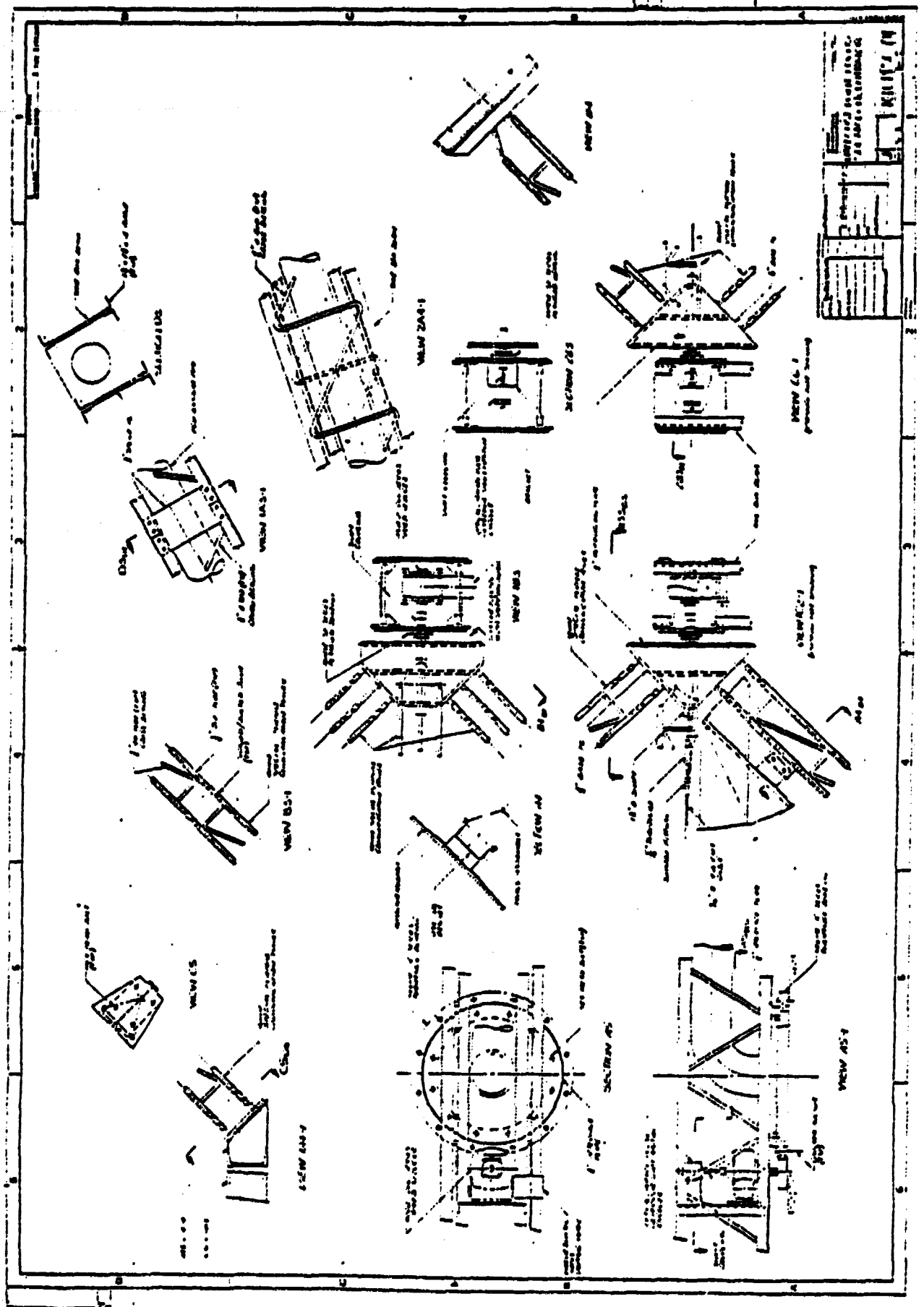

9950-279

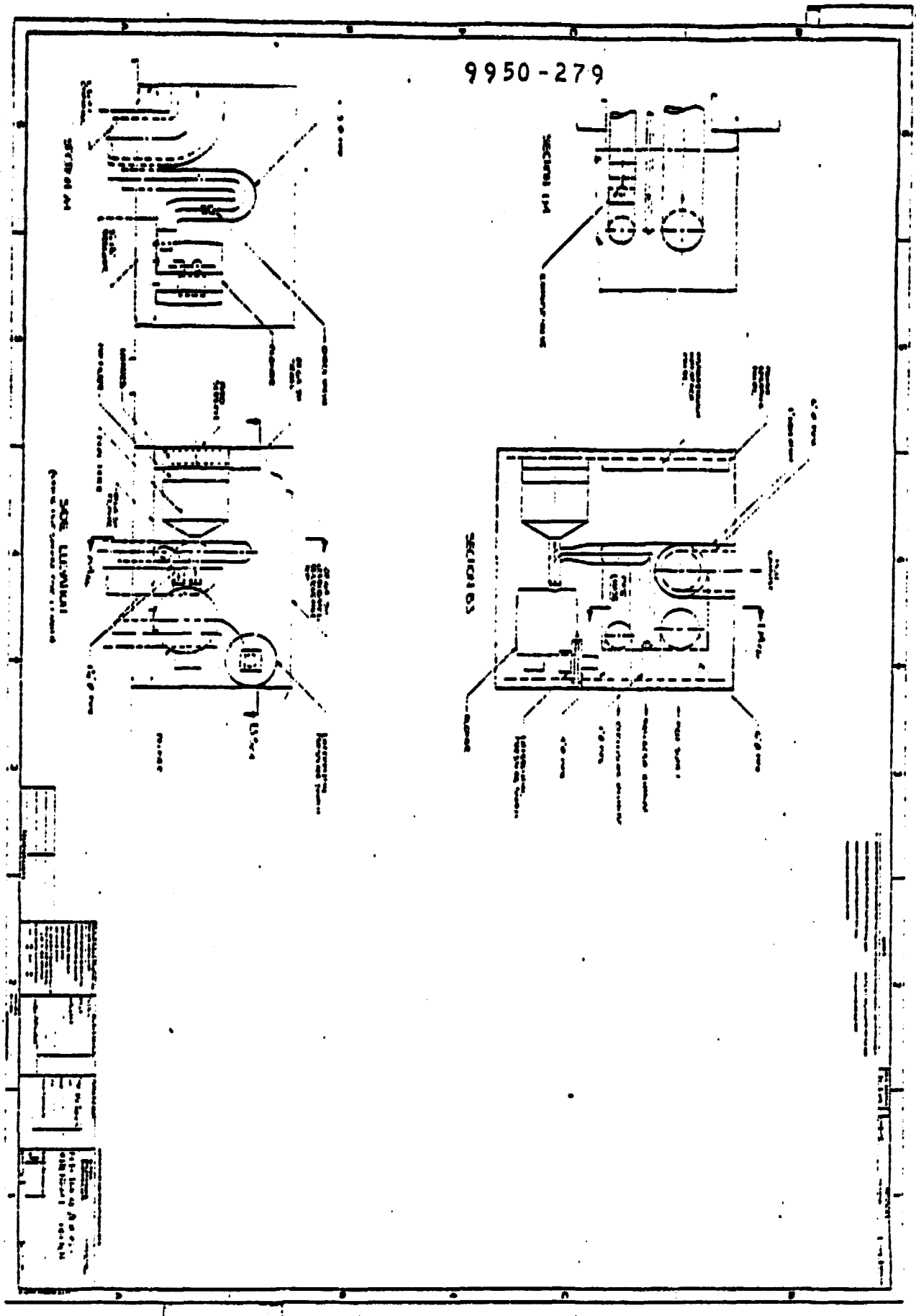

180